

AD 718328

Technical Note N-1141

COMPARATIVE SOLUTIONS FOR THE RESPONSE
OF RESTRAINED, RIGID-BODY UNDERWATER
STRUCTURES TO ACOUSTIC SHOCK

By

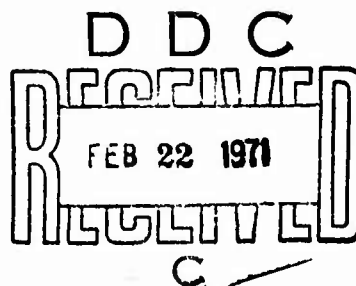
J. G. Hammer and H. S. Zwibel

January 1971

Approved for public release;
distribution unlimited.

NAVAL CIVIL ENGINEERING LABORATORY
Port Hueneme, California 93041

Reproduced by
NATIONAL TECHNICAL
INFORMATION SERVICE
Springfield, Va. 22151



COMPARATIVE SOLUTIONS FOR THE RESPONSE OF RESTRAINED, RIGID-BODY
UNDERWATER STRUCTURES TO ACOUSTIC SHOCK

Technical Note N-1141

ZF 38.512.001.009

by

J. G. Hammer and H. S. Zwibel

ABSTRACT

This study seeks better understanding of the general problem of predicting the response of fixed underwater structures to a shock wave propagating through the water. Two idealized structures are considered; an elastically-restrained rigid sphere and an elastically-restrained rigid cylinder. The shock is assumed to be an exponentially-decaying pressure pulse in an acoustic fluid. Solutions to the exact equations are obtained analytically for the spherical structure and by Bellman's numerical inversion procedure for both structures. Previously obtained solutions for the restrained cylindrical structure, simplified by the Mindlin-Bleich approximation, are found to be in agreement. Response curves are given for both structural types over a range of parameters. The effects of drag are discussed.

ACCESSION for	
CPSTI	WHITE SECTION <input checked="" type="checkbox"/>
BDC	BUFF SECTION <input type="checkbox"/>
UNANNOUNCED	<input type="checkbox"/>
JUSTIFICATION	
BY	
DISTRIBUTION/AVAILABILITY CODES	
DIST.	AVAIL. and/or SPECIAL
/	

Approved for public release; distribution unlimited.

CONTENTS

	<u>Page</u>
INTRODUCTION	1
SPHERICAL STRUCTURE	3
CYLINDRICAL STRUCTURE	10
DRAG EFFECTS	13
FINDINGS AND CONCLUSIONS	14
FIGURES	16
APPENDIXES	
A - Inversion of Fourier-Transformed Equations for Spherical Structure	63
B - Numerical Inversion of Transformed Equations	66
REFERENCES	70
LIST OF SYMBOLS	71

INTRODUCTION

This study continues the analysis that was begun in reference 1, and seeks a better understanding of the general problem of predicting the response of an underwater elastically-restrained structure to a shock wave propagating through the water. This problem is of interest to those who may want to consider the design or vulnerability of fixed ocean-floor structures. There are sufficient differences between this problem and that of a neutrally buoyant submarine, for example, to make one suspect that existing analytical and experimental data may not provide all the answers needed. The fixed ocean-floor structure has several unique considerations: (1) It is not free to move with the water shock or the flow behind it; this alters the loading and produces a greater flow of water past the structure with accompanying drag forces. (2) It is not necessarily neutrally buoyant; it may be denser or less dense than the volume of water it displaces. The effect of this relative density is important in the response of fixed structures. (3) It depends upon the adequacy of the structural restraining members. The design of these may be a critical problem. (4) It is subjected to a different kind of absolute motion and acceleration than would be a free structure such as a submarine. The structure motions must be predicted so that criteria for stable positioning and shock isolation can be met. (5) It is restrained by and tied to the ocean floor. It is thus subject to loading caused by motion of the ocean floor as well as that of the water shock.

Not all of the above considerations can be treated initially. The special problem in the beginning stages of such an analysis is the difficulty in solving any but the most idealized situation. In this study, as in reference 1, a simplified structure is mathematically modeled, and the last of the above considerations is not included. For the water shock an acoustic approximation has been used, which implies certain assumptions about the shock strength and velocity as well as the nature of the fluid surrounding the structure. Although the acoustic approximation is known to be inaccurate, it is not clear how large an error it contributes. In some cases the error may be minor. If the source of the underwater disturbance is sufficiently far from the structure, the shock reaching the structure will be traveling at acoustic speed. Also, any drag forces due to steady flow appear to be quite small. For stronger shocks the principal sources of error probably arise from the neglect of forces produced by non-steady flow, turbulence, and separation of the boundary layer. It was demonstrated in reference 1 that in the case of acceleration the peak values occur before the shock has traversed the structure, so that viscous drag and turbulence have not

yet developed. This would imply that treating the water as an acoustic fluid probably gives a good estimate of peak acceleration. On the other hand, the peak velocity and peak displacement occur at later times so it might be suspected that a larger error is present in the acoustic prediction of these values.

The reason for persisting in the acoustic approximation is that it is the most tractable analytically. However, even the acoustical equations become very difficult to solve as the number of parameters increases. In this study at least two additional parameters are of interest: The relative buoyancy of the structure and the restraint function. A large number of parameters makes it impracticable to run direct numerical solutions of the equations. It is more desirable to try to obtain final solutions as some explicit function of the problem parameters so that results can be obtained for any set of parametric values. This was the approach followed by Murray² for the case of an unrestrained cylinder; but it did not lead to a final analytical solution, and numerical inversion of Fourier transforms was required.

In reference 1 the authors considered the rigid body response of an elastically-restrained cylindrical deep-ocean structure to an acoustic shock. For this problem the method employed by Murray becomes very tedious and an effort was made to find simple procedures of comparable accuracy. Solutions were obtained using the Mindlin-Bleich³ approximation which makes the equation simpler by assuming a plane wave character for the scattered and radiated waves. For the special case of no restraint these solutions were compared with Murray's results and found to be in close agreement.

It was not possible to determine the accuracy of the Mindlin-Bleich approximation for restrained cylinders because no solutions have been found for reference. One of the objectives of this study has therefore been to develop such solutions to the exact equations for the restrained cylinder. This is difficult because solution of the exact equation leads to transformed equations that cannot be inverted analytically. It is necessary to use a numerical inversion procedure as did Murray. His procedure could be followed, but in this more difficult problem that procedure becomes almost prohibitively laborious and time-consuming. Instead, Bellman's numerical inversion procedure⁴ was tried. The appropriateness of doing this was demonstrated for the case of a spherical structure, for which analytical inversion of the transformed equation can be performed and a comparison of results is possible.

This study therefore accomplishes the following:

1. It presents an exact solution for the rigid-body response of an elastically-restrained spherical structure in an acoustic fluid.
2. It demonstrates the appropriateness of the Bellman procedure for inverting the Laplace transforms in the case of the spherical structure by comparison with 1, above.

3. For the case of a restrained cylindrical structure in an acoustic fluid, it presents a solution of the exact equations using Bellman's procedure.

4. It compares solutions using the Mindlin-Bleich approximation for the cylinder with the results of 3, above.

The following sections discuss these results in detail and resulting figures show the calculated response of both spherical and cylindrical structures. The Appendices contain the procedures used for computing inverse transforms.

SPHERICAL STRUCTURE

It is possible to obtain an analytical solution of the equations for a restrained spherical structure. Once that solution is at hand, it can be used as a standard for testing numerical methods of solving the same equations in order to determine the appropriateness of numerical solutions. If a satisfactory numerical procedure exists for the case of the restrained spherical structure, it is reasonable to try the same numerical procedure in the case of the restrained cylindrical structure, for which an exact analytical solution has not been found.

Suppose that an elastically-restrained, spherical deep-ocean structure is subjected to an underwater shock wave. The source of the shock wave is assumed to be sufficiently far from the structure so that the incident shock wave form is a plane wave describable by linear acoustic theory. For simplicity the effects due to reflections from the ocean floor and the ocean surface are not considered.

Figure 1 describes the geometry and shows the coordinate system. The top diagram is for time, $t = 0$. The shock wave is traveling from left to right and time is measured from the instant the shock wave reaches the sphere. The sphere is of radius a and standard spherical coordinates are used; r is the distance from the origin, and θ is the angle measured from the polar axis, which is taken to be in the direction of propagation of the wave. The problem has azimuthal symmetry, so that a second angular coordinate is not required to describe the velocity field. The lower view in Figure 1 shows the configuration at a later time t . The shock wave has advanced the distance ct (c is the acoustic velocity of the fluid) and the sphere has moved its center through a distance z in the propagation direction. For clarity, the z displacement has been grossly exaggerated. Not shown on the lower diagram are the reflected, diffracted and radiated waves.

Three equations describe this dynamical situation. The first expresses equilibrium of forces acting on the sphere. These forces are the inertia force, the elastic restraining force, and the forces due to the acoustic pressures of the incident and scattered and radiated waves. The second equation is the wave equation that describes the propagation

of the acoustic waves. The third equation imposes the condition that the water particle velocity at the surface of the sphere must have a zero normal component relative to the sphere. Physically this states that the surrounding water cannot penetrate into the sphere.

The total pressure force in the propagation direction is obtained by integrating the incremental force in the z direction due to the pressures acting on a strip of width $d\theta$ at θ . This is shown in Figure 2. The area of the strip at angle θ is simply $2\pi a^2 \sin\theta d\theta$. This gives the pressure acting on the strip; the component in the propagation direction is obtained by projecting this pressure force in the z direction. The total horizontal pressure force, therefore, is

$$F_p(a, \theta, t) = - \left[2\pi a^2 \sin\theta \cos\theta d\theta \right] p(a, \theta, t) \quad (1)$$

where $p(a, \theta, t)$ is the pressure distribution at the surface of the sphere at time t . The pressure itself is described through the velocity potential ϕ for the particle velocity distribution. In terms of ϕ the water velocity and pressure are given by

$$u_r(r, \theta, t) = - \frac{\partial}{\partial r} \phi(r, \theta, t) \quad (2)$$

$$p(r, \theta, t) = \mu \frac{\partial \phi}{\partial t}(r, \theta, t) \quad (3)$$

where μ is the density of water. The acoustic field is divided into the incident acoustic field plus the scattered and radiated waves. The incident pulse is assumed to have peak pressure p_0 and to decay with time constant q as given below.

$$p_i(r, \theta, t) = p_0 e^{-\left[\frac{z+a}{c} - t\right]/q} H\left(t - \frac{(z+a)}{c}\right) \quad (4)$$

where $z = r \cos\theta$

In terms of this incident wave, the equations for the system are:

$$m \ddot{z}(t) + k z(t) = - 2\pi a^2 \int_0^\pi \sin\theta \cos\theta \left[p_1(a, \theta, t) + \mu \frac{\partial \phi(a, \theta, t)}{\partial t} \right] d\theta \quad (5)$$

$$\nabla^2 \phi(r, \theta, t) = \frac{1}{c^2} \frac{\partial^2 \phi(r, \theta, t)}{\partial t^2} \quad (6)$$

$$\dot{z}(t) \cos\theta = - \left. \frac{\partial \phi_1(r, \theta, t)}{\partial r} \right|_{r=a} - \left. \frac{\partial \phi(r, \theta, t)}{\partial r} \right|_{r=a} \quad (7)$$

The above equations can be made dimensionless by defining the following parameters:

$$\tau = \left(\frac{c}{a} \right) t$$

$$\rho = \left(\frac{1}{a} \right) r$$

$$\zeta(\tau) = \left(\frac{\mu c^2}{a p_0} \right) z(t)$$

$$\phi_1(\rho, \theta, \tau) = \left(\frac{1}{a p_0 \mu c} \right) \phi(r, \theta, t)$$

$$\chi = \left(\frac{a}{c} \right) \frac{1}{q}$$

$$\omega_0^2 = \frac{k}{m} \left(\frac{a}{c} \right)^2$$

$$S = \mu_s / \mu = \frac{\text{density of structure}}{\text{density of water}}$$

With these transformations, the three equations for the system become:

$$\frac{d^2 \zeta(\tau)}{d\tau^2} + \omega_0^2 \zeta(\tau) = -\frac{3}{2S} \int_0^\pi \sin\theta \cos\theta d\theta \left[H(\tau - 1 - \cos\theta) e^{-\chi(\tau - 1 - \cos\theta)} + \frac{\partial \phi_1}{\partial \tau}(1, \theta, \tau) \right] \quad (8)$$

$$\frac{\partial^2 \phi_1}{\partial \rho^2} + \frac{1}{\rho} \frac{\partial \phi_1}{\partial \rho} + \frac{1}{\rho^2} \frac{\partial^2 \phi_1}{\partial \theta^2} = \frac{\partial^2 \phi_1}{\partial \tau^2}(\rho, \theta, \tau) \quad (9)$$

$$\begin{aligned} \frac{d\zeta(\tau)}{d\tau} \cos\theta &= H(\tau - 1 - \cos\theta) \cos\theta e^{-\chi(\tau - 1 - \cos\theta)} \\ &\quad - \frac{\partial}{\partial \rho} \phi_1(\rho, \theta, \tau) \Big|_{\rho=1} \end{aligned} \quad (10)$$

Rather than deal directly with the time-dependent functions, it is convenient to consider the Fourier transforms of $\zeta(\tau)$ and ϕ_1 . The general relations connecting a function $f(t)$ and its Fourier transform $F(\omega)$ are:

$$f(t) = \frac{1}{\sqrt{2\pi}} \int_{-\infty}^{\infty} e^{i\omega t} F(\omega) d\omega$$

$$F(\omega) = \frac{1}{\sqrt{2\pi}} \int_{-\infty}^{\infty} e^{-i\omega t} f(t) dt$$

Using this transformation, the above set of equations become:

$$(\omega_0^2 - \omega^2) \bar{\zeta}(\omega) = - \frac{3}{2S} \int_0^\pi \sin\theta \cos\theta \, d\theta \left[\frac{1}{\sqrt{2\pi}} \frac{e^{-i\omega t(1+\cos\theta)}}{\chi + i\omega} + i\omega \bar{\phi}_1(1, \theta, \omega) \right] \quad (11)$$

$$\frac{\partial^2 \bar{\phi}}{\partial \rho^2}(\rho, \theta, \omega) + \frac{1}{\rho} \frac{\partial \bar{\phi}_1(\rho, \theta, \omega)}{\partial \rho} + \frac{1}{\rho^2} \frac{\partial^2 \bar{\phi}_1(\rho, \theta, \omega)}{\partial \theta^2} = -\omega^2 \bar{\phi}_1(\rho, \theta, \omega) \quad (12)$$

$$i\omega \bar{\zeta}(\omega) \cos\theta = \frac{1}{\sqrt{2\pi}} \frac{e^{-i\omega(1+\cos\theta)}}{\chi + i\omega} \cos\theta - \frac{\partial \phi_1(\rho, \theta, \omega)}{\partial \rho} \Big|_{\rho=1} \quad (13)$$

where $\bar{\zeta}(\omega)$ is the Fourier transform of $\zeta(\tau)$ and $\bar{\phi}_1(\rho, \theta, \omega)$ is the Fourier transform of $\phi(\rho, \theta, t)$. The middle equation is now in the form of the Helmholtz Equation in spherical coordinates with azimuthal symmetry. The Eigen functions of this equation, which represent outgoing spherical waves, are

$$h_\ell^{(2)}(\omega\rho) P_\ell(\cos\theta)$$

where

$$h_\ell^{(2)}(\omega\rho) = \ell^{\text{th}} \text{ order spherical Hankel Function of the second kind}$$

$$P_\ell(\cos\theta) = \ell^{\text{th}} \text{ order Legendre polynomial}$$

The general solution for the velocity potential, therefore, is given by a linear combination of these Eigen functions, i.e.

$$\bar{\phi}_1(\rho, \theta, \omega) = \sum_{\ell=0}^{\infty} A_\ell(\omega) h_\ell^{(2)}(\omega\rho) P_\ell(\cos\theta) \quad (14)$$

The coupled sets of equations involving $\bar{\zeta}(\omega)$ and $A_1(\omega)$ are obtained by inserting the above expression into the remaining two equations above, multiplying by $P_\ell(\cos\theta)$ and integrating with respect to θ from zero to π . $\bar{\zeta}(\omega)$ appears only in the $\ell = 1$ equation, which corresponds to the rigid-body motion of the sphere. The higher angular modes would contribute to the various deformation modes of the sphere, which are not considered in this report. The two $\ell = 1$ equations that result are:

$$(\omega_0^2 - \omega^2) \bar{\zeta}(\omega) = -\frac{1}{S} \left[\frac{-3I}{\sqrt{2\pi}} \frac{e^{-i\omega}}{\chi + i\omega} j_1(\omega) + i\omega A_1(\omega) h_1^{(2)}(\omega) \right] \quad (15)$$

$$i\omega \bar{\zeta}(\omega) = \frac{3}{\sqrt{2\pi}} \frac{e^{-i\omega} j_1^{(1)}(\omega)}{\chi + i\omega} - \omega A_1(\omega) \frac{d[h_1^{(2)}(\omega)]}{d\omega} \quad (16)$$

The problem has now been reduced to two linear algebraic equations in two unknowns, $\bar{\zeta}(\omega)$ and $A_1(\omega)$. The final expression for $\bar{\zeta}(\omega)$ is:

$$\bar{\zeta}(\omega) = \frac{3}{\sqrt{2\pi}} S \frac{e^{-i\omega}}{\omega^2 \frac{d[h_1^{(2)}(\omega)]}{d\omega} (\chi + i\omega)} \left[\omega_0^2 - \omega^2 + \frac{\omega}{S} \frac{h_1^{(2)}(\omega)}{\frac{d[h_1^{(2)}(\omega)]}{d\omega}} \right] \quad (17)$$

This is not quite as formidable an expression as it appears because the spherical Bessel and Hankel functions are simple linear combinations of sines and cosines. Explicitly these functions are:⁵

$$j_1(\omega) = \frac{\sin\omega}{\omega^2} - \frac{\cos\omega}{\omega}$$

$$h_1^{(2)}(\omega) = \left(\frac{1}{\omega^2} - \frac{1}{\omega} \right) e^{-i\omega}$$

The final expression for $\bar{\zeta}(\omega)$ is obtained by substituting these values for $h_1^{(2)}(\omega)$ and $j_1(\omega)$.

$$\bar{\zeta}(\omega) = \frac{3}{\sqrt{2\pi}} S \frac{\omega}{(i\omega + \chi) \left[(\omega_0^2 - \omega^2)(-2i + 2\omega + i\omega^2) + \frac{\omega^2}{S}(1 - \omega) \right]} \quad (18)$$

The time-dependent displacement $\zeta(t)$ is the inverse, which is given by the following integral:

$$\zeta(t) = \frac{1}{\sqrt{2\pi}} \int_{-\infty}^{\infty} \bar{\zeta}(\omega) e^{i\omega t} d\omega$$

This inversion can be done by contour integration in the complex ω plane to yield general solutions for certain cases, and numerical solutions for other cases. This is discussed in Appendix A.

Typical examples of the time-histories are presented in Figures 3 through 20. The displacement ζ , velocity, $d\zeta/d\tau$, and acceleration, $\frac{d^2\zeta}{d\tau^2}$, are plotted versus time, $\tau = \left(\frac{c}{a}\right) t$, for a variety of the parameters.

The peak acceleration does not appreciably change throughout the range of χ and ω_0 studied. As ω_0 increases, the maximum acceleration in the initial positive peak decreases. However, the magnitude of the first minimum increases. The net effect is an almost constant peak acceleration.

As was to be expected, the peak response increases as S decreases. As was observed for the unrestrained case, the rate of damping also increases as S decreases. A denser structure experiences smaller peak responses. However, its motion will persist for much longer times.

If the transformed equation for $\bar{\zeta}(\omega)$ could not be inverted readily, one could make use of a numerical inversion procedure. One such procedure has been developed by Bellman et al⁴ for Laplace transforms. Since a Fourier transform can be restated to a Laplace transform by an appropriate substitution, the Bellman procedure can be applied to the solution for the sphere. The reason for doing this is to obtain a check on the applicability of the Bellman procedure to this problem by comparing the results with those obtained by contour integration. Once its applicability is established, the Bellman method can be used for the solution for the cylinder, a solution that cannot readily be obtained by contour integration.

The Bellman procedure is described in Appendix B. This procedure was used to invert Equation 18, and the results are shown in Figures 21 through 30, which compare these results with those obtained by contour integration.

The points shown in the figures obtained by the Bellman procedure used a quadrature order N of 5, 6 and 7, and scale factors SF of 1.0 and 3.33. The symbols used on the plots are:

N	SF	
	1.0	3.33
5	X	+
6	□	★
7	⊙	Υ

The agreement for small ω_0 is very good. With increasing natural frequency, the approximation breaks down after the first maximum is reached. The main deficiency from a design point of view is that the first minimum appears underestimated at these higher frequencies. It is expected, however, that actual structures built on the ocean floor will not be that rigidly constrained; hence ω_0 will be relatively small. Bellman's approximate inversion method should then yield reliable design information.

CYLINDRICAL STRUCTURE

The next problem of interest is the motion of an elastically re-strained cylindrical structure subjected to an underwater shock wave. As in the previous section, the effects due to the sea surface and bottom are neglected and the shock wave is considered to be a plane wave that is weak enough to be describable by linear acoustic theory.

The formulation for the cylindrical structure proceeds in a manner analogous to that for the spherical structure. The main differences between the two problems are that the surface area for the cylinder does not contain the factor of $\sin\theta$ and that the independent variables for the acoustic fluid are now cylindrical coordinates rather than spherical coordinates. As a consequence of these differences, the Fourier transform of the cylinder motion contains ordinary Hankel functions rather than spherical Hankel functions and cannot be inverted analytically.

Since the main steps in the mathematical analysis are almost identical with that of the sphere, only a brief treatment of the development will be given. The upper drawing of Figure 31 shows the incident shock wave just arriving at the cylinder. The motion of the cylinder as well as the fluid is independent of the x coordinate, which is perpendicular to the plane of the paper. The z and y as well as r and θ coordinates are shown and are standard Cartesian and Polar coordinates, respectively.

The lower drawing of Figure 31 shows the situation at a time t . The shock wave has moved a distance ct and the cylinder is displaced at a distance z . As with the sphere, the translational motion of the cylinder has been exaggerated for ease of presentation. The equation of motion for the cylinder is

$$m \ddot{z}(t) + k z(t) = -a \int_0^{2\pi} \cos\theta \left\{ p_0 H(ct - a - a \cos\theta) e^{-\frac{(ct - z - a \cos\theta)}{cq}} + \mu \frac{\partial \phi(r, \theta, t)}{\partial t} \right\} \bigg|_{r=a} d\theta \quad (19)$$

where k is the spring constant per unit length of cylinder and m is the mass per unit length of the cylinder. The terms on the righthand side of the equation are the pressure forces due to the fluid (the notation is exactly the same as with the sphere). The wave equation for the motion of the acoustic wave and the boundary condition equation are given below:

$$\frac{\partial^2 \phi}{\partial r^2} + \frac{1}{r} \frac{\partial \phi}{\partial r} + \frac{1}{r^2} \frac{\partial^2 \phi}{\partial \theta^2} = \frac{1}{c^2} \frac{\partial^2 \phi(r, \theta, t)}{\partial t^2} \quad (20)$$

$$\dot{z}(t) \cos\theta = - \frac{\partial \phi(r, \theta, t)}{\partial r} \bigg|_{r=a} + \frac{p_0}{\rho c} H(ct - a - a \cos\theta) \cos\theta e^{-\frac{(ct - a - a \cos\theta)}{cq}} \quad (21)$$

The transformation to dimensionless variables proceeds exactly as it did with the sphere. These transformations and the resulting equations follow:

$$\tau = \left(\frac{c}{a}\right)t$$

$$\rho = \left(\frac{1}{a}\right)r$$

$$\zeta(\tau) = \left(\frac{\mu c^2}{a \rho_0} \right) z(t)$$

$$\phi_1(\rho, \theta, \tau) = \left(\frac{1}{a \rho_0 \mu c} \right) \phi(r, \theta, t)$$

$$\chi = \left(\frac{a}{c} \right) \frac{1}{q}$$

$$S = \mu_s / \mu$$

$$\frac{d^2 \zeta(\tau)}{d\tau^2} + \omega_0^2 \zeta(\tau) = \frac{1}{\pi S} \int_0^{2\pi} \cos \theta \left[H(\tau - 1 - \cos \theta) e^{-\chi(\tau - 1 - \cos \theta)} + \frac{\partial \phi_1}{\partial \tau}(1, \theta, \tau) \right] d\theta \quad (22)$$

$$\frac{\partial^2 \phi_1(\rho, \theta, \tau)}{\partial \rho^2} + \frac{1}{\rho} \frac{\partial \phi_1}{\partial \rho} + \frac{1}{\rho^2} \frac{\partial^2 \phi_1}{\partial \theta^2} = \frac{\partial^2 \phi_1}{\partial \tau^2} \quad (23)$$

$$\frac{d \zeta(\tau)}{d\tau} \cos \theta = H(\tau - 1 - \cos \theta) \cos \theta e^{-\chi(\tau - 1 - \cos \theta)} - \frac{\partial \phi_1(\rho, \theta, \tau)}{\partial \rho} \Big|_{\rho=1} \quad (24)$$

Using the same procedure as with the sphere, these equations are expressed in terms of Fourier transforms. The solution of these transformed equations is straight-forward, but does not lead to any expression involving spherical Hankel functions and Legendre Polynomials as was the case for the sphere. Instead, the solution for the acoustic field is found in terms of ordinary Hankel functions and $\cos n\theta$. The final result for the Fourier transform of the cylinder displacement is given below:

$$\bar{\zeta}(\omega) = \frac{4}{\pi S} \sqrt{\frac{1}{2\pi}} \frac{e^{-i\omega}}{(i\omega + \chi)} \frac{1}{\omega} \frac{d}{d\omega} \left[\frac{H_1^{(2)}(\omega)}{d\omega} \right] \left[-\omega^2 + \frac{\omega H_1^{(2)}(\omega)}{d \left[\frac{H_1^{(2)}(\omega)}{d\omega} \right]} + \omega_0^2 \right]^{-1} \quad (25)$$

The time dependence for the displacement is the inverse, which is given by the usual Fourier integral. Due to the fact that ordinary Hankel functions are much more complicated than spherical Hankel functions, it is not possible to perform the integration analytically. Numerical inversion can be accomplished by using the Bellman procedure, which was demonstrated in the discussion of the sphere and is further explained in Appendix B.

Several examples for the response of cylindrical structures are presented in Figures 32 through 43. The symbols have the meanings previously defined. The displacement, velocity, acceleration, and time are the dimensionless variables pertinent to the cylinder.

It can be seen from these figures that the response of the cylinder is similar to that for the sphere. It is therefore inferred that the reliability of the Bellman method extends to the cylindrical problem in roughly the same parametric range.

Fairly reliable curves can be drawn through these points, and additional points can be readily calculated using larger values of N in the Bellman procedure. The values chosen, however, appear adequate for the determination of the peak response in the parametric range of interest.

In reference 1 the solution to the cylinder problem was obtained using the Mindlin and Bleich approximation. Good agreement was obtained between this approximate solution and Murray's exact solution for an unrestrained cylinder. In Figures 44 through 46 a comparison of these previous results with the present calculations shows that the Mindlin and Bleich approximation must be reasonably accurate for the restrained cylinder too. The Mindlin-Bleich results follow those from the exact calculation until the velocity becomes negative. The reason for this is the different treatment of the radiative force. In the Mindlin-Bleich approximation this force is always 180 degrees out of phase with the velocity; in the exact formulation the radiative force is an integral operator and bears no such constant phase relation with the velocity.

DRAG EFFECTS

Thus far the real nature of water, namely its wetness, has been neglected. Due to viscosity the actual flow will differ from that obtained in the preceding analysis. One immediate result is that drag forces will be present.

The drag forces due to idealized steady flow, however, would be quite small compared to the main pressure forces. For example, consider the usual expression for the drag force on a sphere. This is given by:

$$F_D = \frac{1}{2} \rho C_D \pi a^2 U^2 \quad (26)$$

where C_D is the drag coefficient and U is the relative speed of the sphere through the fluid. Assuming that $U = U_0 = P_0/(\mu c)$, i.e., the fluid particle velocity at the front of the shock wave, the drag force becomes

$$F_D = \frac{1}{2} \mu C_D \pi a^2 \left[\frac{P_0}{\mu c} \right]^2 \quad (27)$$

From this one readily calculates the dimensionless acceleration,

$$\left[\frac{d^2 r}{d\tau^2} \right]_D = \frac{3}{8} C_D \frac{U_0}{Sc} \quad (28)$$

where $\left[\frac{d^2 r}{d\tau^2} \right]_D$ is the acceleration due solely to the drag term. This can be compared with the main pressure contribution for a specific numerical example. For $S = 1$, $C_D = 2$ and $P_0 = 1,000$ psi, one gets

$$\left[\frac{d^2 r}{d\tau^2} \right]_D = 2.25 \times 10^{-3}$$

The calculated peak acceleration from Figure 32 is 0.7; therefore, the drag force is about 0.3% of the direct force. For larger incident pressures this percentage increases; however, the linear-acoustic theory itself collapses before this drag contribution is appreciable.

In addition to this small perturbation, the change in the flow resulting from the separation of the boundary layer may appreciably alter the scattering and radiative properties of the sphere. If this is the case, then inviscid theory could conceivably be in error by much more than the 0.3% estimated above for the contribution of direct drag. At the present time there seems to be little information on this subject.

FINDINGS AND CONCLUSIONS

The response of spherical and cylindrical structures due to a weak, plane acoustic shock wave has been presented. Exact expressions for the Fourier transform were obtained. For the sphere the inverse was obtained exactly; however, in order to invert the transform for the cylinder, an approximation was necessary. This approximate method applied to a sphere was compared with the exact solution for the sphere

and found to be acceptable for the range of parameters that will be encountered for a deep ocean structure. It can be concluded from the similarity of results for the sphere and cylinder that the approximate method is appropriate for the cylinder in the same parametric range as for the sphere.

The direct drag effects due to the viscosity of the water were estimated to be negligible. Indirect effects due to the perturbed flow could not be estimated, and a theoretical analysis of this effect would be very difficult. A series of small-scale experiments should be performed in order to investigate the magnitude of this effect.

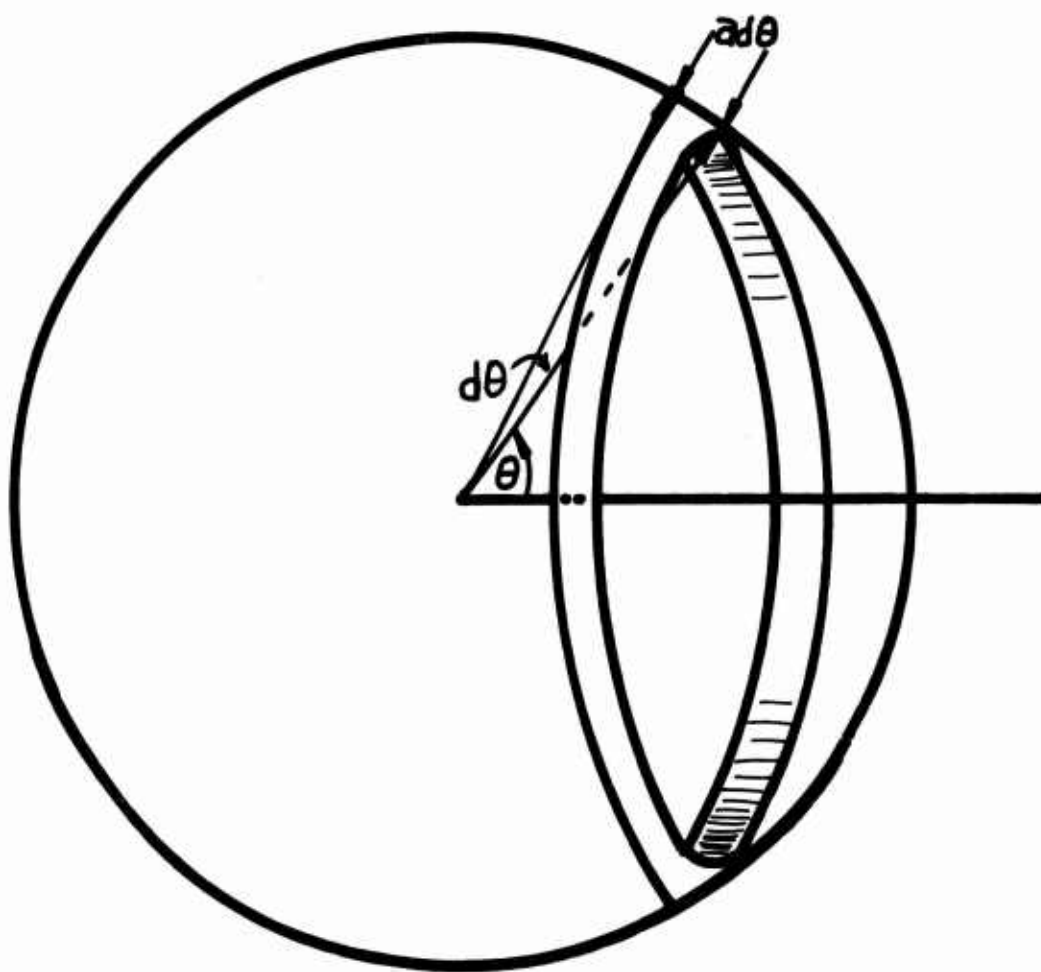


Figure 2. Detail for Pressure Calculation.

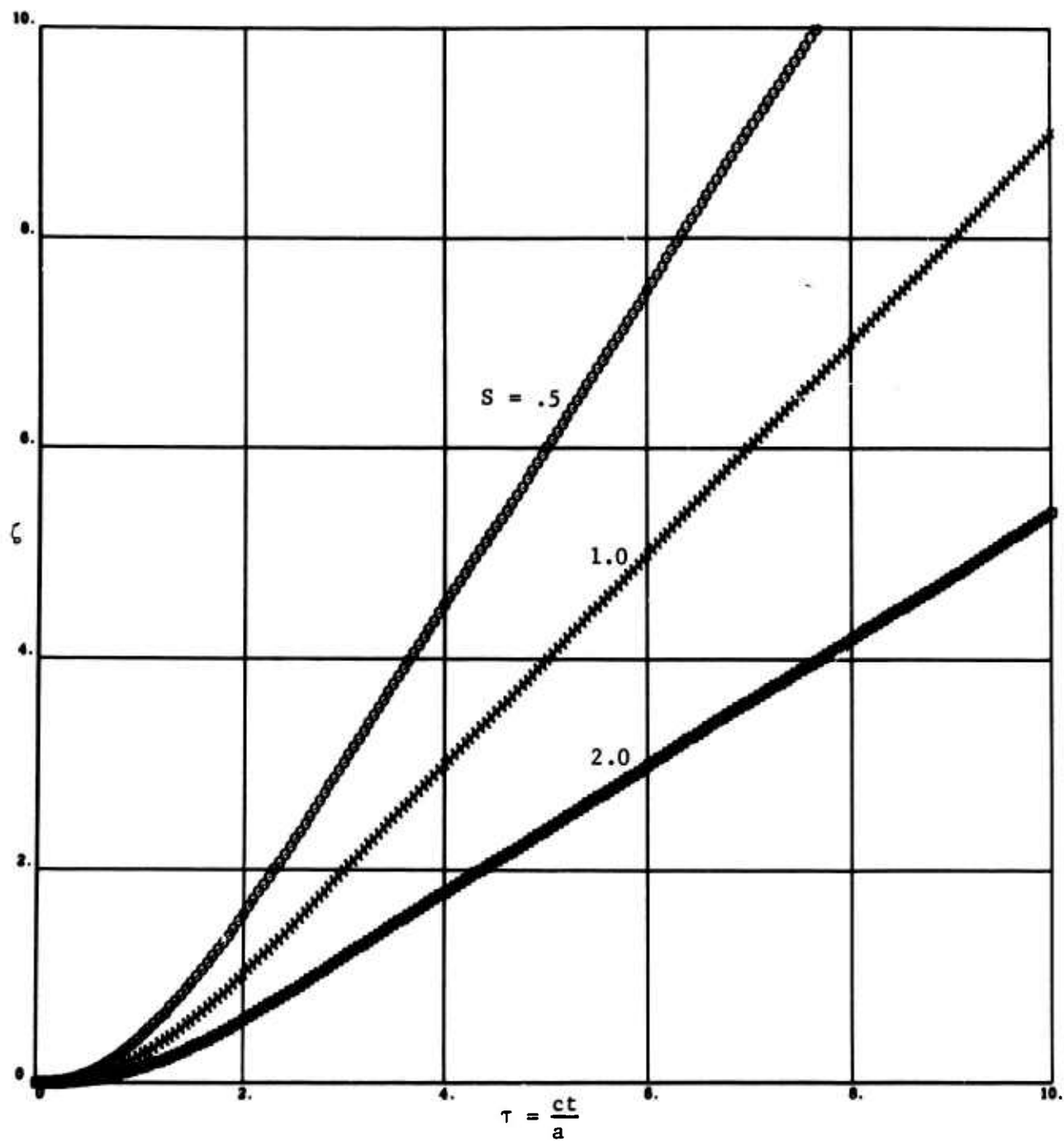


Figure 3. Displacement Versus Time for Unrestrained Sphere; Step Pulse Incident.

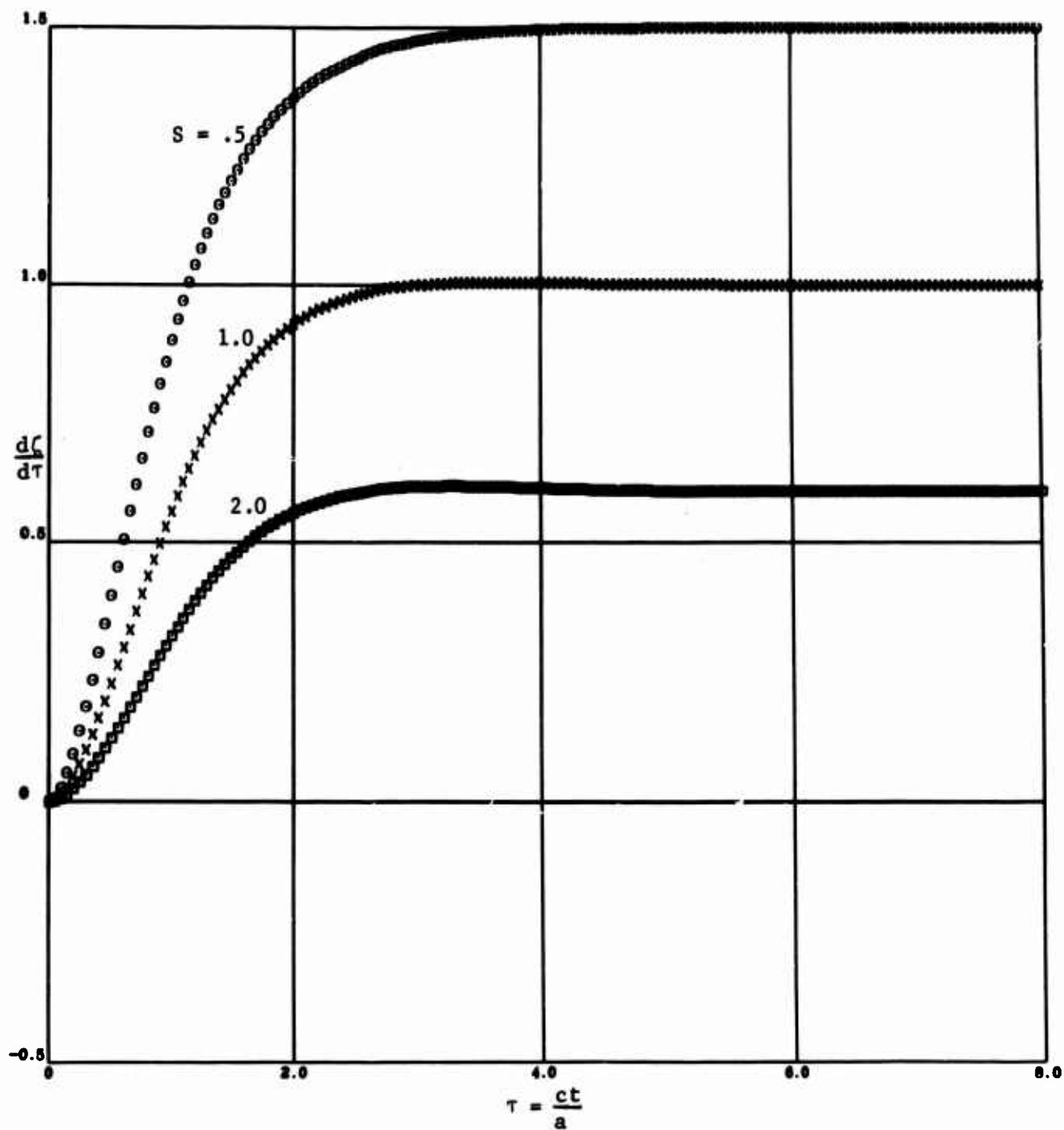


Figure 4. Velocity Versus Time for Unrestrained Sphere; Step Pulse Incident.

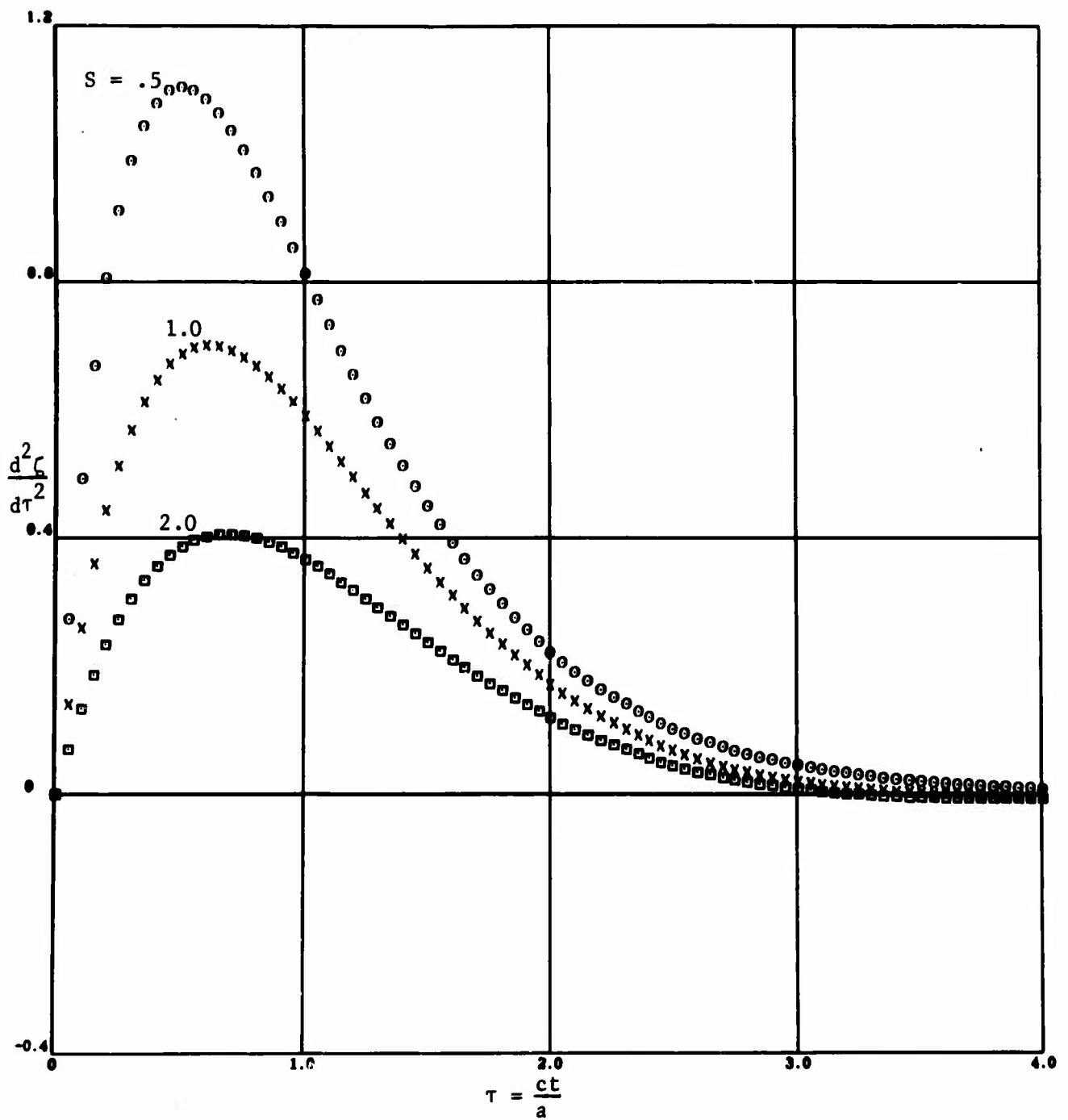


Figure 5. Acceleration Versus Time for Unrestrained Sphere; Step Pulse Incident.

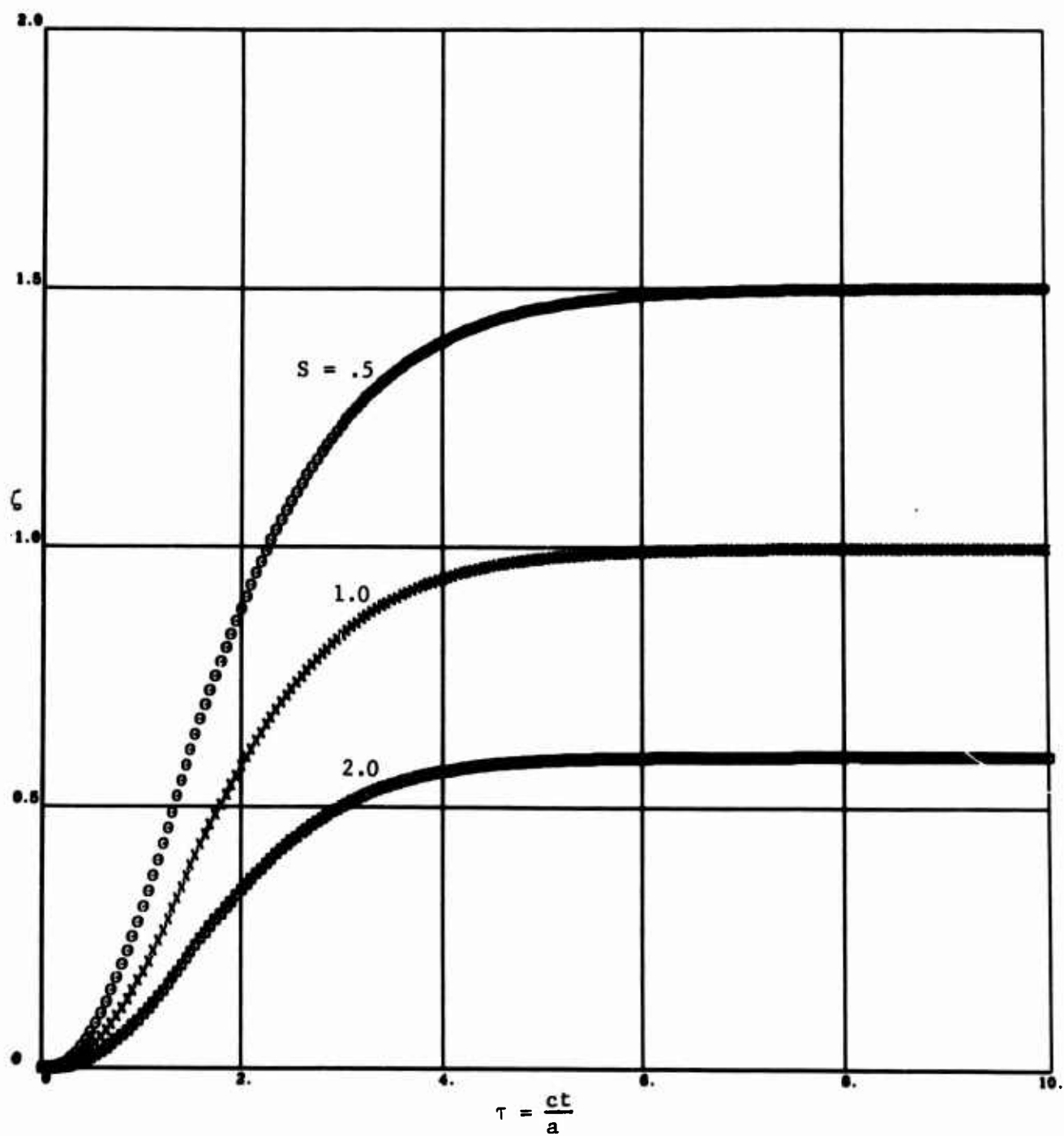


Figure 6. Displacement Versus Time for Unrestrained Sphere; Short ($\chi = 1$) Pulse Incident.

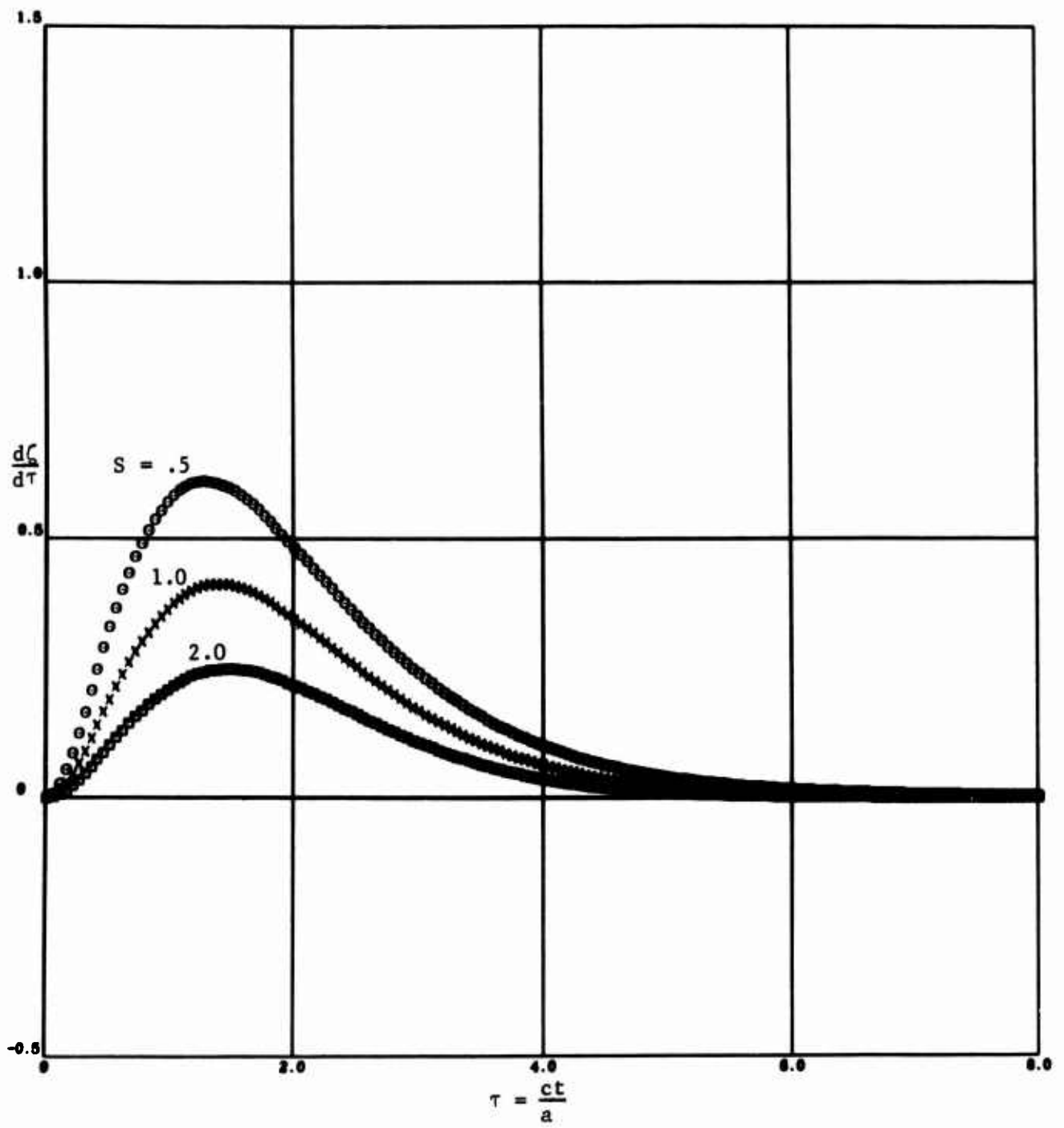


Figure 7. Velocity Versus Time for Unrestrained Sphere; Short ($\chi = 1$) Pulse Incident.

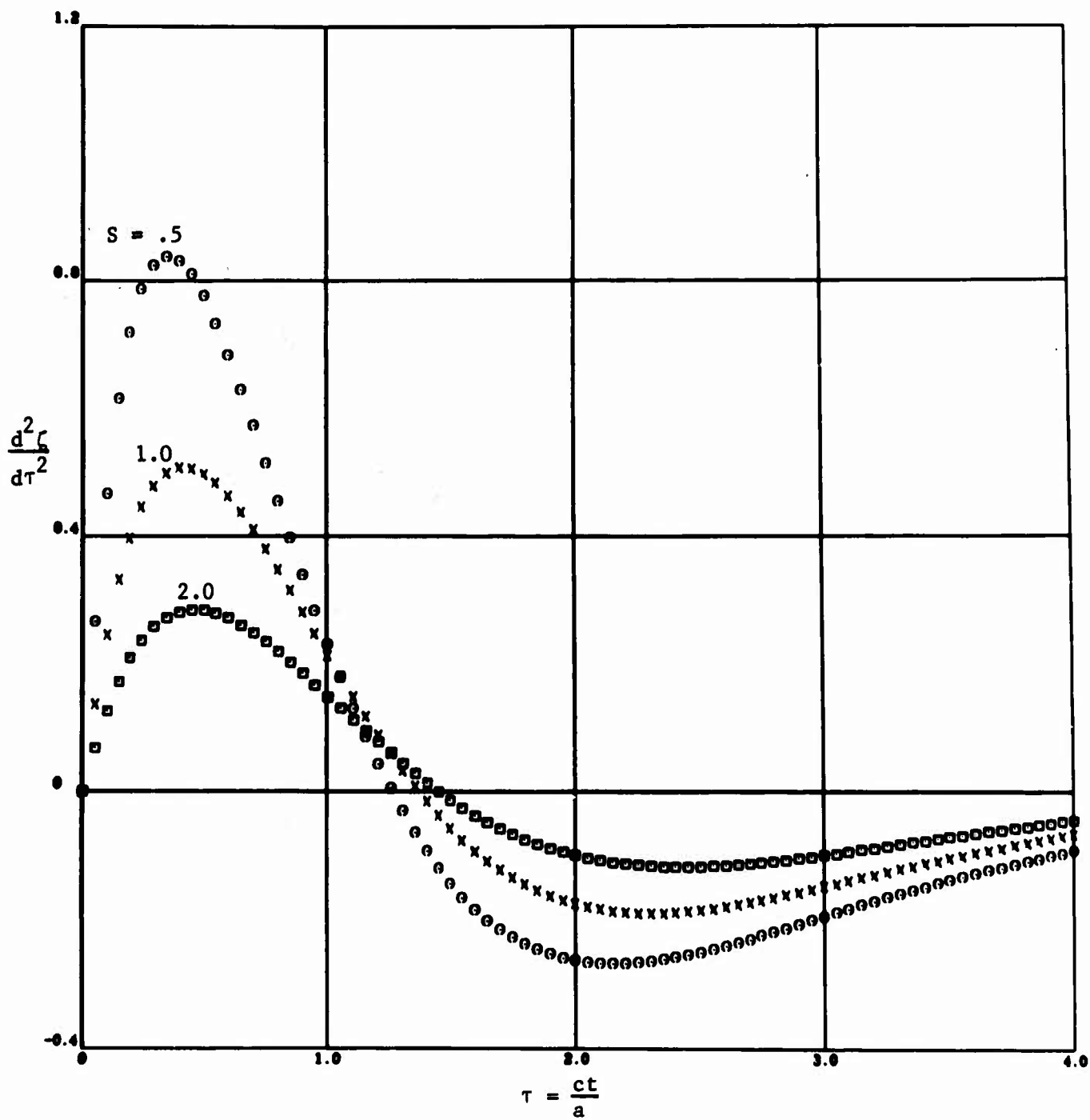


Figure 8. Acceleration Versus Time for Unrestrained Sphere; Short ($\chi = 1$) Pulse Incident.

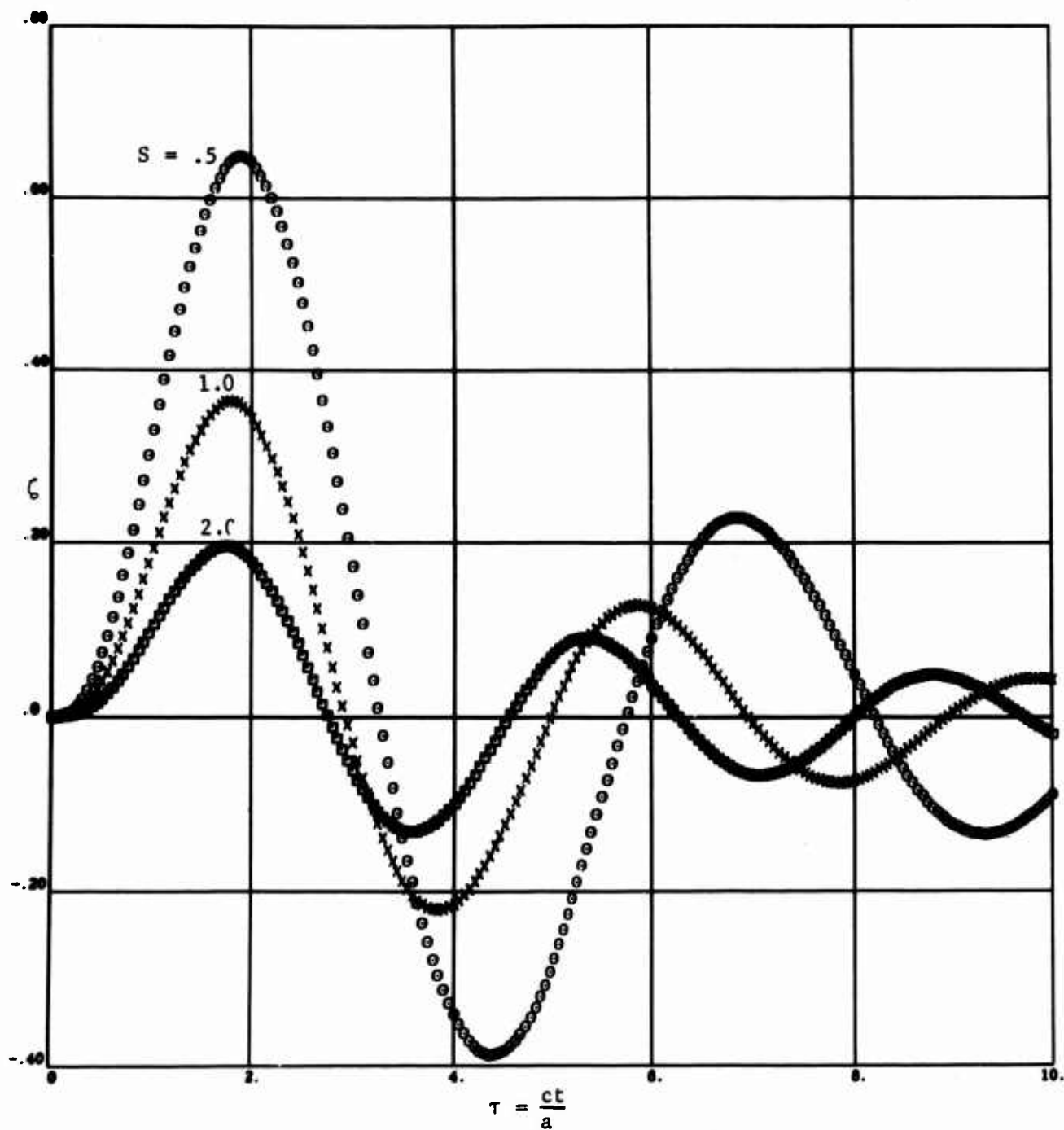


Figure 9. Displacement Versus Time for Restrained ($\omega_0 = 2$) Sphere; Step Pulse Incident.

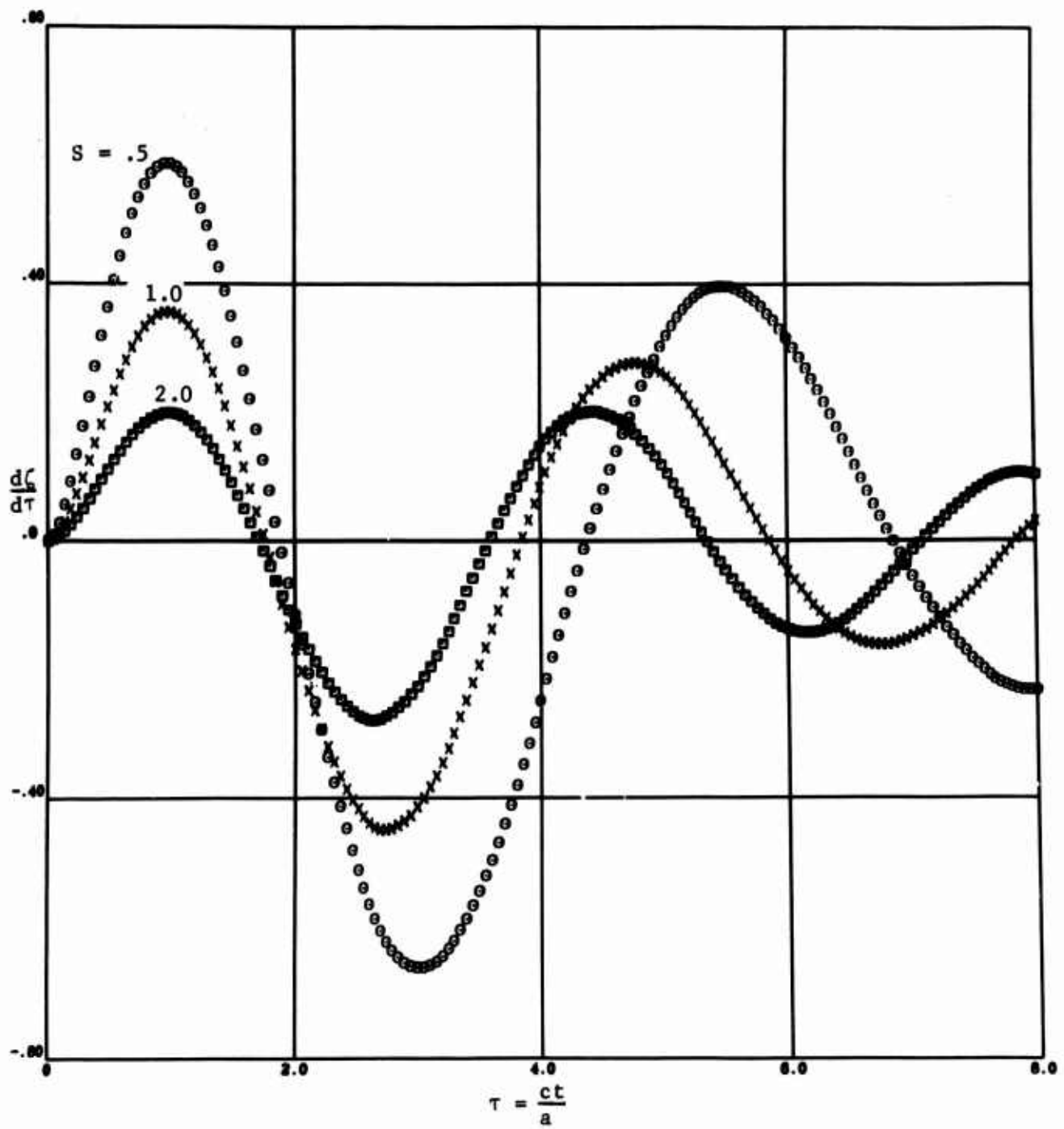


Figure 10. Velocity Versus Time for Restrained ($\omega_0 = 2$) Sphere; Step Pulse Incident.

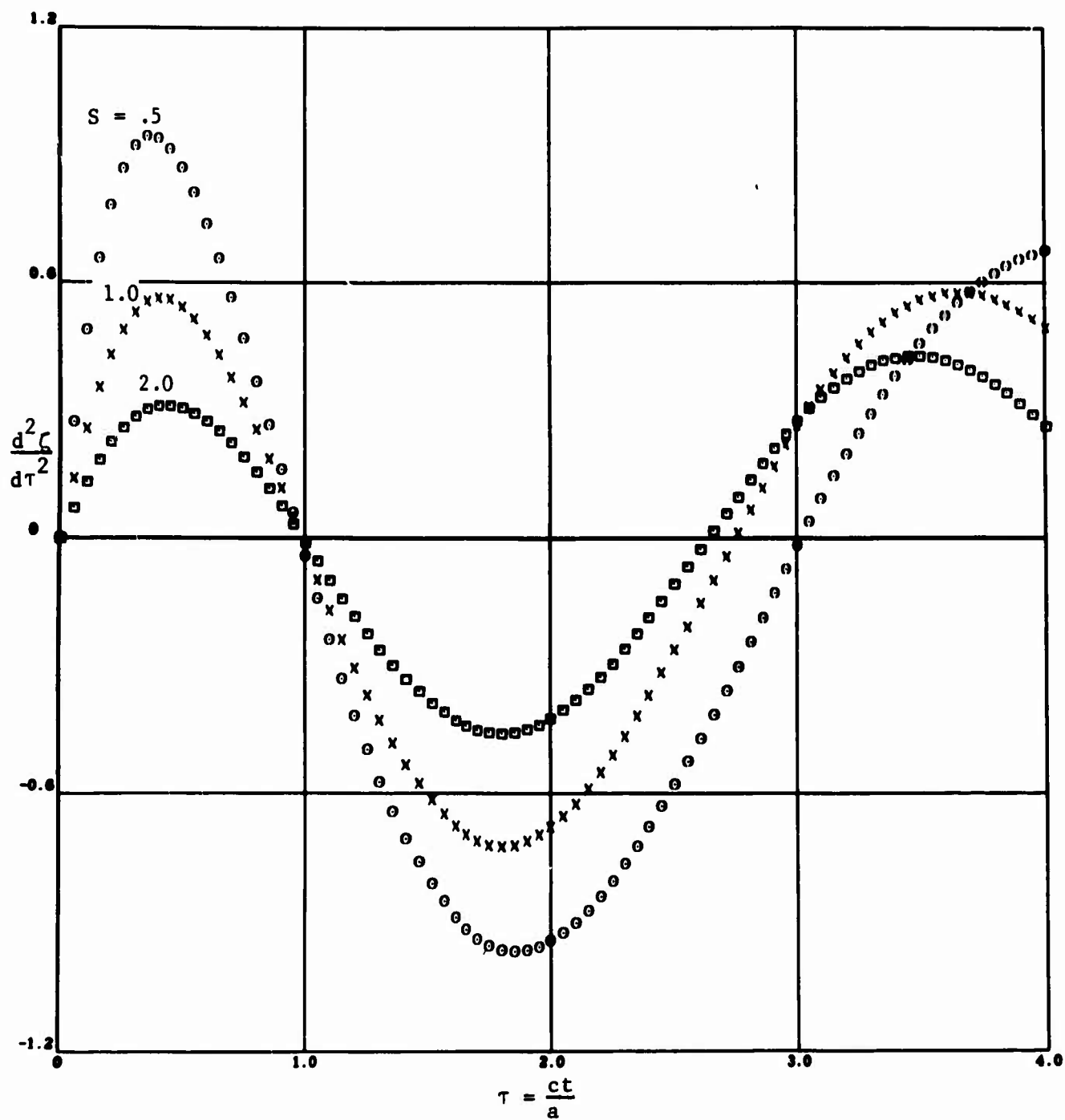


Figure 11. Acceleration Versus Time for Restrained ($\omega_0 = 2$) Sphere; Step Pulse Incident.

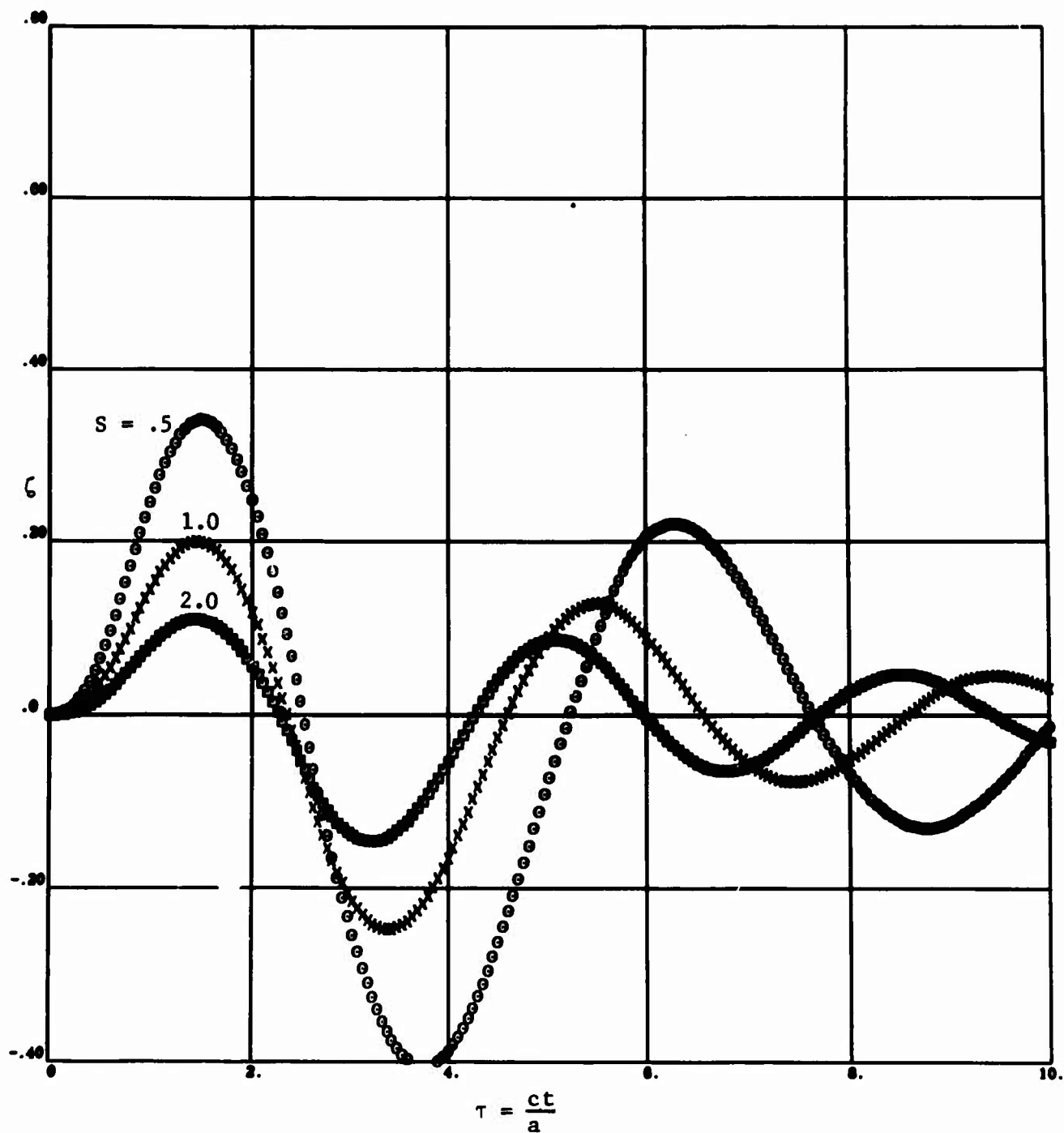


Figure 12. Displacement Versus Time for Restrained ($\omega_0 = 2$) Sphere;
Short Pulse ($\chi = 1$) Incident.

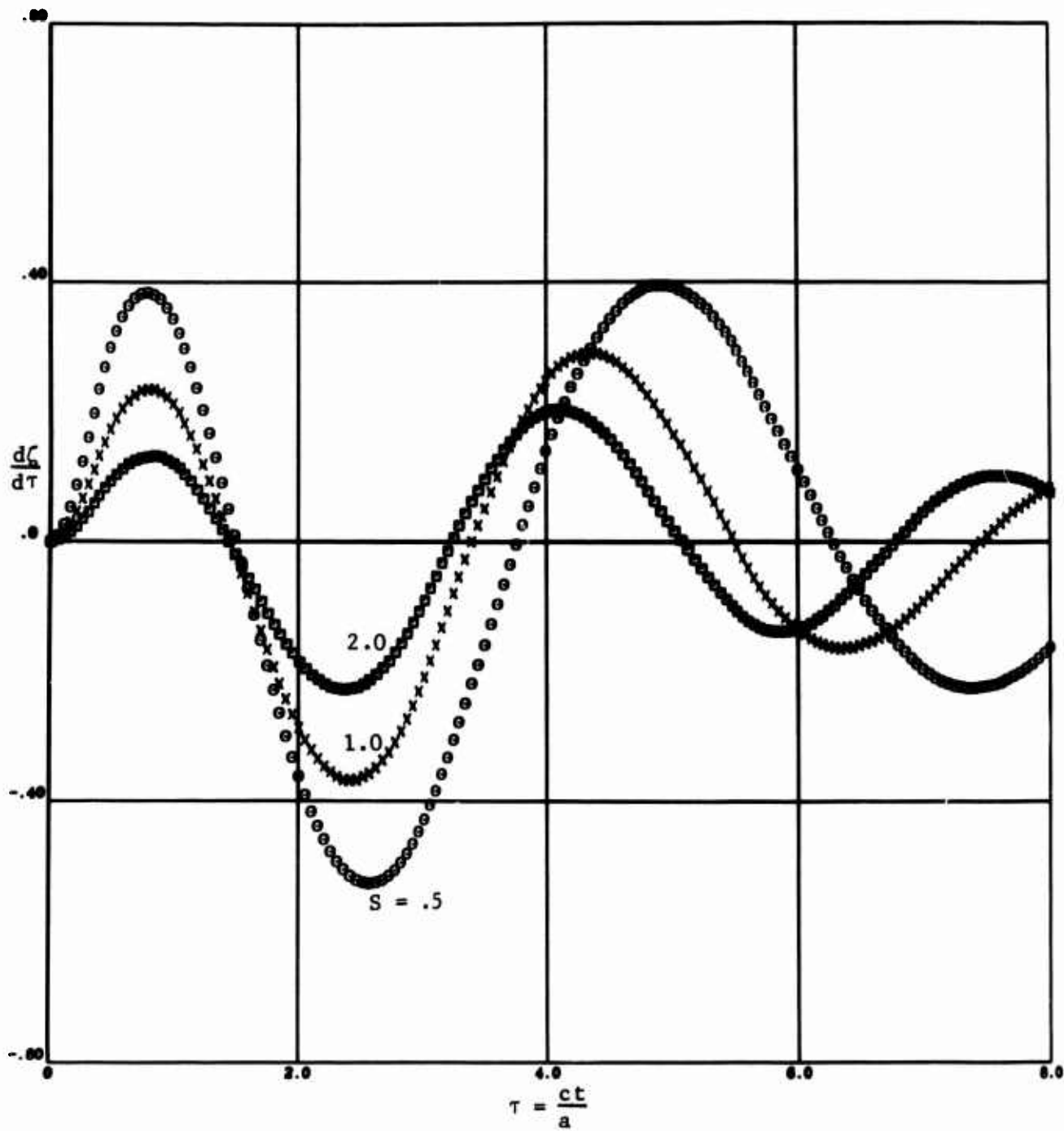


Figure 13. Velocity Versus Time for Restrained ($\omega_0 = 2$) Sphere; Short Pulse ($\chi = 1$) Incident.

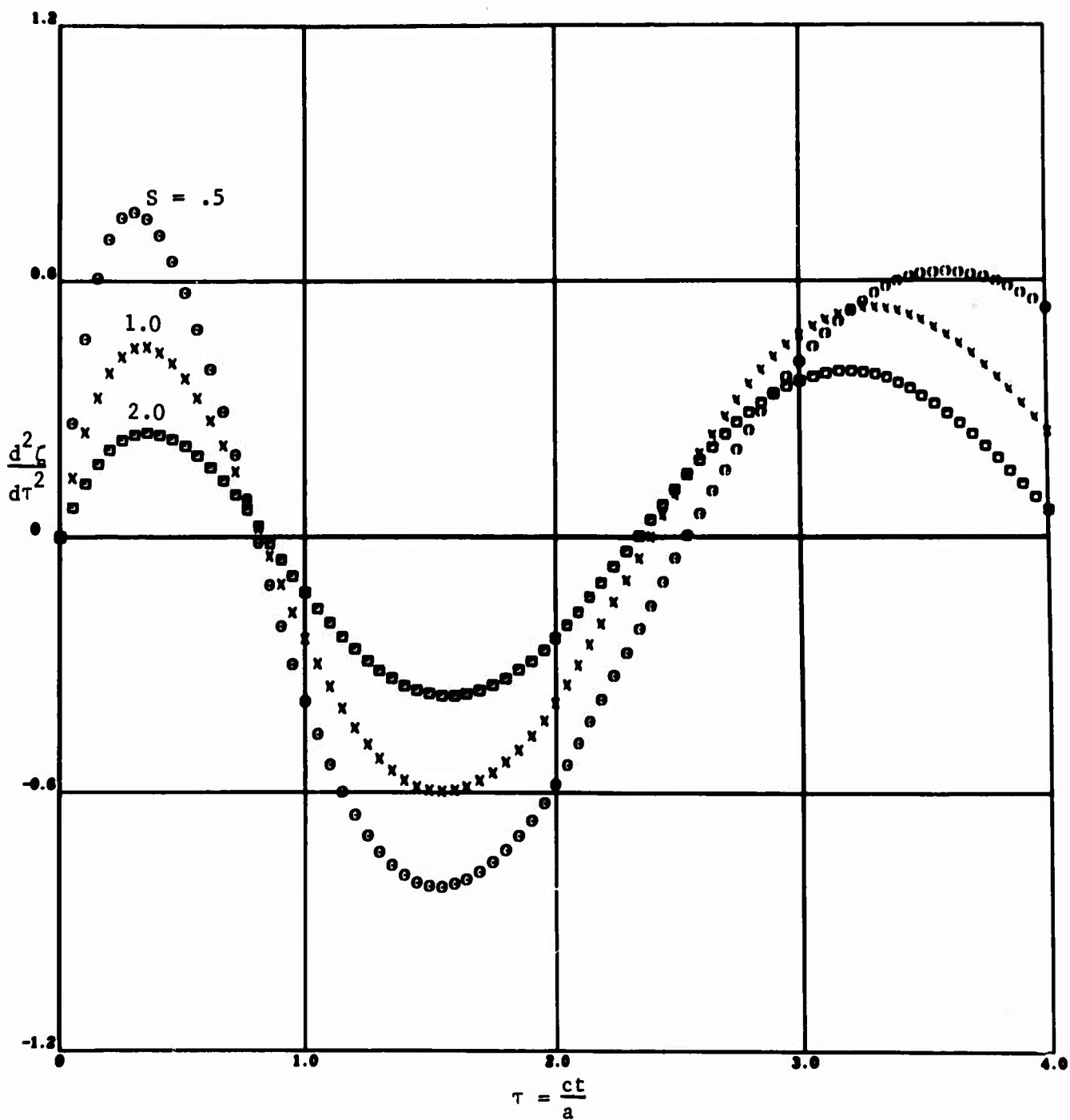


Figure 14. Acceleration Versus Time for Restrained ($\omega = 2$) Sphere;
Short Pulse ($\chi = 1$) Incident.

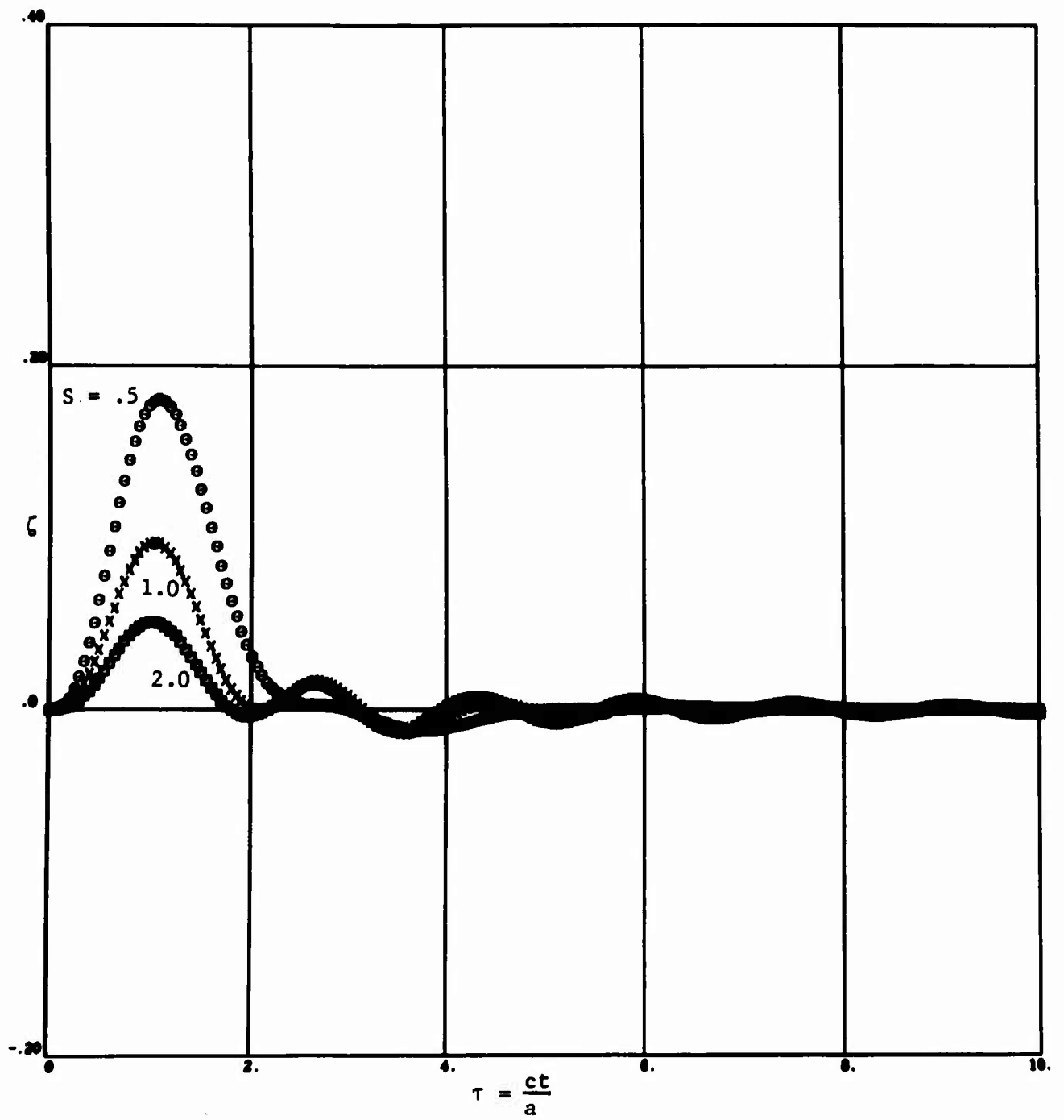


Figure 15. Displacement Versus Time for Restrained ($\omega_0 = 4$) Sphere; Step Pulse Incident.

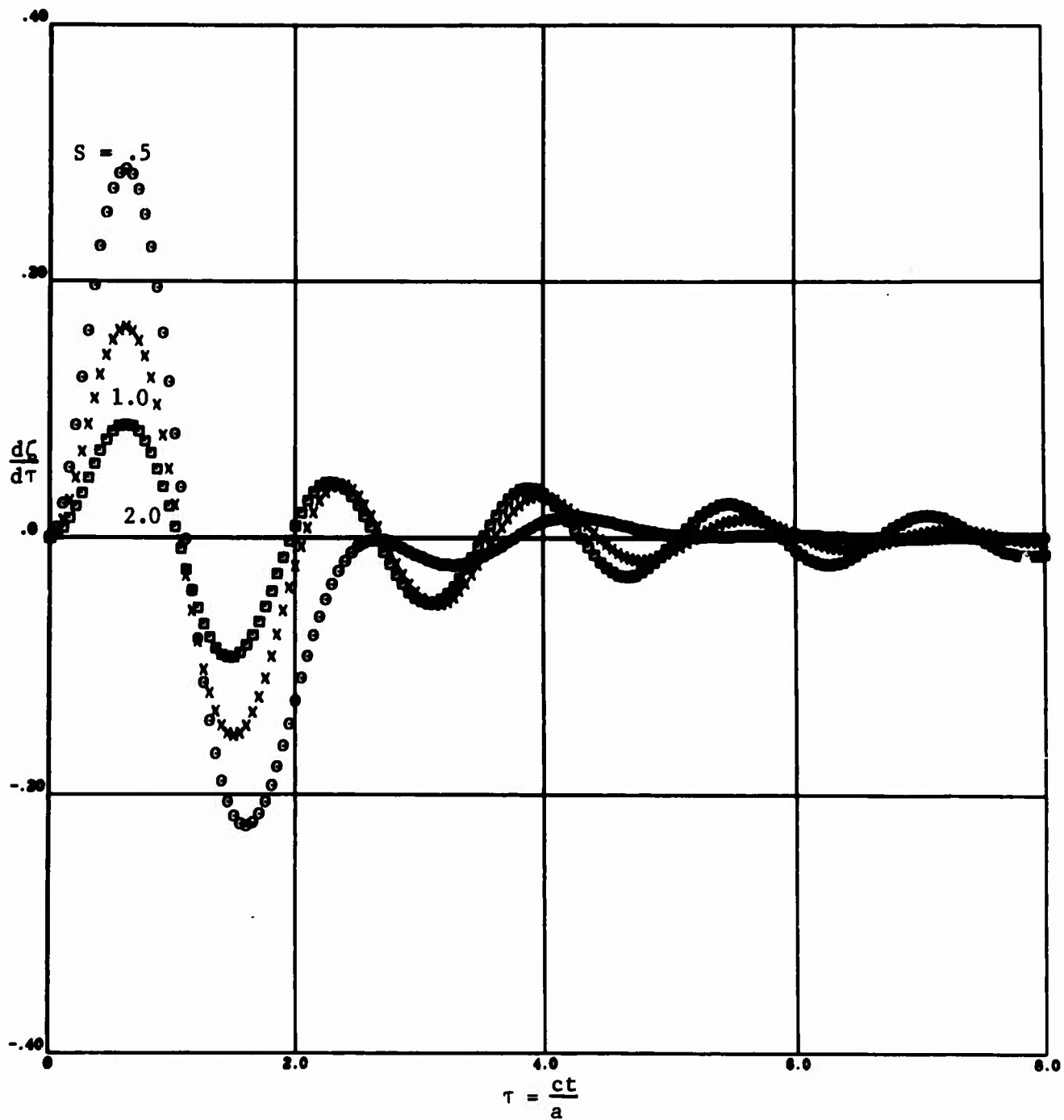


Figure 16. Velocity Versus Time for Restrained ($\omega_0 = 4$) Sphere; Step Pulse Incident.

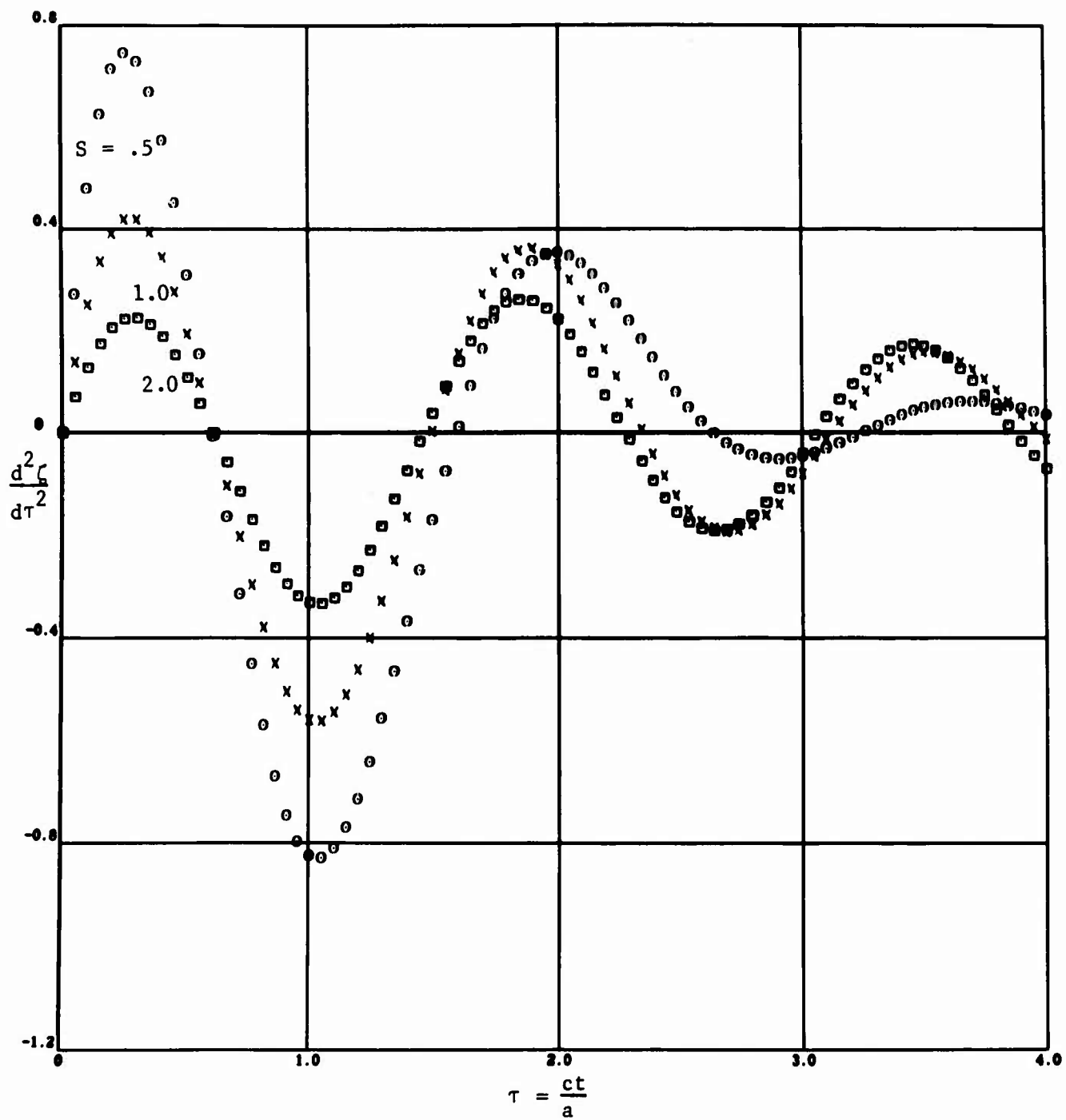


Figure 17. Acceleration Versus Time for Restrained ($\omega_0 = 4$) Sphere; Step Pulse Incident.

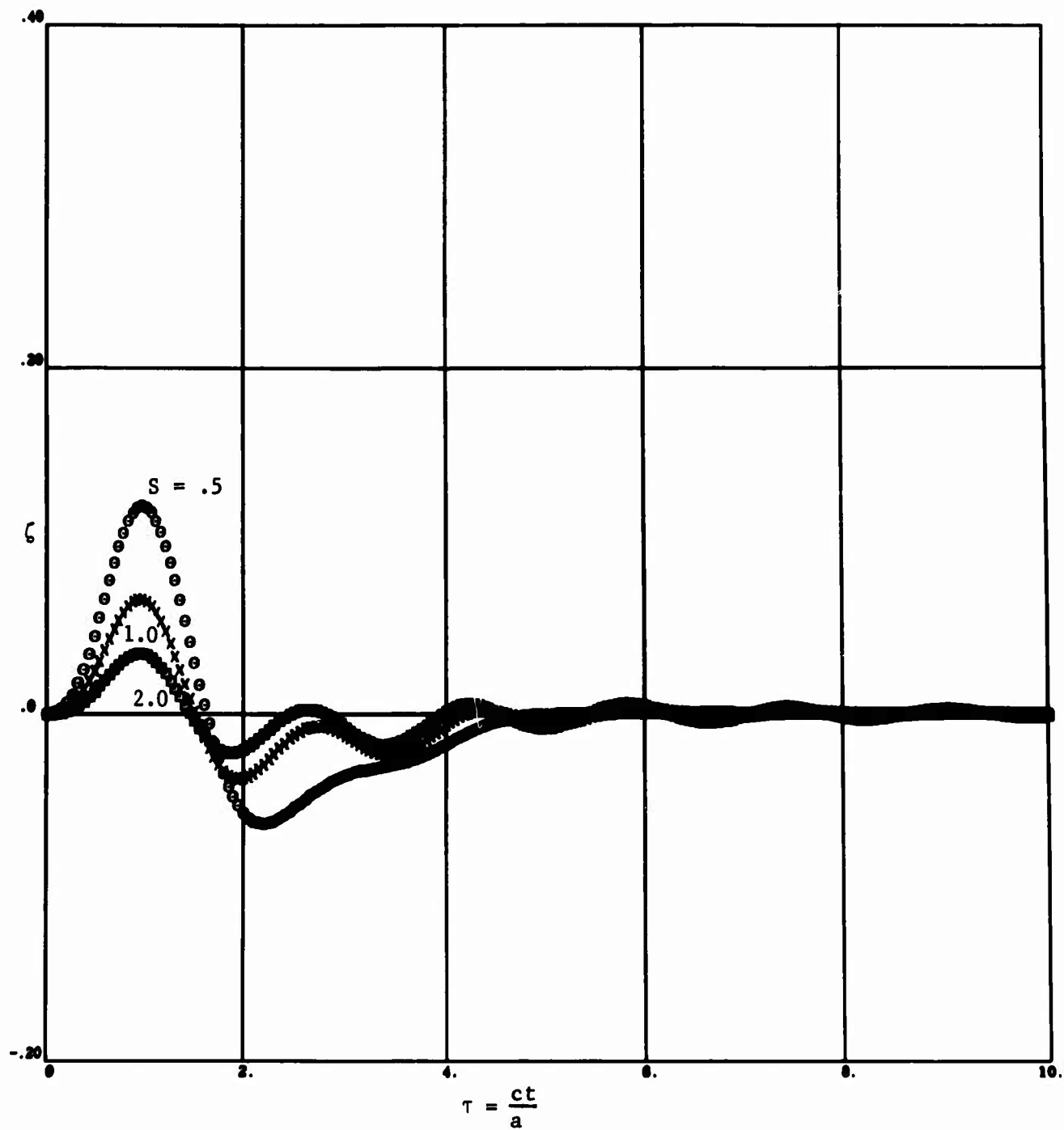


Figure 18. Displacement Versus Time for Restrained ($\omega_0 = 4$) Sphere;
Short Pulse ($\chi = 1$) Incident.

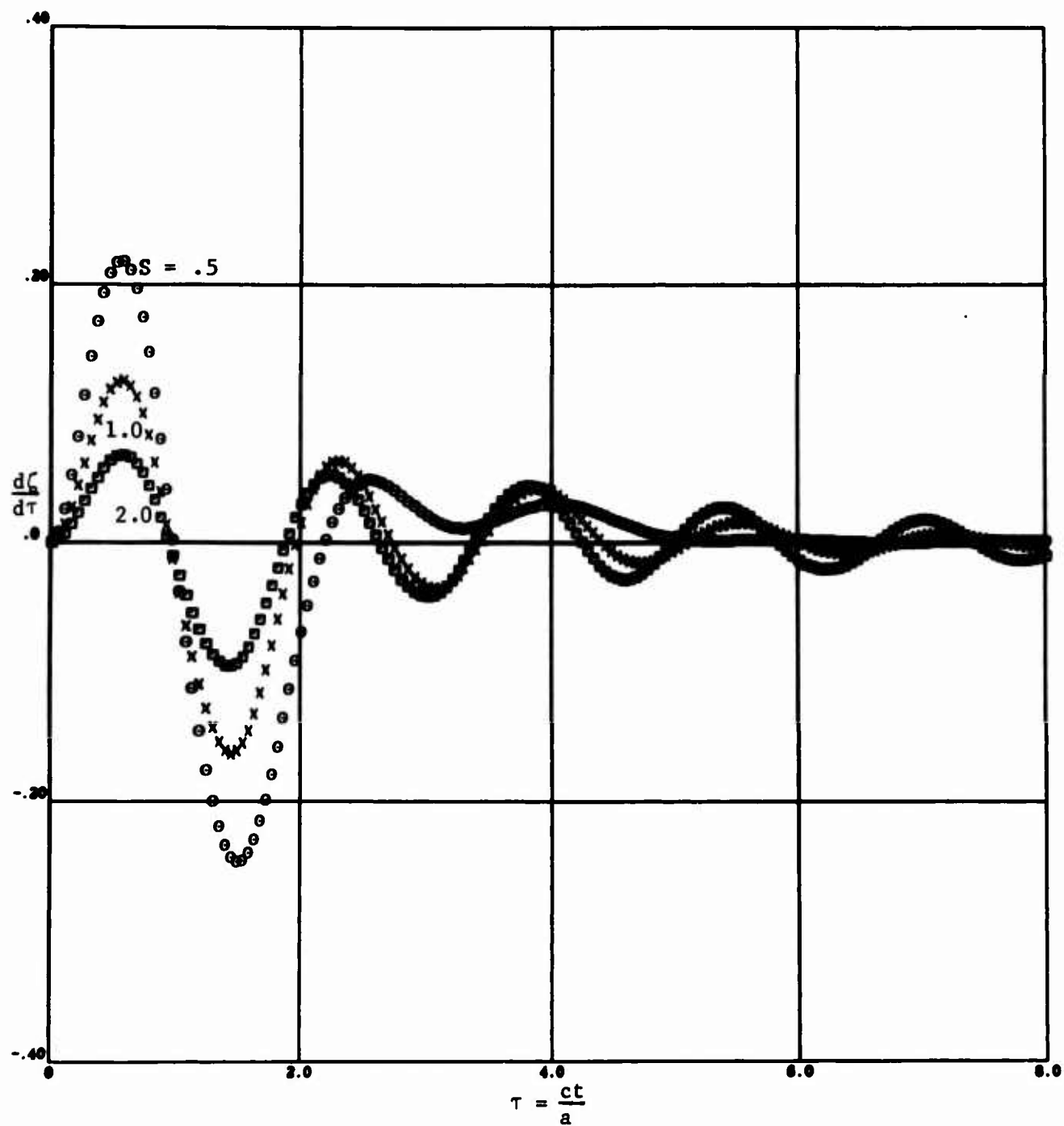


Figure 19. Velocity Versus Time for Restrained ($\omega_0 = 4$) Sphere; Short Pulse ($\chi = 1$) Incident.

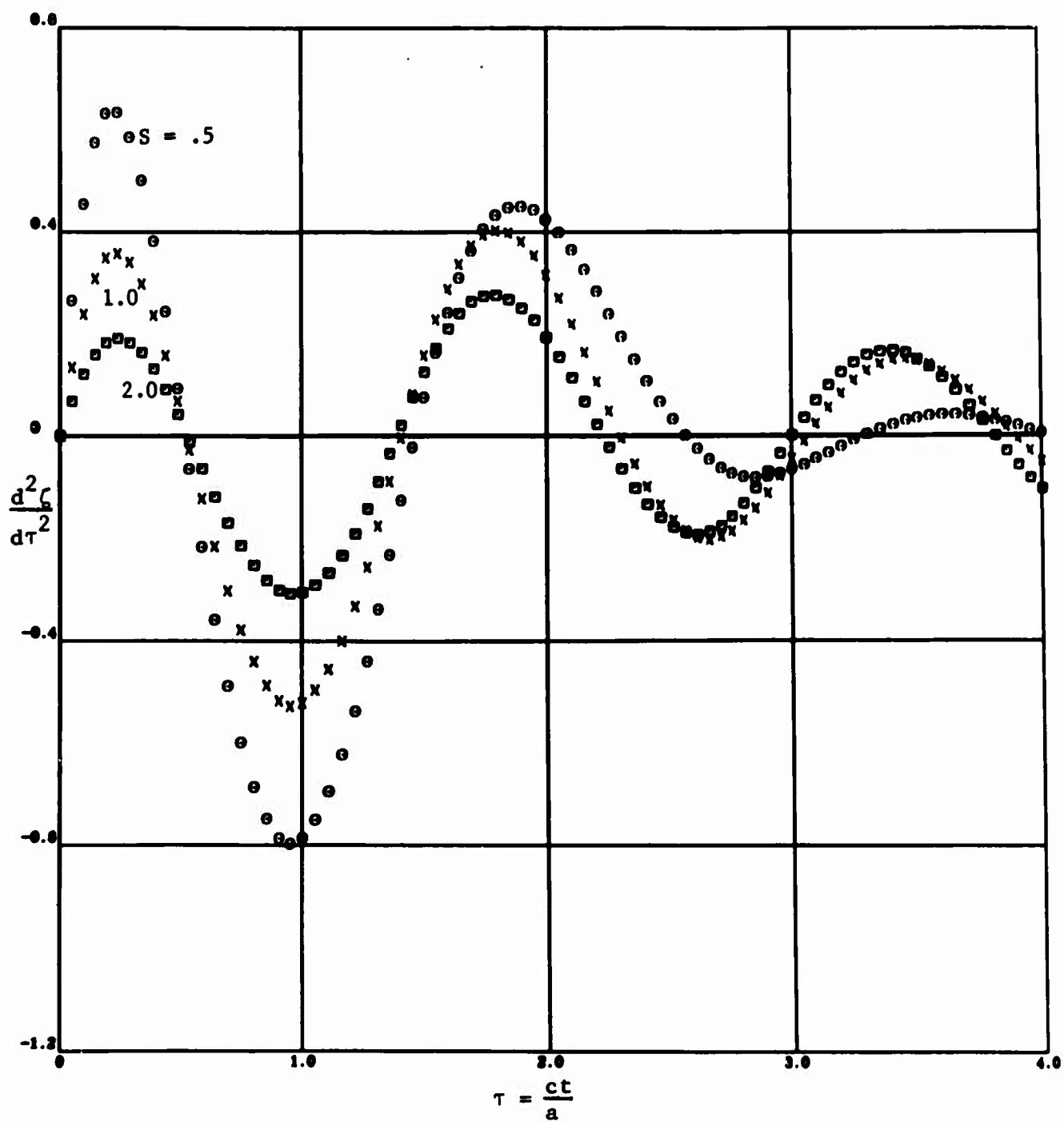


Figure 20. Acceleration Versus Time for Restrained ($\omega_0 = 4$) Sphere; Short Pulse ($\chi = 1$) Incident.

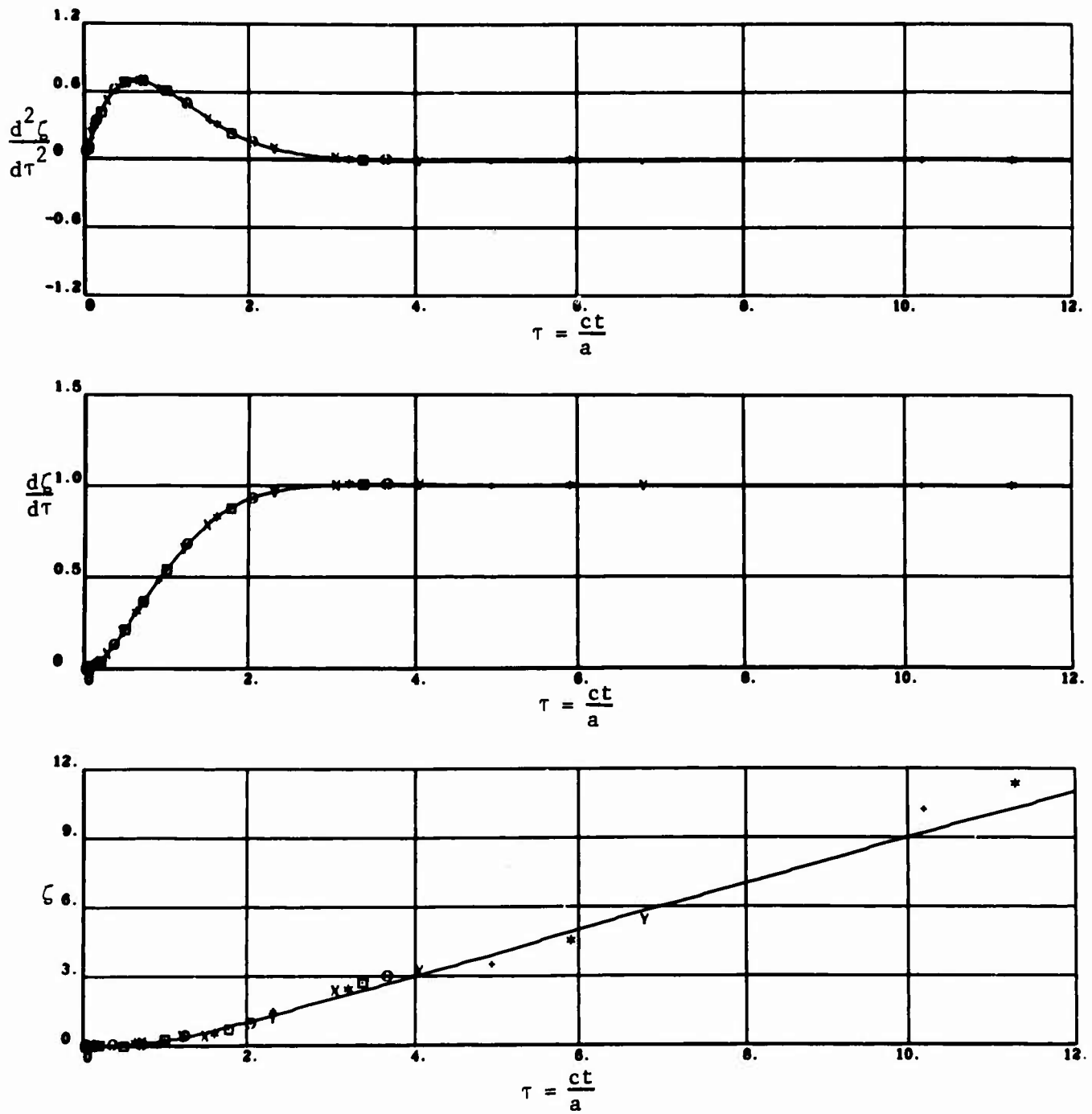


Figure 21. Comparison of Bellman's Method With Exact Solution for Unrestrained, Neutrally Buoyant Sphere; Step Incident Pulse.

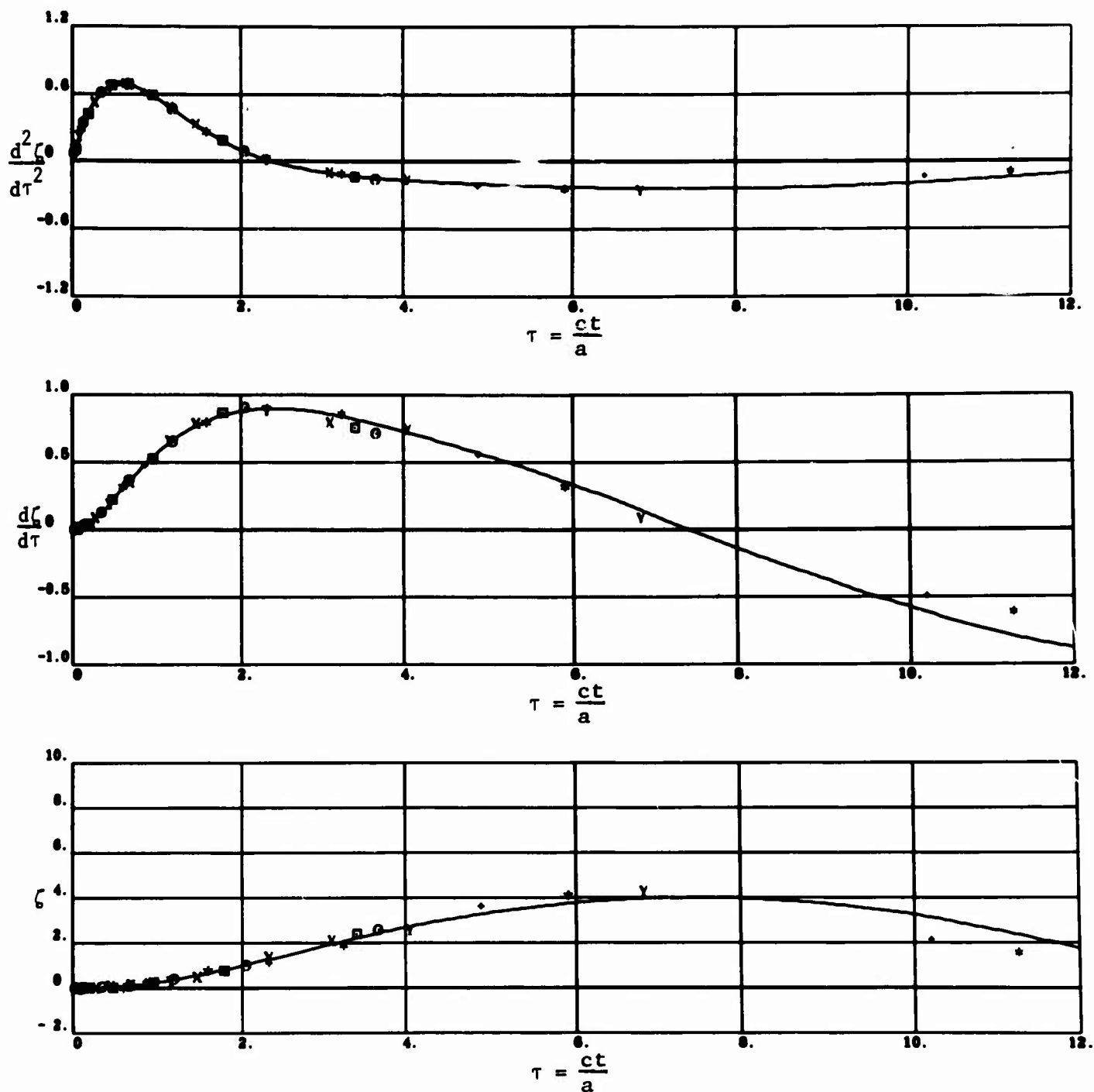


Figure 22. Comparison of Bellman's Method With Exact Solution for Restrained ($\omega = 0.3$), Neutrally Buoyant Sphere; Step Pulse Incident.

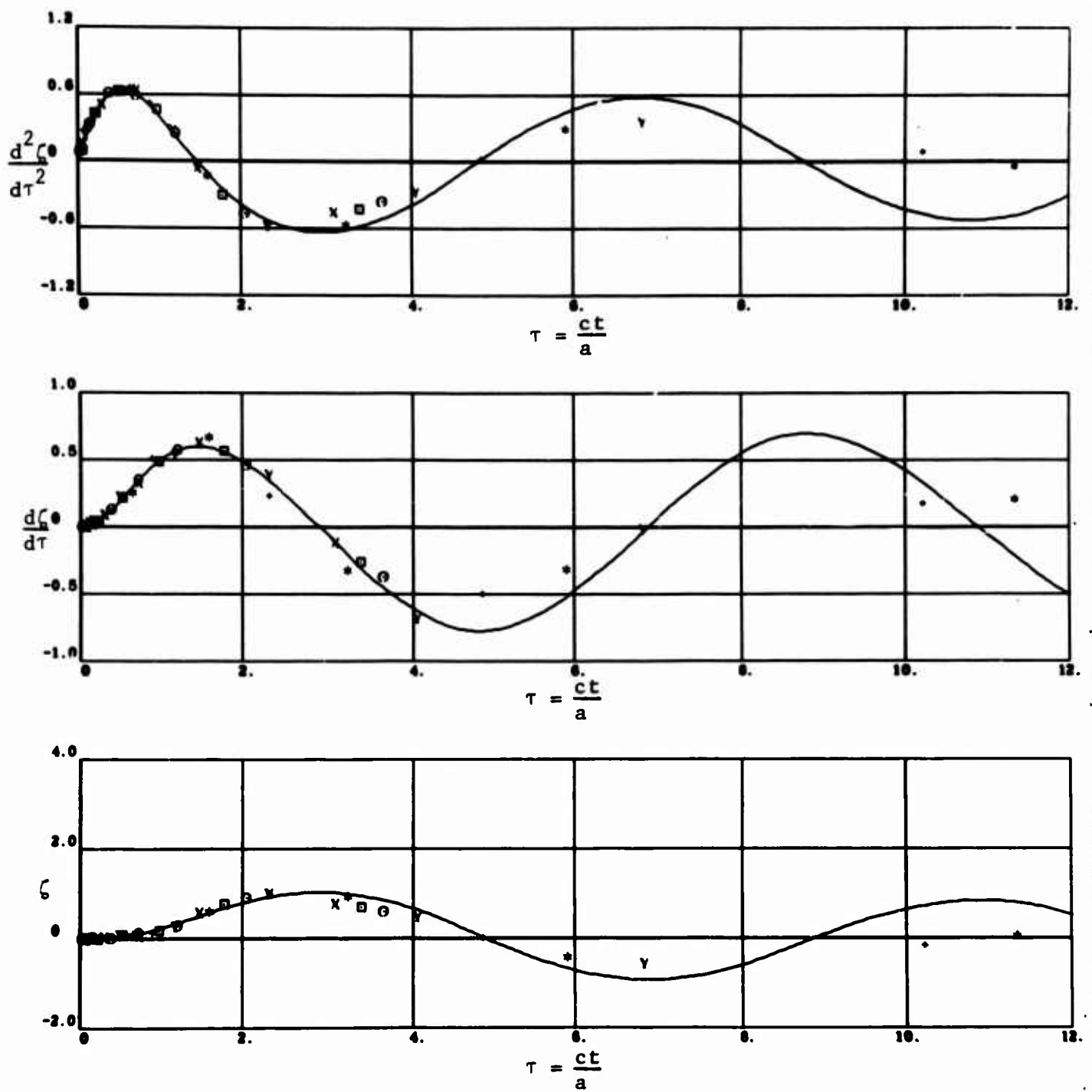


Figure 23. Comparison of Bellman's Method With Exact Solution for Restrained ($\omega = 1.0$), Neutrally Buoyant Sphere; Step Pulse Incident.

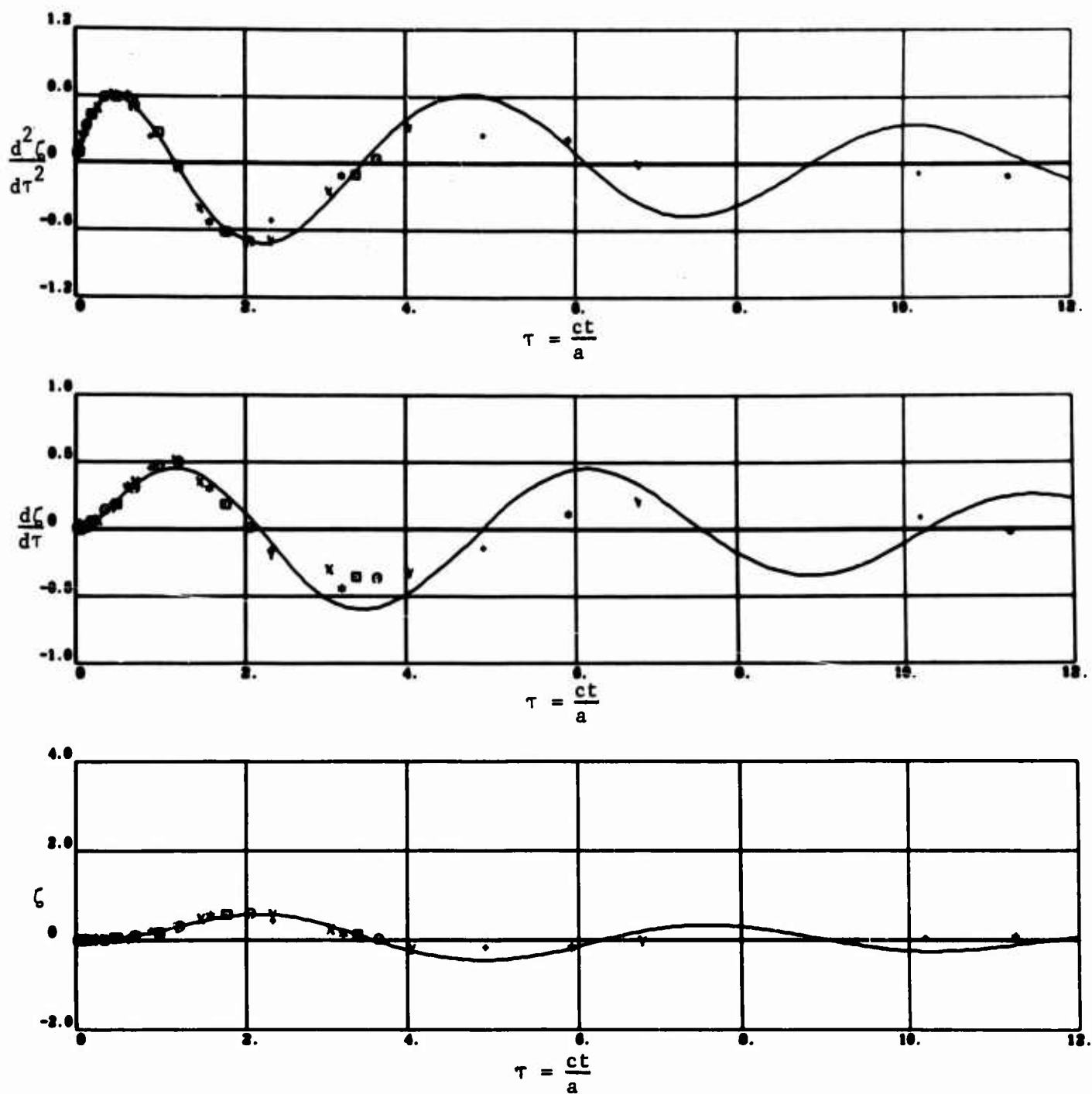


Figure 24. Comparison of Bellman's Method With Exact Solution for Restrained ($\omega = 1.5$), Neutrally Buoyant Sphere; Step Pulse Incident.

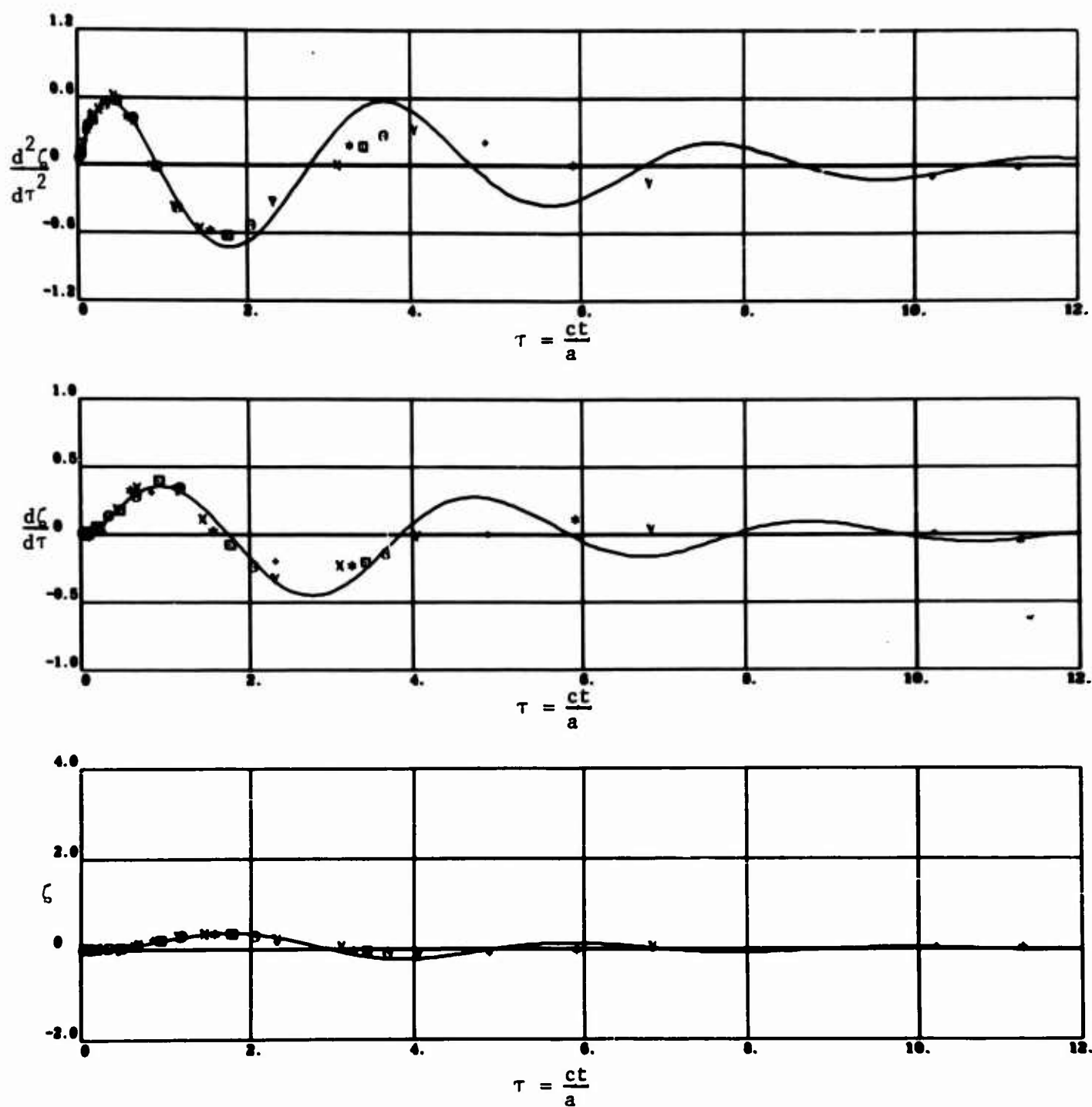


Figure 25. Comparison of Bellman's Method With Exact Solution for Restrained ($\omega = 2.0$), Neutrally Buoyant Sphere; Step Pulse Incident.

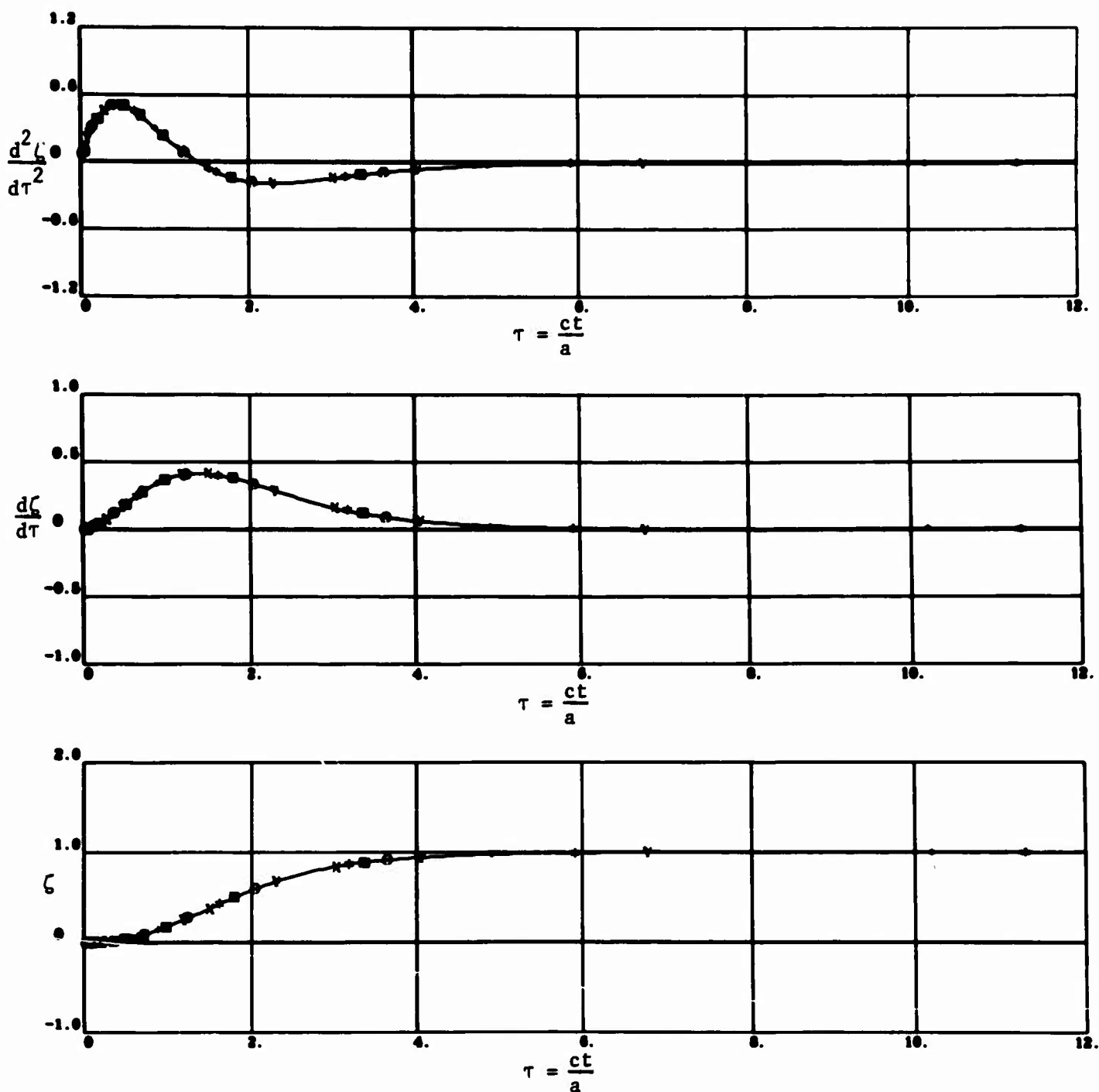


Figure 26. Comparison of Bellman's Method With Exact Solution for Unrestrained, Neutrally Buoyant Sphere; Short Pulse ($\chi = 1$) Incident.

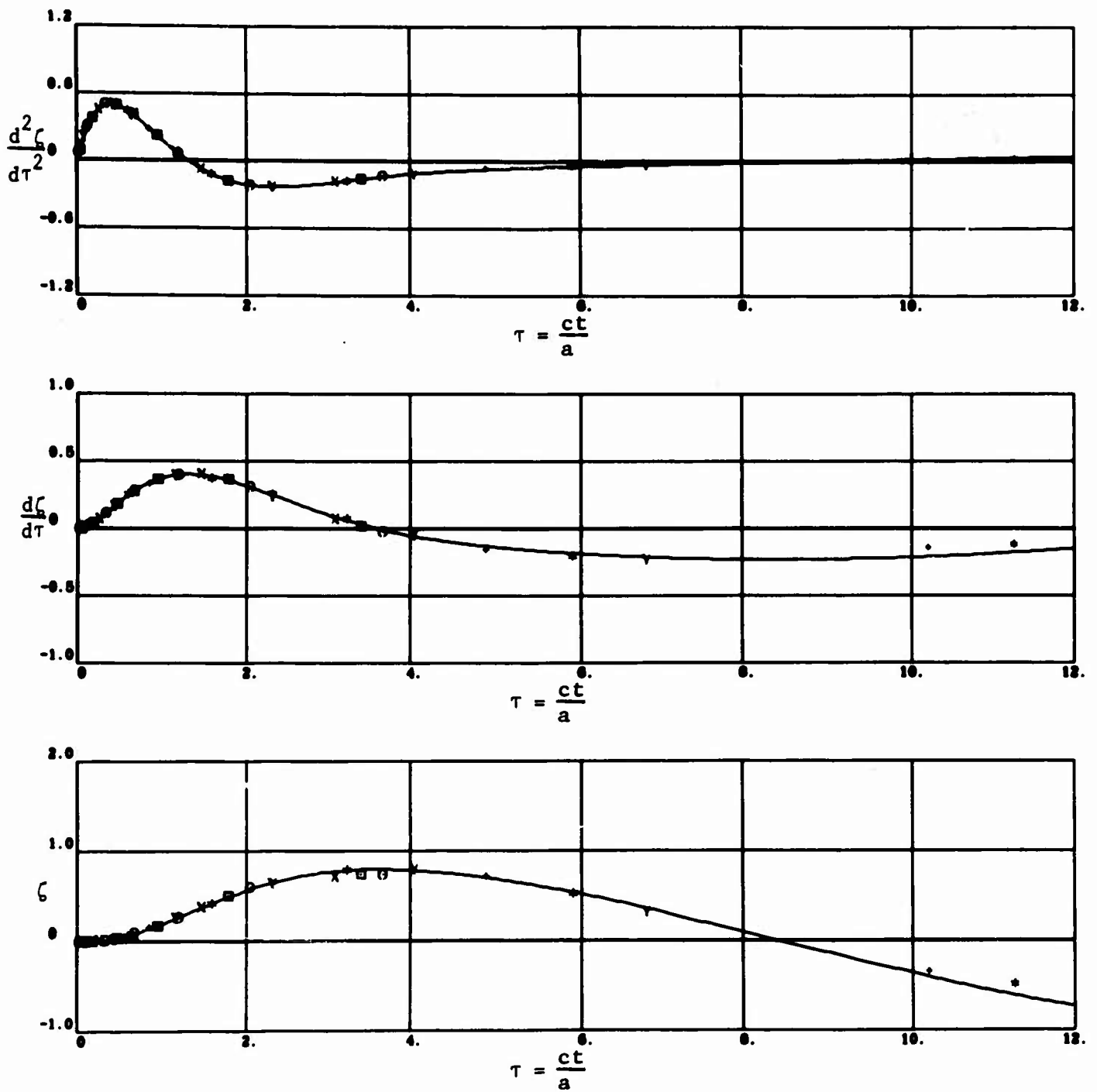


Figure 27. Comparison of Bellman's Method With Exact Solution for Restrained ($\omega = 0.3$) Neutrally Buoyant Sphere; Short Pulse ($\chi = 1$)^o Incident.

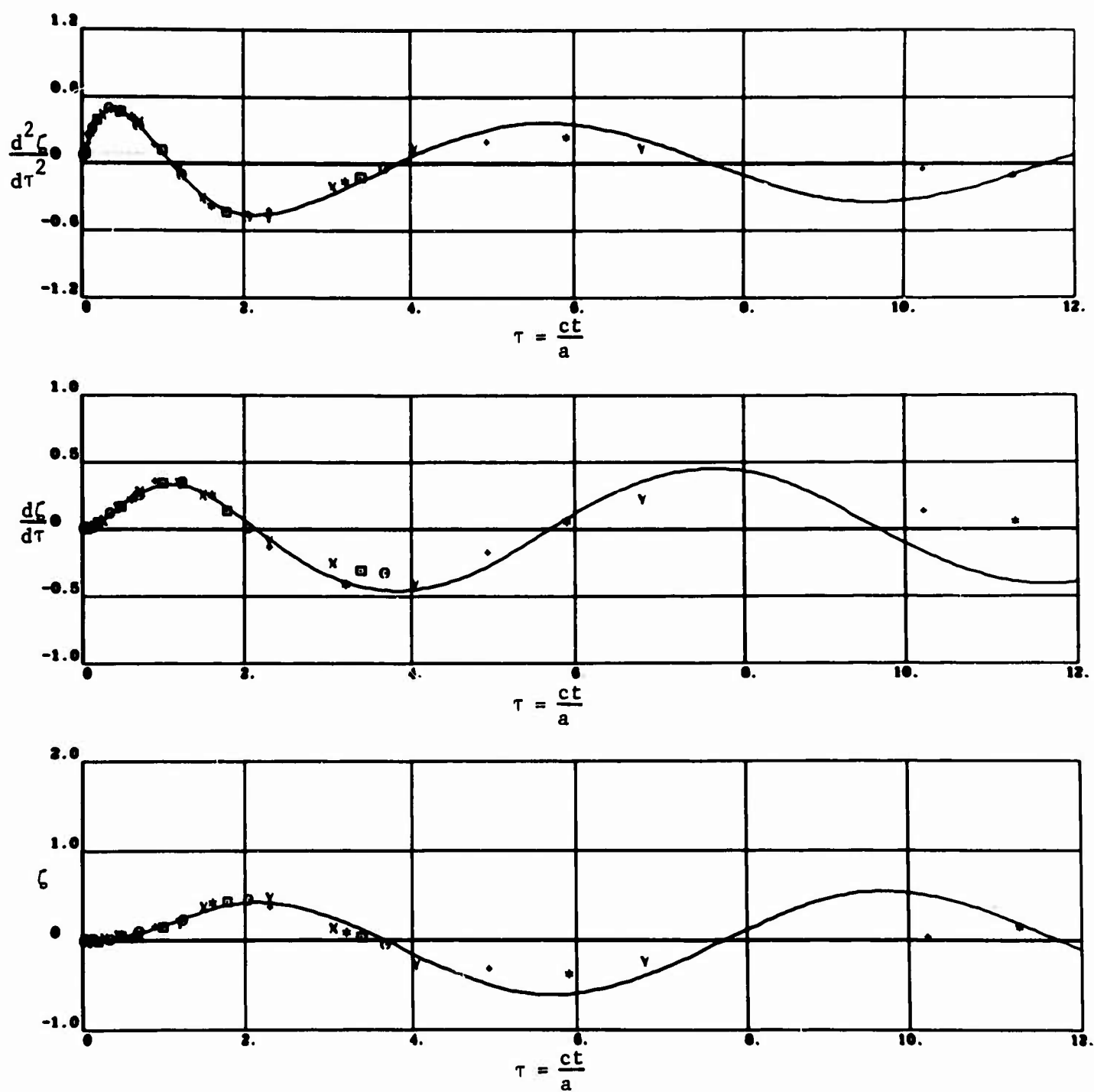


Figure 28. Comparison of Bellman's Method With Exact Solution for Restrained ($\omega = 1.0$) Neutrally Buoyant Sphere; Short Pulse ($\chi = 1$)^o Incident.

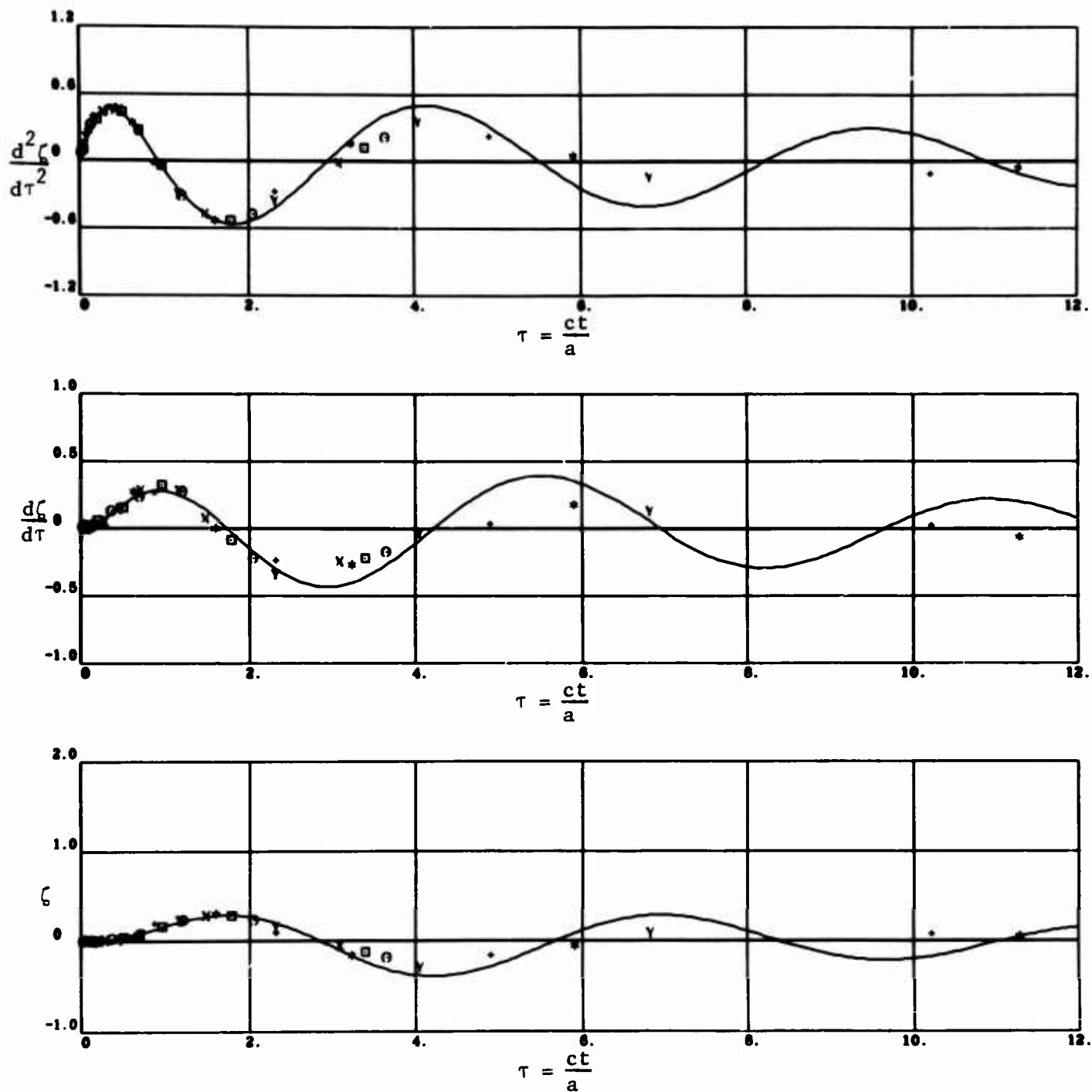


Figure 29. Comparison of Bellman's Method With Exact Solution for Restrained ($\omega = 1.5$) Neutrally Buoyant Sphere; Short Pulse ($\chi = 1$)^o Incident.

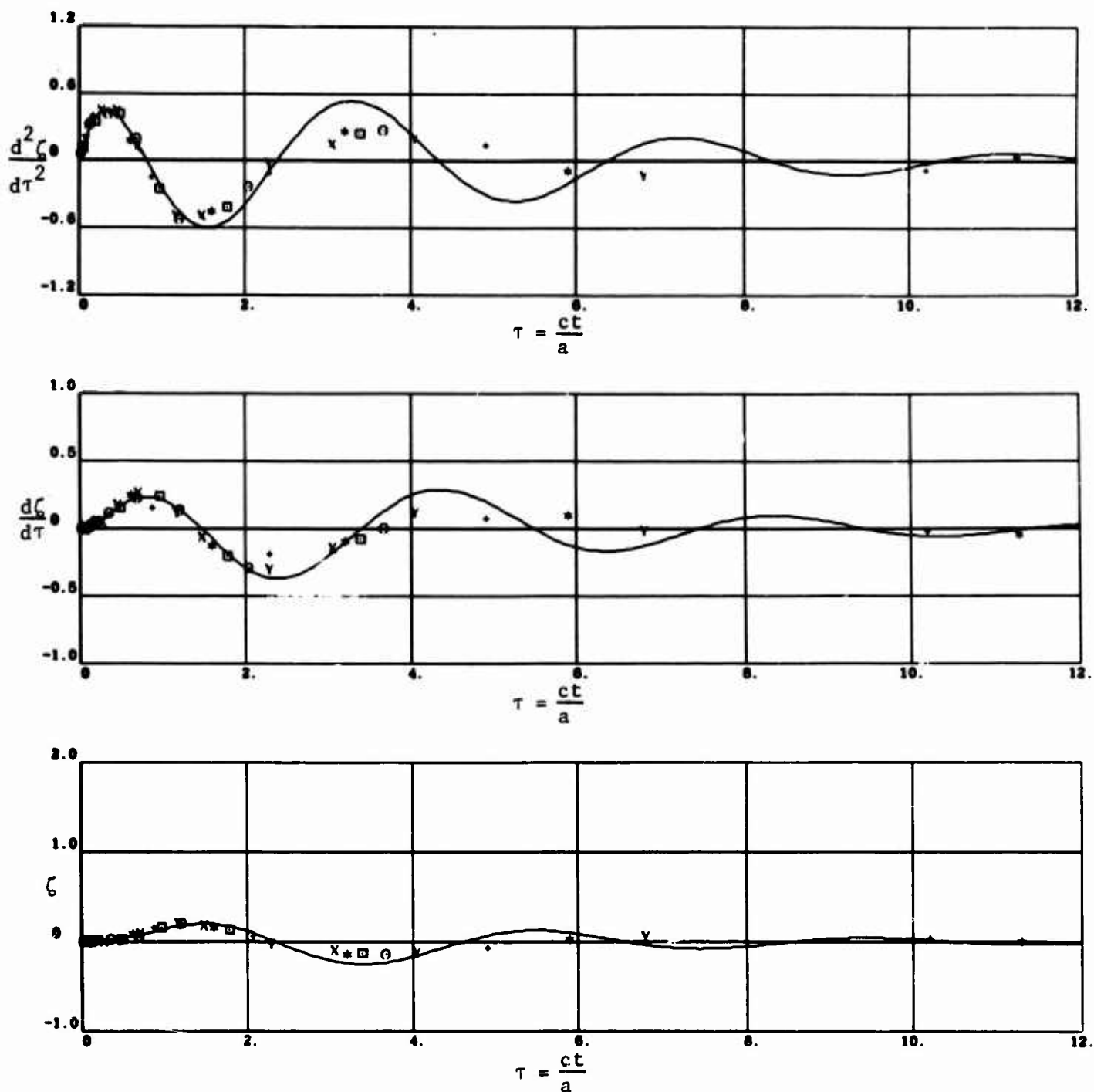


Figure 30. Comparison of Bellman's Method With Exact Solution for Restrained ($\omega = 2.0$) Neutrally Buoyant Sphere; Short Pulse ($\chi = 1$)^o Incident.

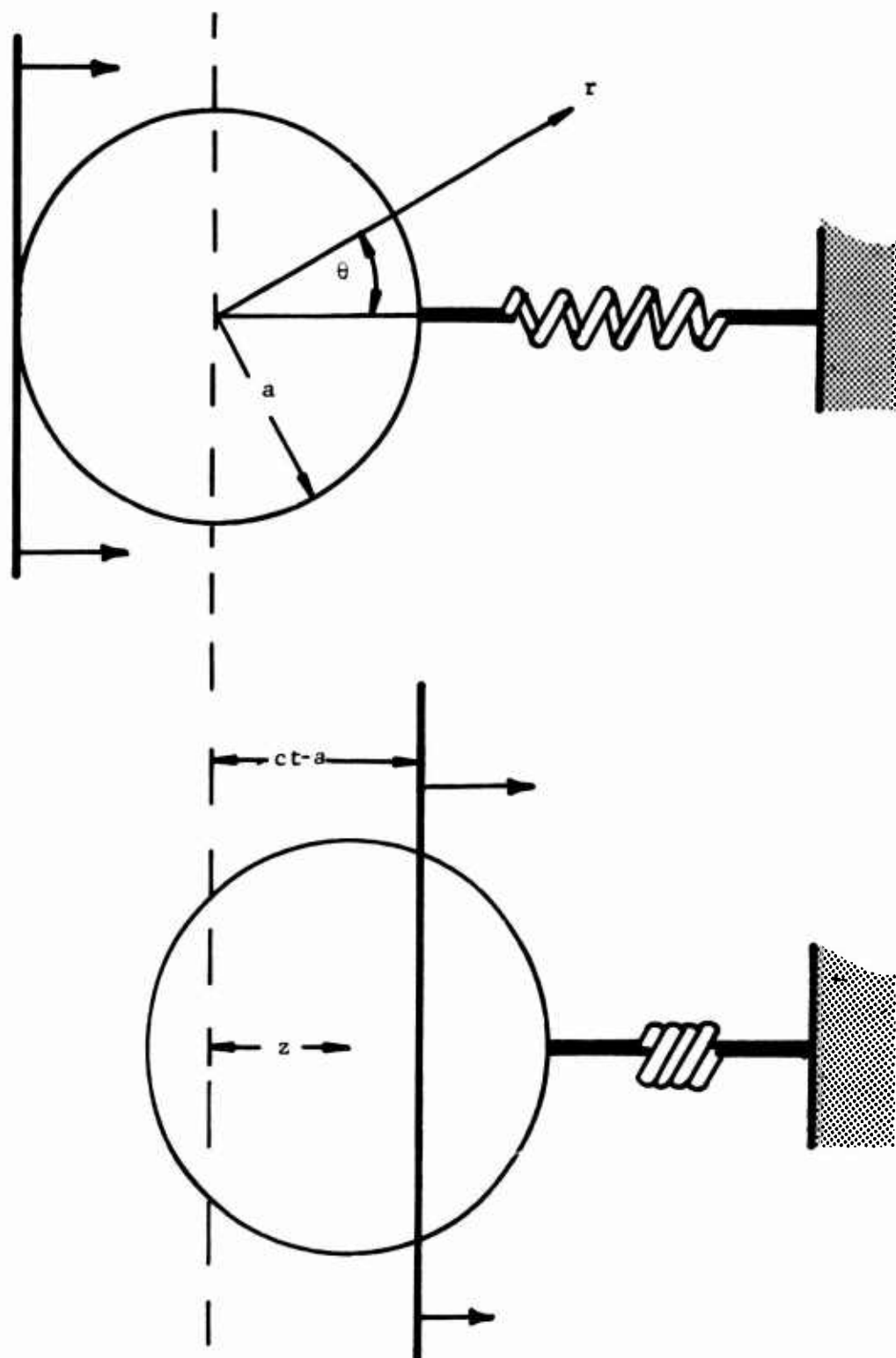


Figure 31. Geometry and Incident Shock Wave Diagram for Cylindrical Structure.

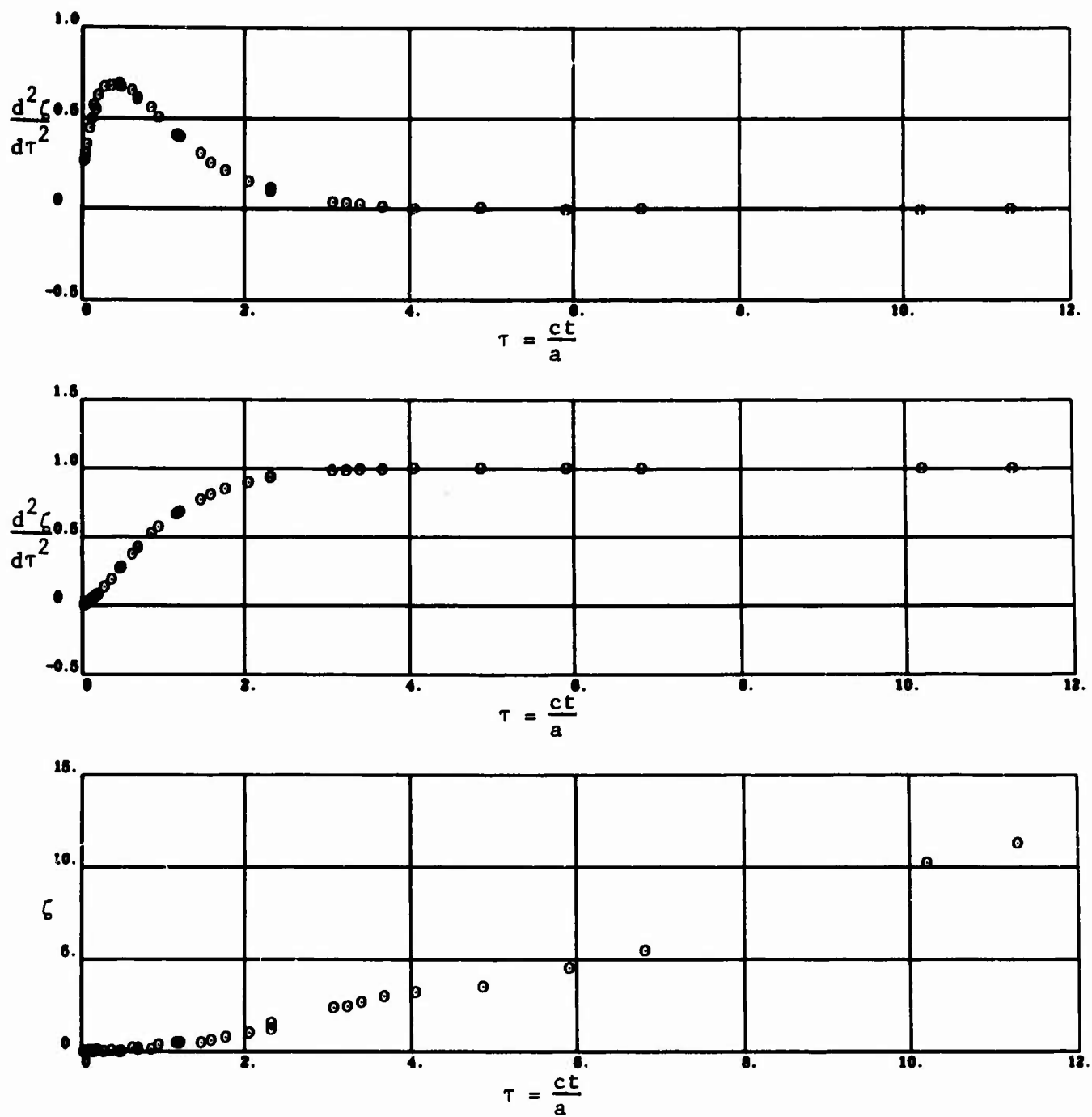


Figure 32. Response Versus Time for Neutrally Buoyant, Unrestrained Cylinder; Step Pulse Incident.

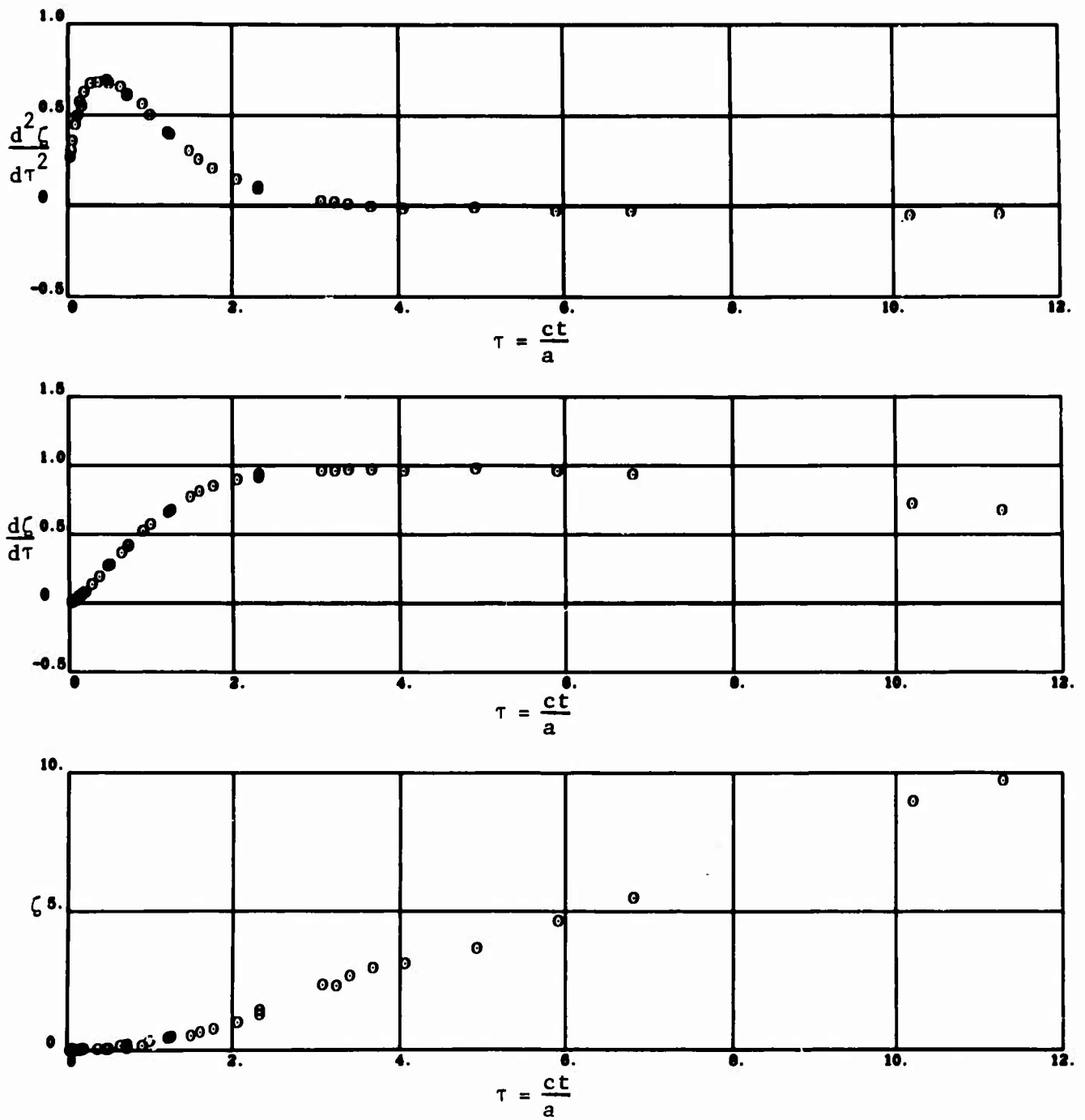


Figure 33. Response Versus Time for Neutrally Buoyant, Restrained ($\omega = 0.1$) Cylinder; Step Pulse Incident.

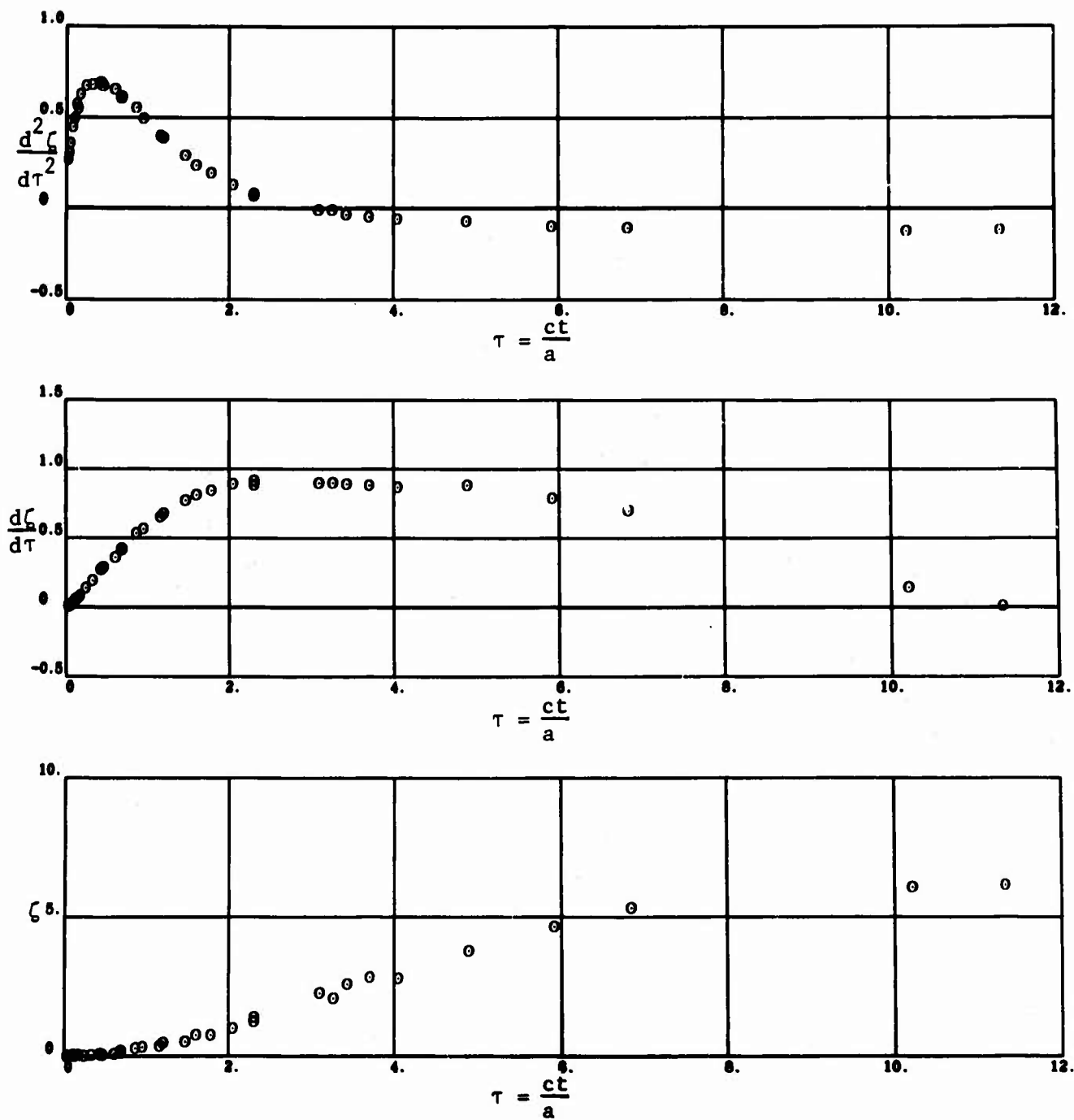


Figure 34. Response Versus Time for Neutrally Buoyant, Restrained ($\omega_0 = 0.2$) Cylinder; Step Pulse Incident.

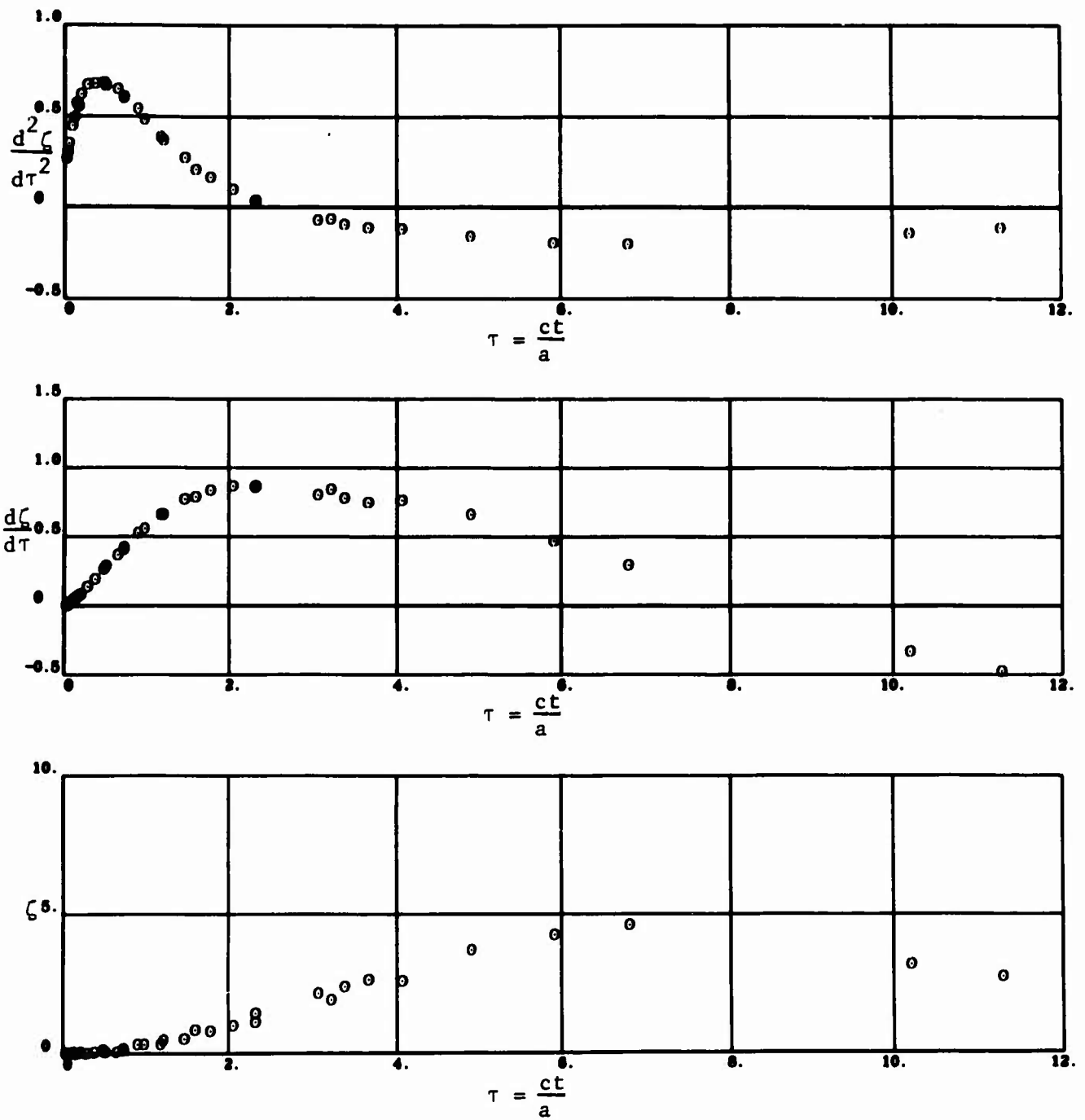


Figure 35. Response Versus Time for Neutrally Buoyant, Restrained ($\omega_0 = 0.3$) Cylinder; Step Pulse Incident.

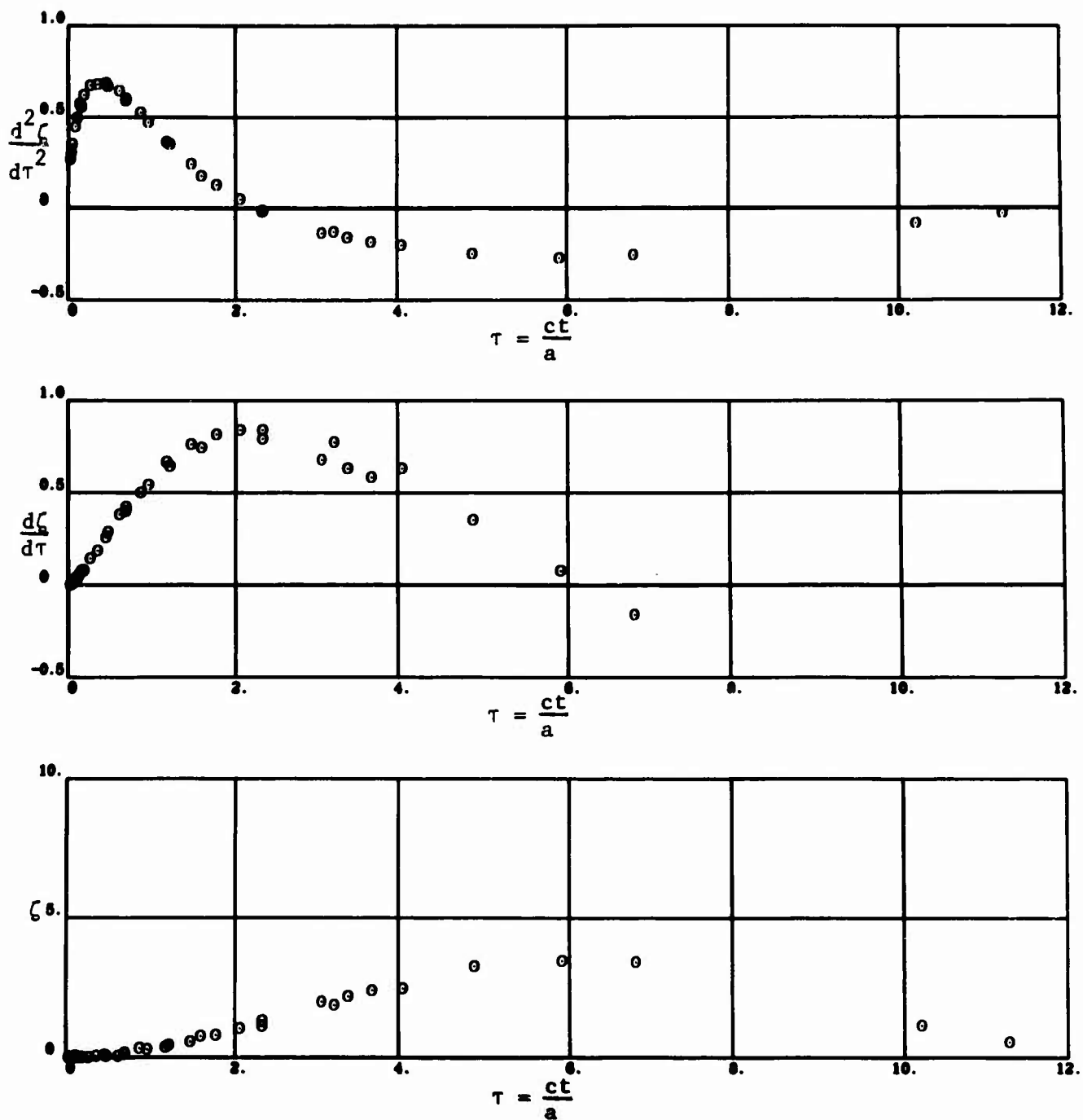


Figure 36. Response Versus Time for Neutrally Buoyant, Restrained ($\omega_0 = 0.4$) Cylinder; Step Pulse Incident.

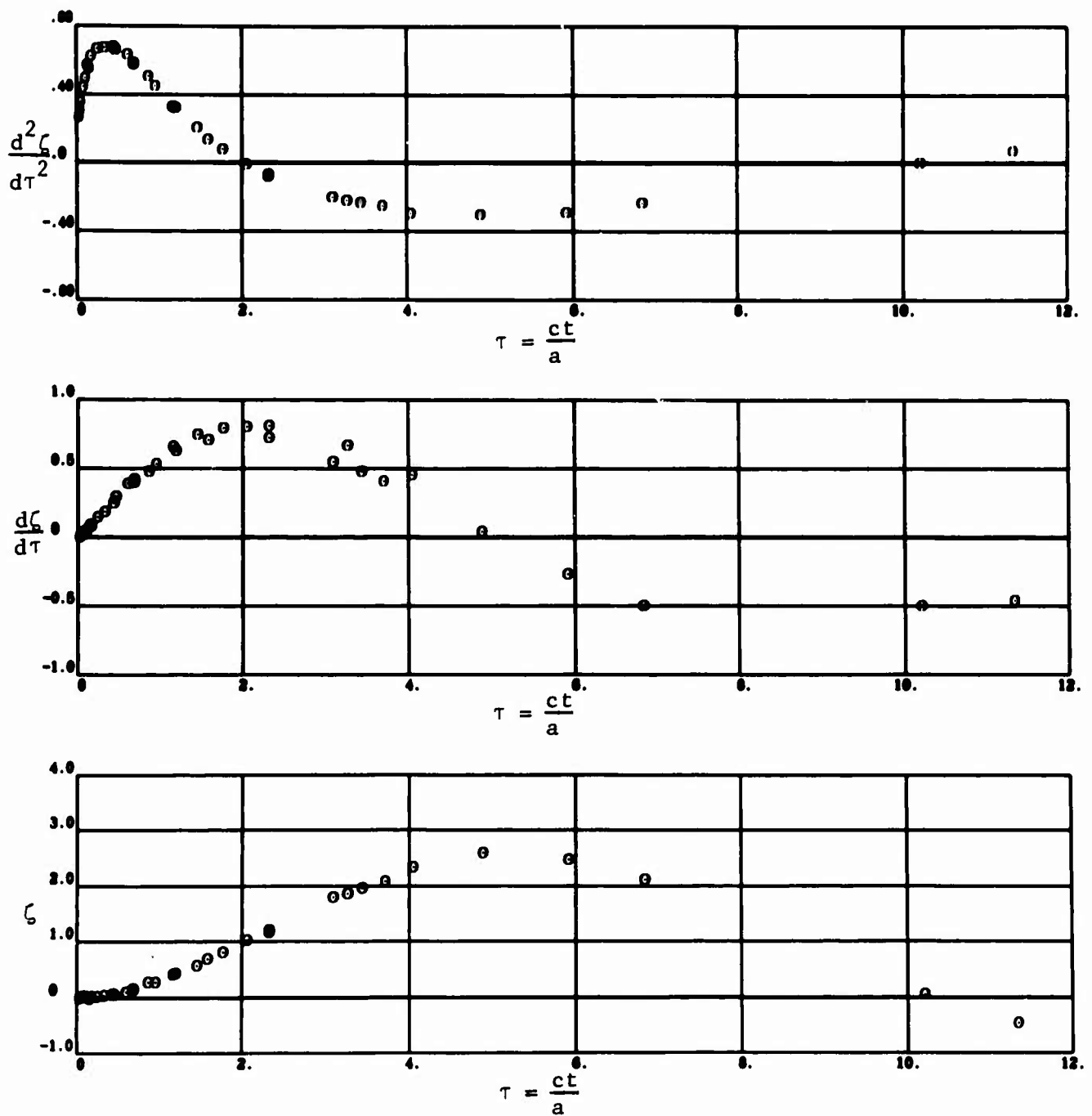


Figure 37. Response Versus Time for Neutrally Buoyant, Restrained ($\omega_0 = 0.5$) Cylinder; Step Pulse Incident.

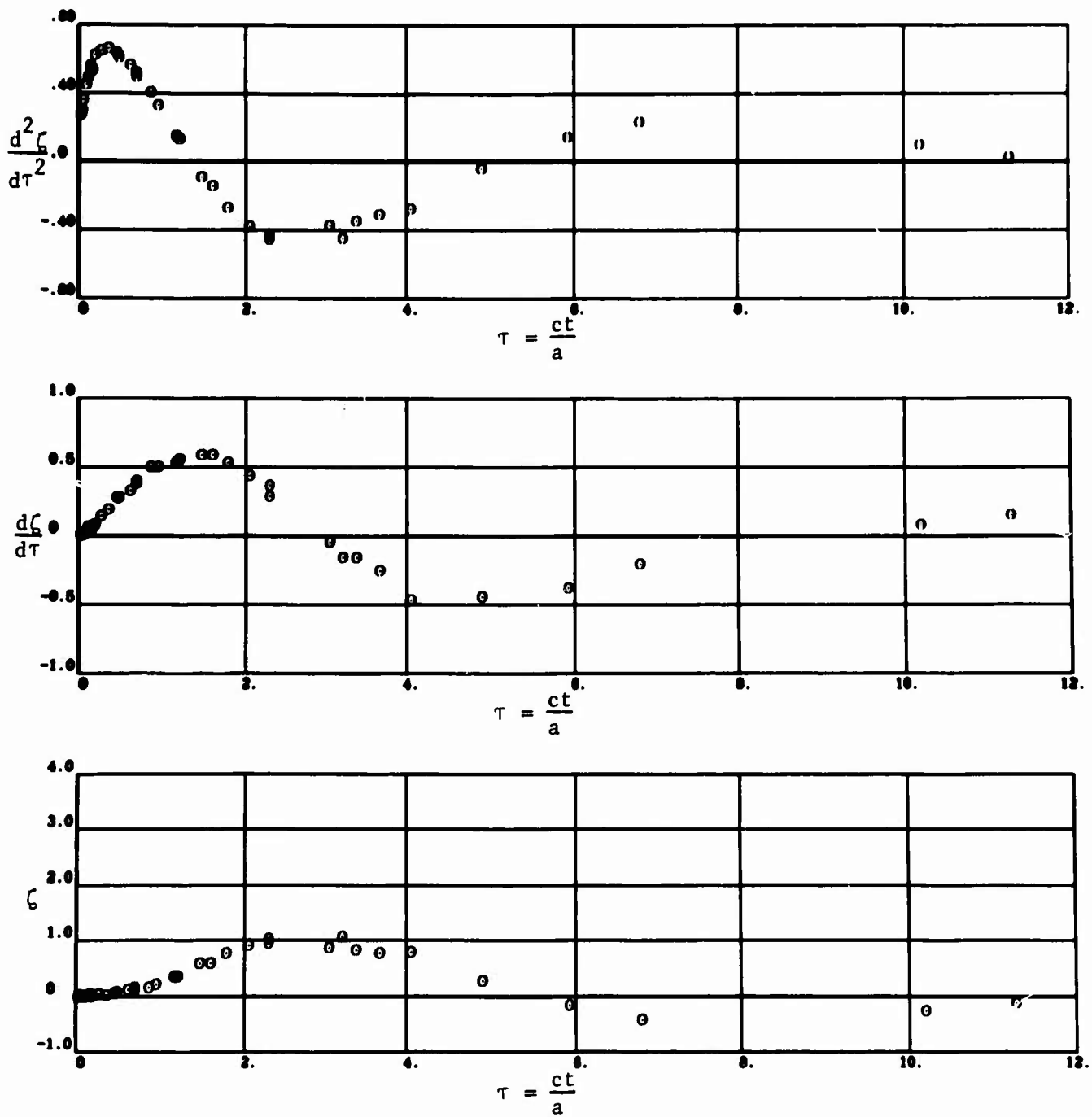


Figure 38. Response Versus Time for Neutrally Buoyant, Restrained ($\omega_o = 1.0$) Cylinder; Step Pulse Incident.

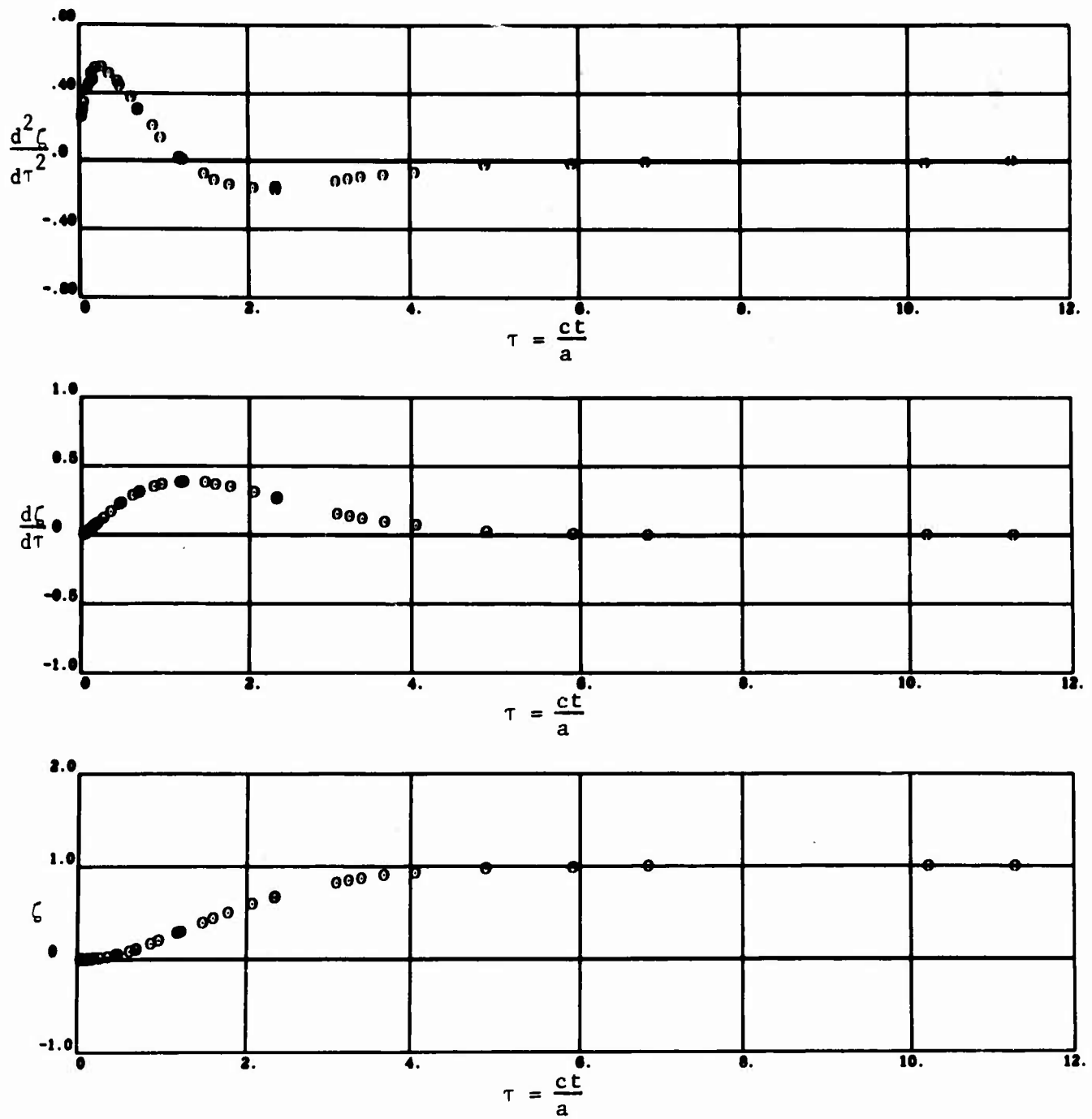


Figure 39. Response Versus Time for Neutrally Buoyant, Unrestrained Cylinder; Short Pulse ($\chi = 1$) Incident.

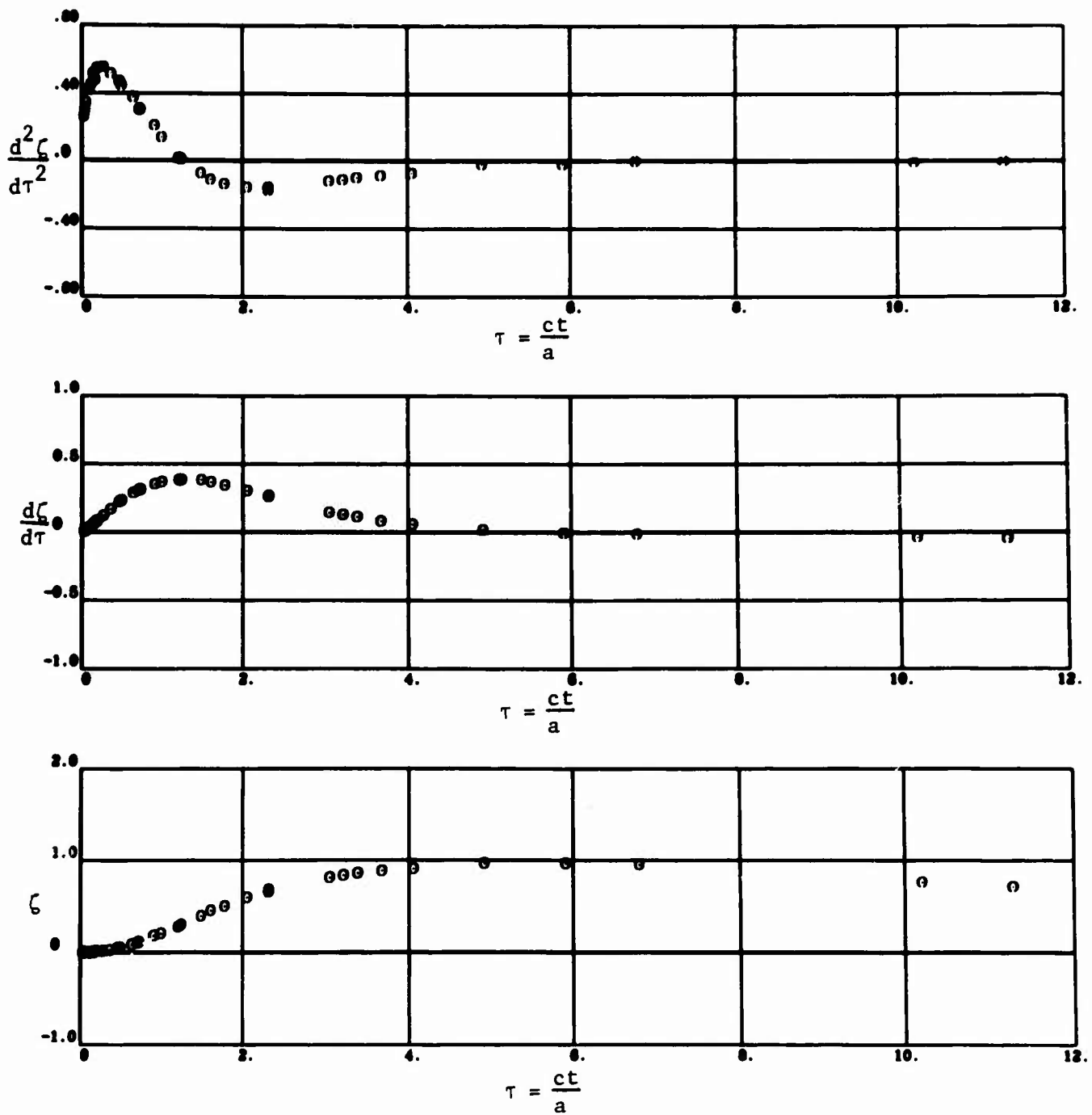


Figure 40. Response Versus Time for Neutrally Buoyant, Restrained ($\omega_0 = 0.1$) Cylinder; Short Pulse ($\chi = 1$) Incident.

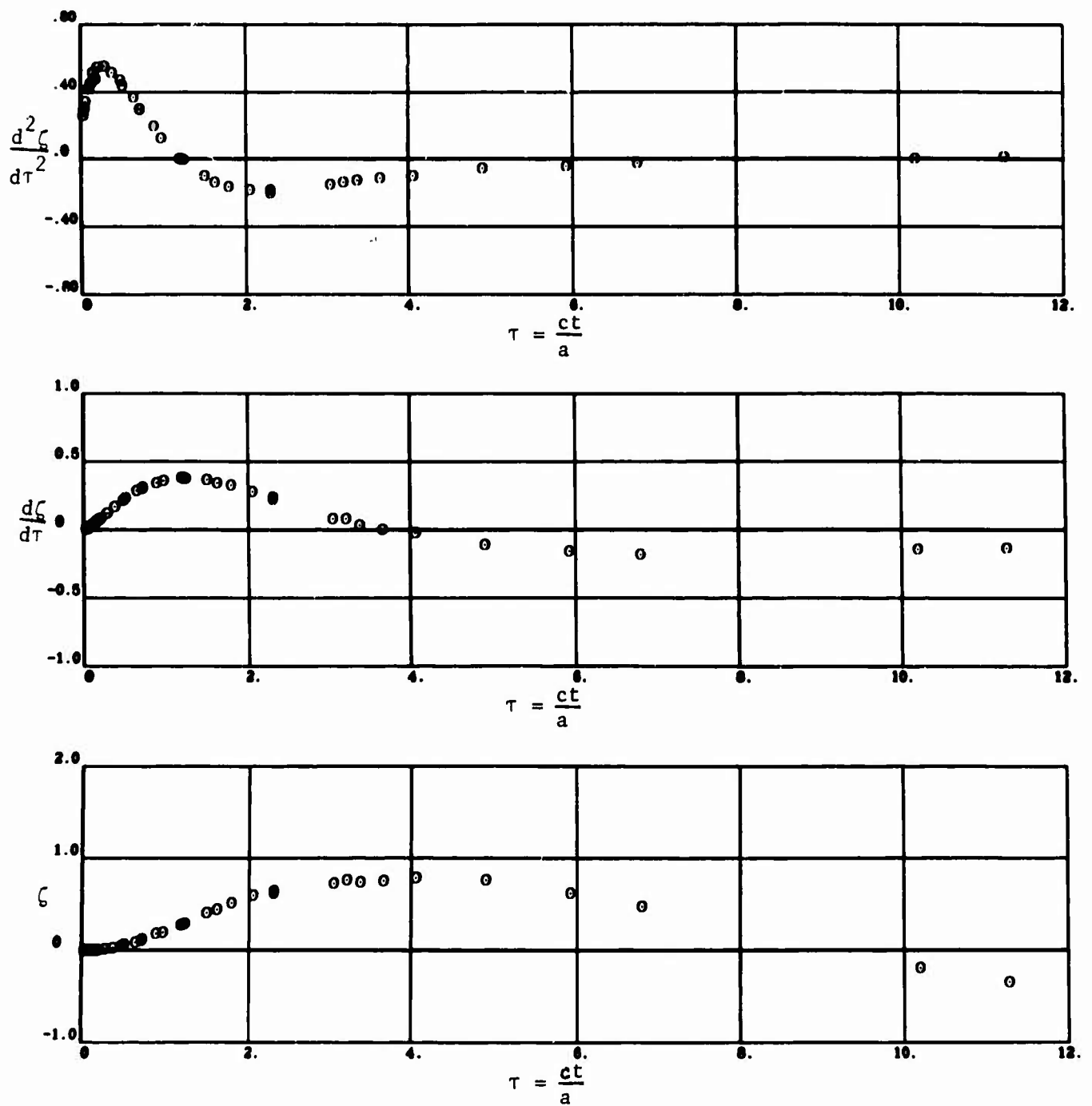


Figure 41. Response Versus Time for Neutrally Buoyant, Restrained ($\omega_0 = 0.3$) Cylinder; Short Pulse ($\chi = 1$) Incident.

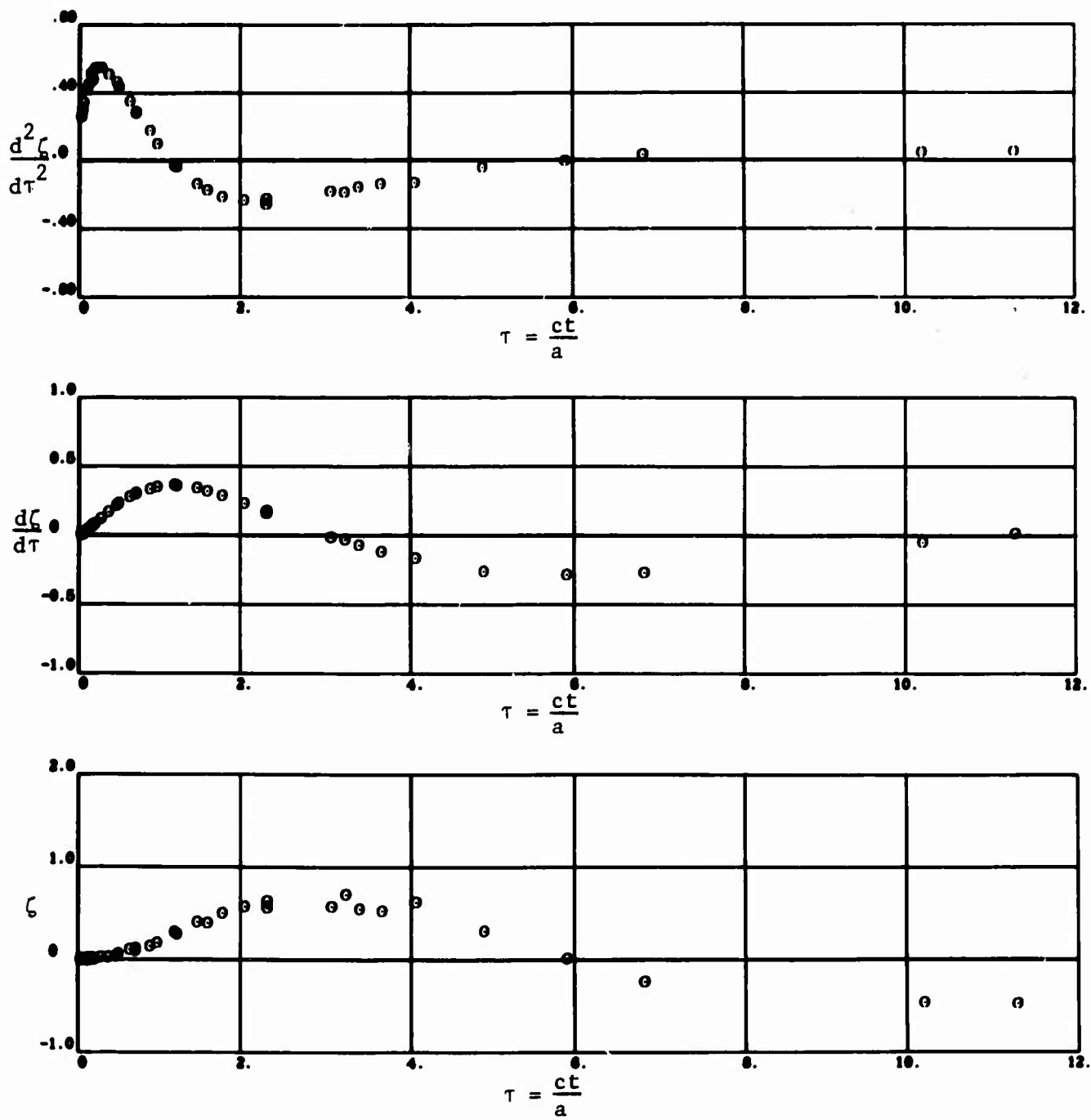


Figure 42. Response Versus Time for Neutrally Buoyant, Restrained ($\omega_0 = 0.5$) Cylinder; Short Pulse ($\chi = 1$) Incident.

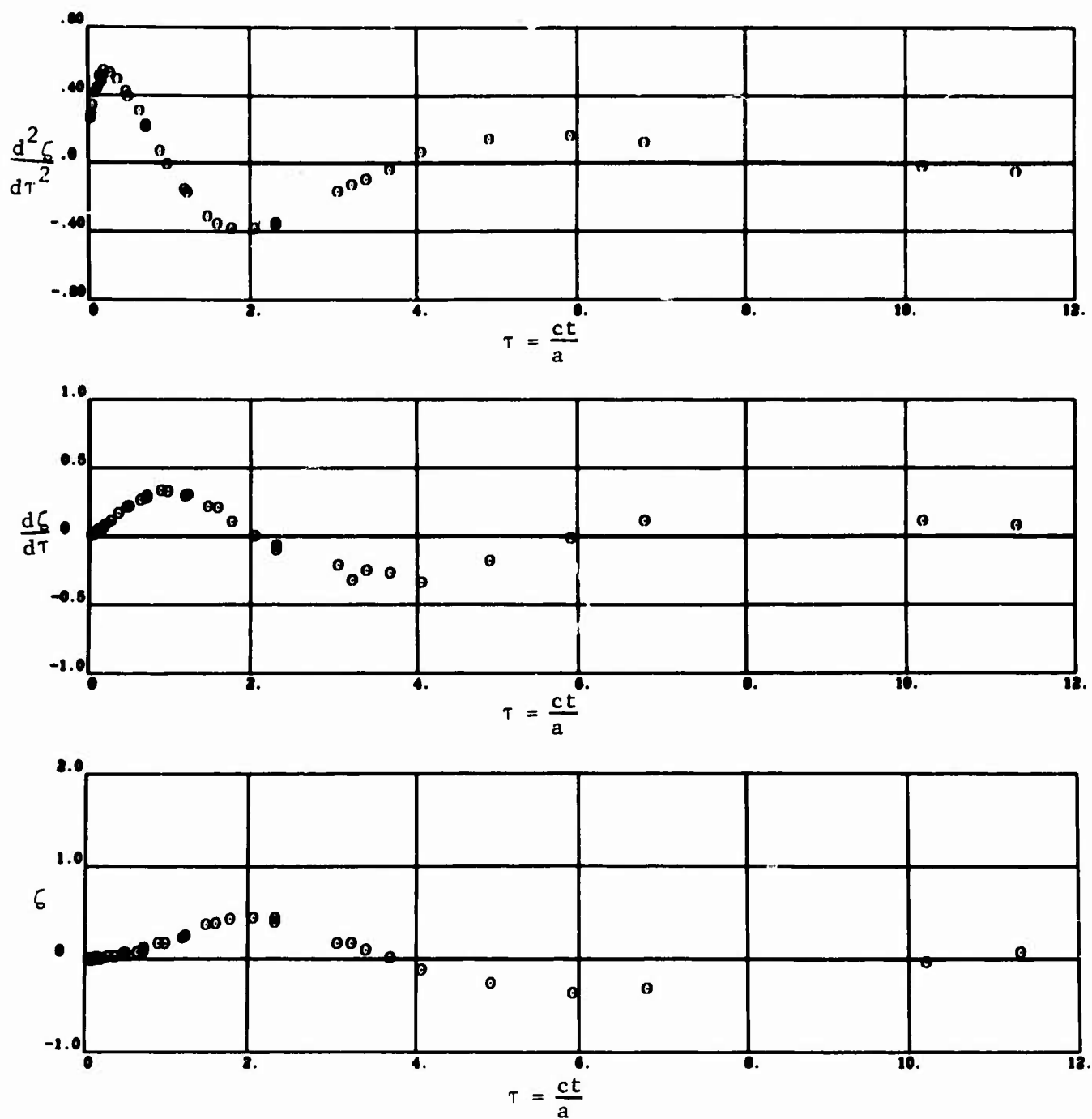


Figure 43. Response Versus Time for Neutrally Buoyant, Restrained ($\omega_0 = 1.0$) Cylinder; Short Pulse ($\chi = 1$) Incident.

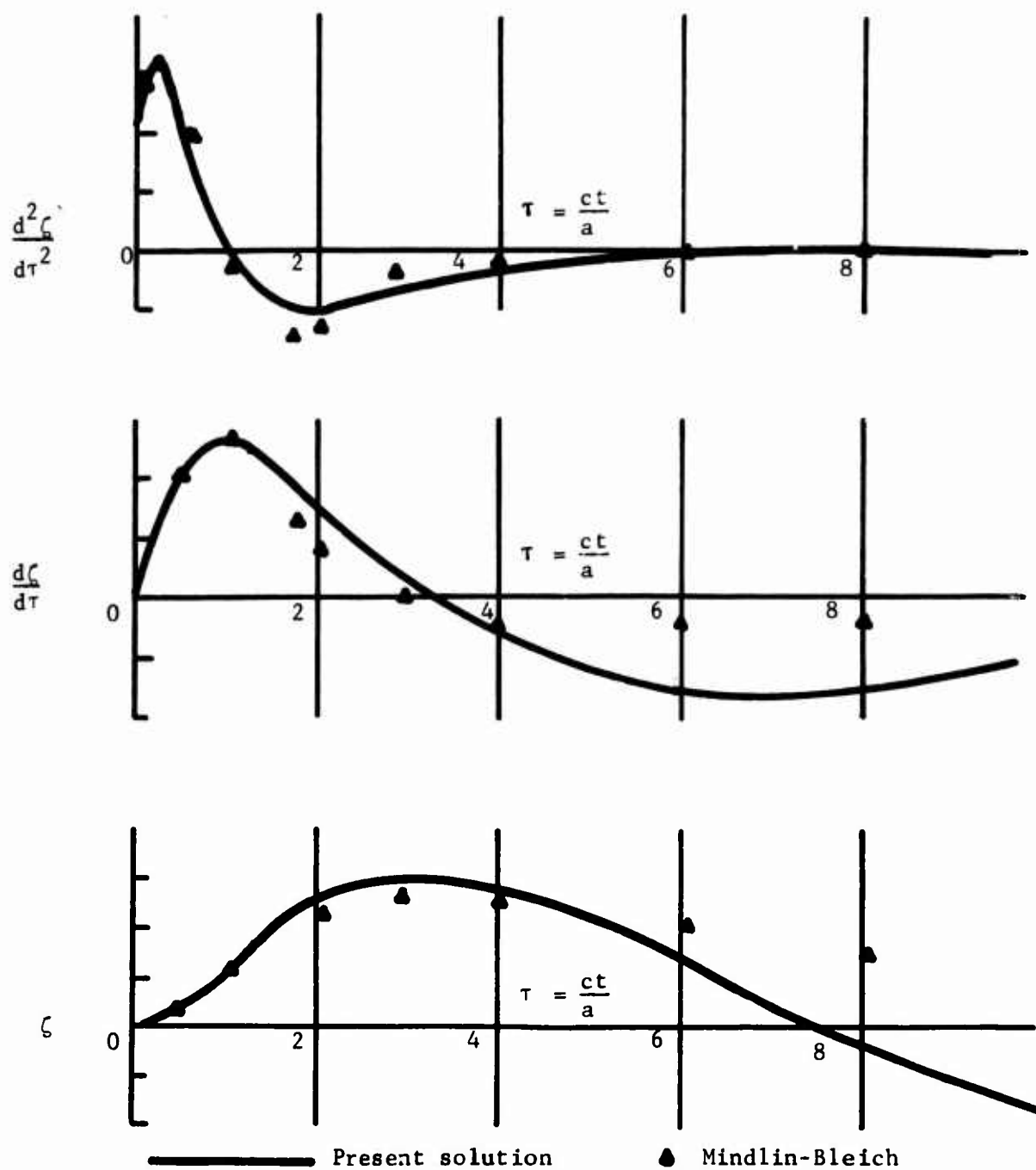


Figure 44. Comparison of Mindlin-Bleich Approximation With Present Calculation for a Buoyant ($S = 0.5$), Restrained ($\omega_o = 0.47$) Cylinder; Short Pulse ($\chi = 1$) Incident.

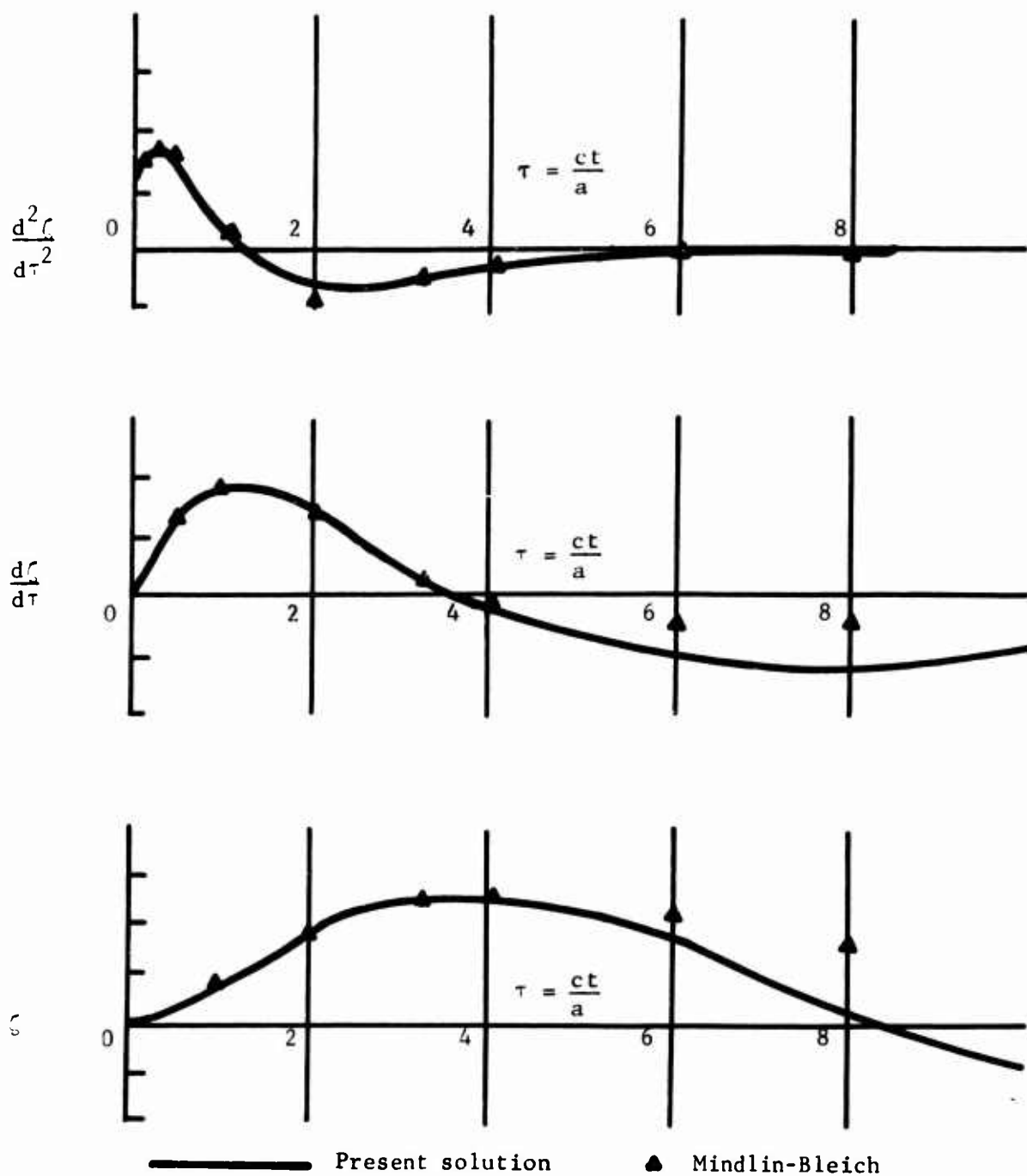


Figure 45. Comparison of Mindlin-Bleich Approximation With Present Calculation for a Neutrally Buoyant, Restrained ($\omega_0 = 0.33$) Cylinder; Short Pulse ($\chi = 1$) Incident.

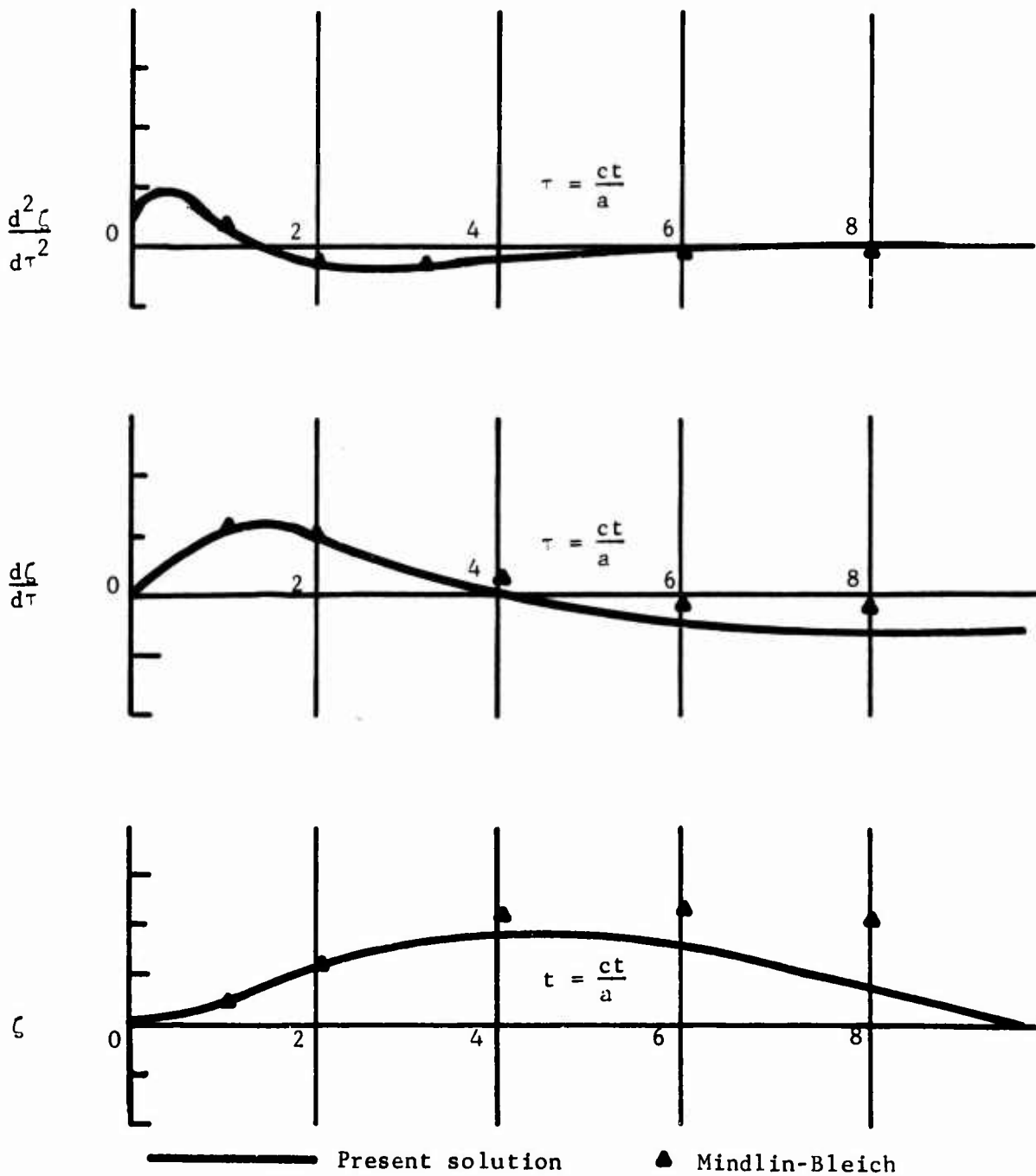


Figure 46. Comparison of Mindlin-Bleich Approximation With Present Calculation for a Heavy ($S = 2.0$), Restrained ($\omega = 0.23$) Cylinder; Short Pulse ($\chi = 1$) Incident.

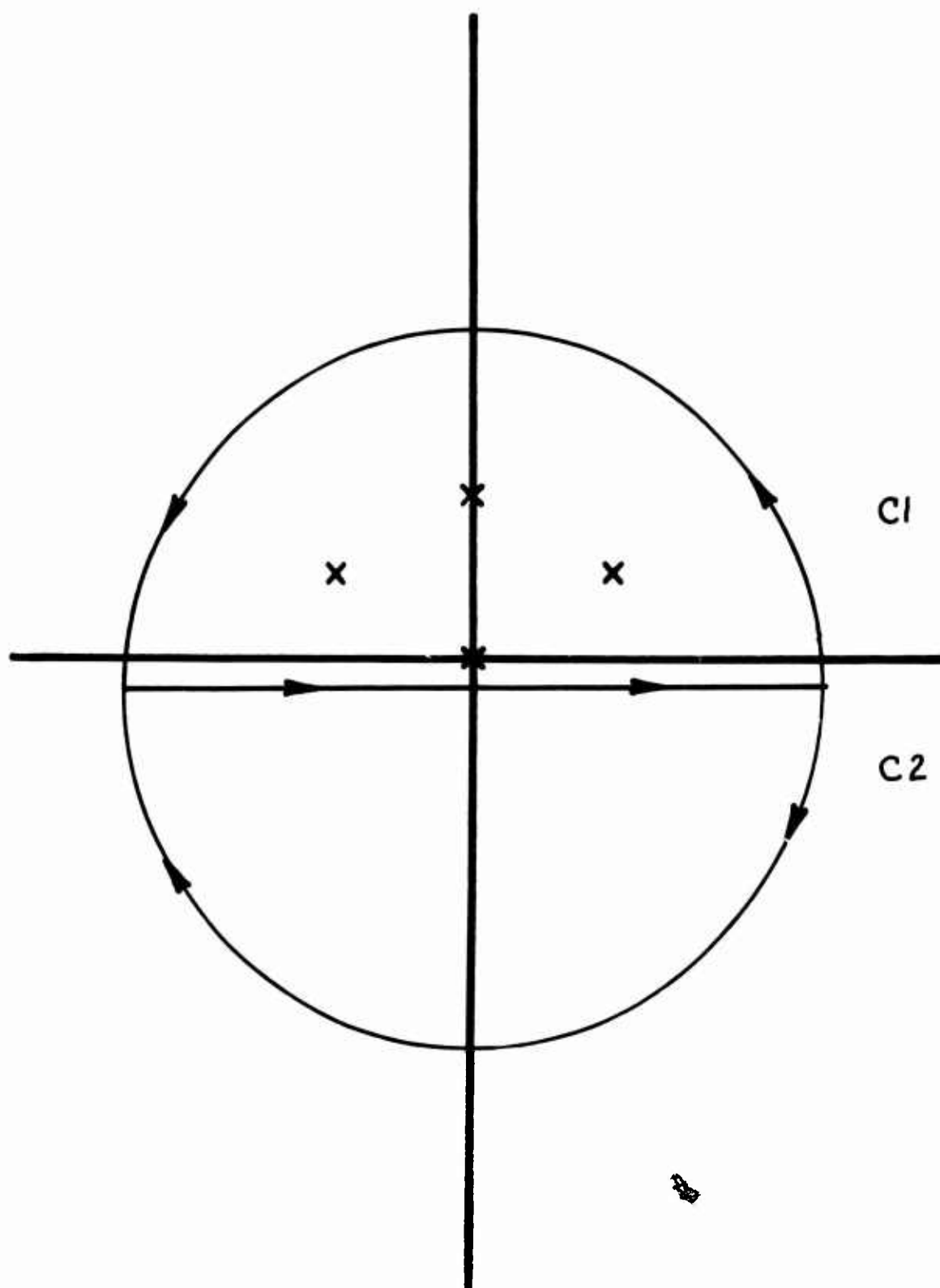


Figure 47. Location of Poles and Contours Used for Unrestrained Sphere.

Appendix A

INVERSION OF FOURIER-TRANSFORMED EQUATIONS FOR SPHERICAL STRUCTURE

The integral for $\zeta(t)$ that appears in Equation 18 on page 9 can be done by contour integration in the complex ω plane. In general there will be contributions from five poles, one at $\omega = iX$ and the others at the roots of the quartic equation

$$i\omega^4 + \left(2 + \frac{1}{S}\right)\omega^3 - 1\left(2 + \omega_0^2 + \frac{1}{S}\right)\omega^2 - 2\omega_0^2\omega + 2i\omega_0^2 = 0 \quad (A-1)$$

The roots of this equation can be shown to lie in the upper half plane, as they must to insure causality. It is not possible to solve the quartic equation in closed form for arbitrary S and ω_0 . However, for $\omega_0 = 0$ the quartic equation breaks down into a double root at $\omega = 0$ and two roots that are the solutions of the remaining quadratic equation. For ω_0 not equal to 0, recourse must be made to numerical methods in order to obtain a particular solution. In terms of these roots, x_i , $\zeta(t)$ is

$$\zeta(t) = \frac{3i}{S} \sum_{i=1}^5 \frac{x_i e^{ix_i t}}{\prod_{\substack{j=1 \\ j \neq i}}^5 (x_i - x_j)} \quad (A-2)$$

where $x_5 = iq$ and x_i , $i = 1, \dots, 4$ are the roots of the quartic. It should be noted, that in case of multiple roots this solution is not valid.

It is instructive to look at the inversion integral for the case $\omega_0 = 0$ in some detail. For this case, the above inverse of Equation 18 becomes

$$\zeta(t) = \frac{3}{2\pi S} \int_{-\infty}^{\infty} \left[\frac{e^{i\omega t}}{\omega(\omega - iX) \left[\omega - \left(1 + \frac{1}{2S}\right)i - \sqrt{\left(1 + \frac{1}{2S}\right)\left(1 - \frac{1}{2S}\right)} \right]} \right. \\ \left. \left[\omega - \left(1 + \frac{1}{2S}\right)i + \sqrt{\left(1 + \frac{1}{2S}\right)\left(1 - \frac{1}{2S}\right)} \right] \right] d\omega \quad (A-3)$$

Figure 47 shows the location of the poles in the complex ω plane, as well as the two contours, C1 and C2. For negative values of t the exponential along the contour C2 goes to zero. There are no poles within this contour; hence the result is zero. As stated above, this is simply due to causality. Namely, before the shock wave hits the sphere, it shouldn't move. For t greater than zero the contour can be closed in the upper half of the plane. This is C1 in Figure 47, and this contour encloses all four poles. The integral along the real axis is displaced slightly below it, so that the pole at $\omega = 0$ is inside the contour. The value of the integral is $2\pi i$ times the sum of the residue.

The general feature of the solution can be readily determined without explicitly presenting the cumbersome algebra. If $\chi = 0$, there is a first order pole at $\omega = 0$. The residue at $\omega = 0$ times $2\pi i$ then represents the asymptotic displacement of the sphere, i.e.

$$\zeta(\infty) = \frac{3/\chi}{2S + 1}$$

If $\chi = 0$, then the pole at $\omega = 0$ is of second order so that

$$\zeta(\tau) \xrightarrow{\tau \rightarrow \infty} \frac{3\tau}{2S + 1}$$

hence

$$\frac{d \zeta(\tau)}{d\tau} \xrightarrow{\tau \rightarrow \infty} \frac{3}{2S + 1}$$

The poles at

$$\omega = +\left(1 + \frac{1}{2S}\right) \pm \sqrt{\left(1 + \frac{1}{2S}\right)\left(1 - \frac{1}{2S}\right)}$$

yield exponentially damped contributions; the damping increases inversely with S . It is interesting to observe that even without a restraint force these contain an oscillatory component for S greater than one-half. It is not obvious what the physical cause is for this oscillation. However, it is rather strongly damped out in time and would probably not be measurable. (Murray² observes the same type of oscillations for the motion of an unrestrained cylinder.) For S smaller than one-half, the motion no longer is oscillatory but is exponentially damped. It is interesting to observe that for S equal to one and $\chi \neq 0$, $\zeta(\infty)$ is equal to $\frac{1}{\chi}$ which is simply the distance a particle of water in front of the shock wave would move during the decay time of the pulse. For $\chi = 0$ on the other hand,

$$\frac{dr}{d\tau} \longrightarrow 3/(2S + 1)$$

which for S greater than one is less than the particle velocity in the shock wave. For $S = 1$ the sphere moves with the shock wave, and for S less than 1, it moves faster than the particle velocity in the shock wave. This is not an unreasonable result, since from potential theory it is well known that an accelerated sphere will lead or lag the water velocity depending on whether the density is less than or greater than the water density. Since with the potential theory there is no force on the submerged object due to uniform flow, this motion will persist. On the other hand the inclusion of drag forces would maintain the asymptotic velocity of the sphere equal to that of the water particle velocities.

Appendix B

NUMERICAL INVERSION OF TRANSFORMED EQUATIONS

Although an exact solution for the motion of the sphere can be obtained, this is not possible for a cylindrical structure because the solution to the transformed equation cannot be readily inverted. A numerical inversion of the Laplace transform for the cylinder response can be obtained, however, using a method due to Bellman, Kalaba and Lockett.⁴ It is expected that the motion of the sphere and the cylinder will be qualitatively similar, so that the limitations of Bellman's method in this application can be determined by applying it to the motion of the sphere.

The solution obtained for the sphere was based on the Fourier transform, whereas Bellman's method requires the Laplace transform. Due to the fact that the system is at rest for negative times, the Laplace transform $F_L(\sigma)$ is related to the Fourier transform $F_F(\omega)$ by

$$F_L(\sigma) = \sqrt{2\pi} F_F(-i\sigma)$$

In order to demonstrate this, let $F_F(\omega)$ be the Fourier transform of $f(t)$; then

$$F_F(\omega) = \frac{1}{\sqrt{2\pi}} \int_{-\infty}^{\infty} e^{-i\omega t} f(t) dt \quad (B-1)$$

Then since $f(t) = 0$ when t is less than zero, this becomes

$$F_F(\omega) = \frac{1}{\sqrt{2\pi}} \int_0^{\infty} e^{-i\omega t} f(t) dt \quad (B-2)$$

The above expression for $\omega = -i\sigma$ is

$$F_F(-i\sigma) = \frac{1}{\sqrt{2\pi}} \int_0^{\infty} e^{-\sigma t} f(t) dt \quad (B-3)$$

However, the Laplace transform of $f(t)$ is

$$F_L(\sigma) = \int_0^{\infty} e^{-\sigma t} f(t) dt \quad (B-4)$$

hence

$$F_L(\sigma) = \sqrt{2\pi} F_F(-i\sigma) \quad (B-5)$$

as was to be shown. With this relation the Laplace transform for the spherical problem can be readily obtained from the Fourier transform solution.

To describe Bellman's method for inverting the Laplace transform let $F(\sigma)$ be the Laplace transform of $f(t)$, hence

$$F(\sigma) = \int_0^{\infty} e^{-\sigma t} f(t) dt \quad (B-6)$$

For the numerical integration, limits of zero to one are easier to handle. This is accomplished by the following change of variable.

$$y = e^{-t} \quad (B-7)$$

which when inserted into (B-6) gives

$$F(\sigma) = \int_0^1 y^{\sigma-1} f(-\ln y) dy \quad (B-8)$$

This integral can be approximated by an N -term quadrature formula (Bellman uses Gauss-Legendre, although others may work as well). Equation (B-8) therefore becomes

$$F(\sigma) = \sum_{n=1}^N w_n y_n^{\sigma-1} f(-\ln y_n) \quad (B-9)$$

where the y_n and w_n depend on the particular quadrature formula used. This represents one equation for the N unknowns, $(f(-\ln y_n), n = 1, 2, \dots, N)$. N equations are obtained by substituting N different values for σ . Taking this set to be $\sigma = 1, 2, \dots, N$, equation (B-9) yields the following set.

$$F(j) = \sum_{n=1}^N w_n y_n^{j-1} f(-\ln y_n); j = 1, 2, \dots, N \quad (B-10)$$

In matrix form equation (B-10) is

$$\{F\} = [A]\{f\} \quad (B-11)$$

where

$$\{F\} = \begin{pmatrix} F(1) \\ F(2) \\ \vdots \\ F(N) \end{pmatrix}; \{f\} = \begin{pmatrix} f(-\ln y_1) \\ \vdots \\ f(-\ln y_N) \end{pmatrix}$$

$$[A] = \begin{pmatrix} y_1^{1-1} w_1 & \dots & y_n^{1-1} w_n \\ \vdots & & \vdots \\ y_1^{N-1} w_1 & \dots & y_n^{N-1} w_n \end{pmatrix}$$

The usefulness of the method is due to the fact that $[A]^{-1}$ is problem-independent. The solution of equation (B-11) is

$$\{f\} = [A]^{-1} \{F\} \quad (B-12)$$

Numerical values for $f(-\ln y_n)$ are readily obtained once $[A]^{-1}$ is known. For Gauss-Legendre quadrature, Bellman has tabulated $[A]^{-1}$ and $-\ln y_n$ for values of N from 3 to 15. It should be noted that $[A]$ is ill-conditioned, hence double precision (16 digits) is needed to carry out the indicated operations in equation (B-12).

Since $t = -\ln y$, N values of $f(t)$ can be obtained by solving equation (B-12) for N values of $f(-\ln y)$. Unfortunately, the t_n values are rather small and tend to cluster near $t = 0$ for the range of N given by Bellman. This problem can be avoided, however, and $f(t)$ determined for larger values of t by using the fact that the Laplace transform of $f(\alpha t)$ is given by $\frac{1}{\alpha} F(\sigma/\alpha)$ where $F(\sigma)$ is the Laplace transform of $f(t)$. Therefore, equation (B-12) becomes

$$f(\alpha t_i) = \frac{1}{\alpha} \sum_{j=1}^N A_{ij}^{-1} F(j/\alpha) \quad (B-13)$$

Other methods to extend the time domain are discussed in reference 4 and will not be discussed here.

REFERENCES

1. Naval Civil Engineering Laboratory. Technical Note N-1062: Rigid body response of an elastically-restrained cylindrical deep ocean structure to detonation-induced underwater shock, by H. S. Zwibel and J. G. Hammer. Port Hueneme, California, Nov 1969.
2. Norfolk Naval Shipyard. Underwater Explosions Research Division. U.E.R.D. Report 1-55: Interaction of a spherical acoustical wave with a beam of circular cross section, by W. W. Murray. Portsmouth, Virginia, Jan 1955.
3. R. D. Mindlin and H. H. Bleich. "Response of an elastic cylindrical shell to a transverse step, shock wave," Journal of Applied Mechanics, Jun 1953, pp. 189-195.
4. R. Bellman, R. E. Kalaba and J. A. Lockett. Numerical inversion of the Laplace transform. New York, American Elsevier Publishing Co., Inc., 1966.
5. E. Merzbacher. Quantum mechanics. New York, John Wiley and Sons, Inc., 1961, pp. 204-206.

LIST OF SYMBOLS

a	Radius of sphere or cylinder
c	Acoustic velocity in water
$h_\ell^{(2)}$	Hankel function, ℓ^{th} order, 2 nd kind
J_ℓ	Bessel function
j	Summation index
k	"Spring" constant of restraint
ℓ	Summation index
m	Unit mass of sphere or cylinder
n	Summation index
p	Unit pressure
P_0	Peak pressure of incident pulse
q	Time decay-constant
r	Radial distance
s	Ratio of structure density to water density
t	Time
u, \dot{u}	Water particle velocity and acceleration
u_0	Water particle velocity at front of shock wave
w	Weighting factor
z, \dot{z}, \ddot{z}	Displacement, velocity, acceleration of structure in direction of shock propagation
A_ℓ	Frequency dependent amplitude of ℓ^{th} mode
C_D	Drag coefficient
C_M	Mass coefficient
F_D	Drag force
F_I	Inertia force
H	Heavyside step function
N	Quadrature order, Bellman method
P_ℓ	Legendre polynomial, ℓ^{th} order
α	Scaling factor
γ	Spherical coordinate measured in vertical plane

ζ	Dimensionless translational distance
$\bar{\zeta}$	Fourier transform of ζ
θ	Spherical or cylindrical coordinate
μ	Mass density of water
ρ	Dimensionless radial distance
σ	Laplace variable
τ	Dimensionless time
ϕ	Potential function
$\bar{\phi}$	Fourier transform of ϕ
χ	Dimensionless time constant
ω	Angular frequency (rad/sec)
ω_0	Fundamental frequency of structure in air

Unclassified

Security Classification

DOCUMENT CONTROL DATA - R & D		
(Security classification of title, body of abstract and indexing annotation must be entered when the overall report is classified)		
1. ORIGINATING ACTIVITY (Corporate author)		2a. REPORT SECURITY CLASSIFICATION
Naval Civil Engineering Laboratory Port Hueneme, California 93041		Unclassified
		2b. GROUP
3. REPORT TITLE		
Comparative Solutions for the Response of Restrained, Rigid-Body Underwater Structures to Acoustic Shock		
4. DESCRIPTIVE NOTES (Type of report and inclusive dates)		
Final November 1969 - August 1970		
5. AUTHOR(S) (First name, middle initial, last name)		
J. G. Hammer and H. S. Zwibel		
6. REPORT DATE	7a. TOTAL NO. OF PAGES	7b. NO. OF REFS
January 1971	73	5
8a. CONTRACT OR GRANT NO.		9a. ORIGINATOR'S REPORT NUMBER(S)
b. PROJECT NO. ZF 38.512.001.009		Technical Note N-1141
c.		9b. OTHER REPORT NO(S) (Any other numbers that may be assigned this report)
d.		
10. DISTRIBUTION STATEMENT		
Approved for public release; distribution unlimited.		
11. SUPPLEMENTARY NOTES		12. SPONSORING MILITARY ACTIVITY
<i>See also</i>		Director of Navy Laboratories Washington, D. C. 20360
13. ABSTRACT		
<p>This study seeks better understanding of the general problem of predicting the response of fixed underwater structures to a shock wave propagating through the water. Two idealized structures are considered; an elastically-restrained rigid sphere and an elastically-restrained rigid cylinder. The shock is assumed to be an exponentially-decaying pressure pulse in an acoustic fluid. Solutions to the exact equations are obtained analytically for the spherical structure and by Bellman's numerical inversion procedure for both structures. Previously obtained solutions for the restrained cylindrical structure, simplified by the Mindlin-Bleich approximation, are found to be in agreement. Response curves are given for both structural types over a range of parameters. The effects of drag are discussed.</p>		

DD FORM 1473

NOV 68

(PAGE 1)

S/N 0101-807-6801

Unclassified

Security Classification

Unclassified
Security Classification

14 KEY WORDS	LINK A		LINK B		LINK C	
	ROLE	WT	ROLE	WT	ROLE	WT
Blast effects Shock waves Underwater acoustics Dynamic response Underwater structures Drag						